INTEGRATING COMPUTATIONAL FLUID DYNAMICS AND BIOLOGICAL MODEL TO ASSESS WASTEWATER REACTOR DESIGN

Albert Vilà-Rovira

Universitat de Girona

DOCTORAL THESIS

Integrating computational fluid dynamics and biological models to assess wastewater reactor design

Albert Vilà i Rovira

2017

Programa de Doctorat en Ciència i Tecnologia de l'Aigua

Dirigida per: Jesús Colprim Galceran, Maria Dolors Balaguer Condom, Maël Ruscalleda Beylier

Tutor/a: Jesús Colprim Galceran

Memòria presentada per optar al títol de doctor/a per la Universitat de Girona

List of publications

The list of publications derived from this thesis is presented:

1. **Vilà-Rovira, A**., Puig, S., Balaguer, M.D. and Colprim, J., 2015. Anode hydrodynamics in bioelectrochemical systems. RSC Advances, 5(96), pp. 78994-79000.

2. **Vilà-Rovira, A**., Ruscalleda, M., Balaguer, M.D. and Colprim, J. Multiphase Hydrodynamic Simulations and Biological Modelling of an Anammox Reactor. (summited)

List of symbols

Hydrodynamics

D_{im}	Mass diffusion coefficient [$m^2 \cdot s^{-1}$]
D_{iT}	Thermodiffusion (Soret) coefficient [$kg \cdot m^{-1} \cdot s^{-1}$]
div	Divergence of a vector [-]
D_T	Thermal conductivity [$m^2 \cdot s^{-1} \cdot K^{-1}$]
E	Energy [J]
E_I	Internal energy [J]
g	Gravity vector [$m \cdot s^{-2}$]
grad	Gradient vector [-]
J_i	Diffusion term [$kg \cdot m^{-2} \cdot s^{-1}$]
P	Pressure [Pa]
Re	Reynolds number [-]
R_i	Species reaction source term [$kg \cdot m^{-3} \cdot s^{-1}$]
S	Source term [-]
T	Temperature [K]
t	Time [s]
u	Velocity vector [$m \cdot s^{-1}$]
u_i	Velocity vector component, i=x,y or z. [$m \cdot s^{-1}$]
x	Position vector [m]
x_i	Position vector component, i=x,y or z. [m]
Y_i	Species mass fraction [-]
ϕ	General scalar variable, vector or matrix [-]
ρ	Density [$kg \cdot m^{-3}$]
θ	*Normailized time (ratio of time to space time)*
ε	*Turbulent dissapation rate ($m^2 \cdot s^{-3}$)*
κ	*Turbulent kinetic energy ($m^2 \cdot s^{-2}$)*
φ, Φ	*General value , average of general value.*
Sc	*Schmidt Number(-)*

Multiphase

D_p	Bubble or particle diameter [m]
τ_P	Bubble or particle relaxation time [s]

A_i Bubble or particle interfacial area [m^2]

λ_q Bulk viscosity of phase q [$kg \cdot s^{-1} \cdot m^{-1}$]

C_D Drag coefficient [-]

f Drag coefficient function [-]

F Force (N)

R_{pq} Interaction forces between phases p and q [N]

μ_q Shear viscosity of phase q [$kg \cdot s^{-1} \cdot m^{-1}$]

V Total volume [m^3]

α Volume fraction [-]

V_i Volume of phase *i* [m^3]

Pe Peclet Number

L Length

D Diameter

VF Volume Fraction

Biological model

S_S Readily biodegradable organic matter state variable [kg COD$\cdot m^{-3}$]

S_I Inert soluble organic matter state variable [kg COD$\cdot m^{-3}$]

X_S Slowly biodegradable substrate state variable [kg COD$\cdot m^{-3}$]

S_I Non-biodegradable soluble substrate [kg COD$\cdot m^{-3}$]

$X_{I/P}$ Inert/particulate organic matter substrate state variable [kg COD$\cdot m^{-3}$]

X_{BH} Heterotrophic biomass sate variable [kg COD$\cdot m^{-3}$]

X_{BA} Autotrophic biomass state variable [kg COD$\cdot m^{-3}$]

μ_{max} Maximum growth rate [s^{-1}]

q_a substrate consumption rate anadiphilic microorgansims [mg S$\cdot mg^{-1}$ X$\cdot d^{-1}$]

q_m substrate consumption rate methanogenic microorgansims [mg S·mg^{-1} X·d^{-1}]

q_a^{max} màximum substrate consumption rate anadiphilic microorgansims [mg S·mg^{-1} X·d^{-1}]

q_m^{max} màximum substrate consumption rate methanogenic microorgansims [mg S·mg^{-1} X·d^{-1}]

K_{Sa} half saturation constants for anodiphilic microorganisms [mg S·L^{-1}·d^{-1}]

K_{Sm} half saturation constants for methanogenic microorganisms [mg S·L^{-1}·d^{-1}]

M_{ox} oxidized fraction of mediator [mg S·L^{-1}·d^{-1}]

Y_{AMX} Yield coefficient for anammox microorganisms' growth [g COD·g^{-1} N]

i_{NBM} Nitrogen content of anammox microorganisms [g COD·g^{-1} N]

μ_{AMX}^{growth} Maximum growth rate for anammox microorgansims [d^{-1}]

S_{NH4} ammonium nitrogen concentration [mg N·L^{-1}]

S_{NO2} nrite nitrogen concentration [mg N·L^{-1}]

K_{NH4}^{AMX} Half saturation constant for ammonium of anammox microorganisms [mg N·L^{-1}]

K_{NO2}^{AMX} Half saturation constant for nitrite of anammox microorganisms [mg N·L^{-1}]

X_{AMX} anammox microorganisms' concentration [mg COD·L^{-1}]

TN Total Nitrogen

Abreviations

MBR Membrane Bioreactor

RTD Residence Time Distribution

CEM	Cation Exchange Membraane
Anammox	Anaerobic ammonium oxidation
PN	Partial Nitritaion
DO	Dissolved Oxygen
NLR	Nitrogen Loading Rate
UASB	Upflow Anaerobic Sludg Blanket
AMX	Anammox
BES	Bioelectrochemical Systems
CFD	Computational Fluid Dynamics
COD	Chemical Oxygen Demand
CSTR	Continuous Stirred Tank Reactor
MFC	Microbial Fuell Cells
SBR	Sequencing Batch Reactor
UDF	User Defined Function
TAN	Total Anode volume Compartment
NAC	Net Anode Volume Compartment
HRT	Hydraulic Retention Time
ASM	Activated Sludge Models
MEC	Microbial Electrolysis Cell

List of Figures

List of tables

A la Iria, a en Jan i a l'Abril

"*tal com sembris recolliràs*"

Acknowledgements

Aquesta part de la tesi he de reconèixer que és la que m'ha costat mes però que segurament hauré escrit més ràpid. És la part més emotiva per mi perquè significa que (per fi) s'ha acabat un projecte personal i professional que m'ha omplert moltíssim.

En primer lloc - i si pogués ho escriuria en lletres molt més grans - vull agrair moltíssim – però moltíssim – a en Jesús i la Marilós haver-me donat l'oportunitat de fer aquesta tesi. Crec que si pogués tornar enrere, no hauria escollit cap altre temàtica ni tipus de recerca: he après moltíssim, i a sobre he fet recerca del que més m'ha agradat, doncs la modelització i la simulació sempre m'ha semblat sempre ha estat del meu interès. Gràcies de veritat per haver-me permès haver fet la tesi doctoral, i per haver-la fet del que l'he fet. Gràcies, moltes gràcies. Encara recordo que tot va començar quan estava cercant un màster per poder fer - només un màster -, vaig anar al despatx d'en Jesús demanant unes pràctiques de màster i al final l'he acabat fent més "grossa" del que m'imaginava. Jesús, encara tinc present el dia que em vas proposar treballar en CFDs, i de veritat que t'estic molt agraït, al principi em vaig acollonir però al mateix temps sabia que en el fons era un repte i els reptes són per enfrontar-los. Gràcies per haver seguit confiant sempre, a pesar del que ha costat. Marilós, moltes gràcies també per l'esforç enorme que has fet corregint i corregint - i tornant a corregir - capítols i capítols, i papers, i per les hores de despatx discutint termes i equacions, aportant-me sempre una mirada més crítica i pràctica. Gràcies de veritat, moltes gràcies (sí, em repeteixo però aquest cop ho faig expressament!).

En segon lloc vull agrair molt i molt l'esforç de dues persones més que han estat també molt importants en aquest camí: Maël i Sebas. Maelus, ha estat un plaer haver pogut treballar amb tu. Has estat el que més contacte directe he tingut, potser del que més he après de processos, de reactors, de plantes pilots, de moltíssimes coses que no estan enlloc escrites però són molt importants. Gràcies per les hores de discussió, de fer balanços, de tractar dades, hores de cotxe anant a les plantes. Gràcies Melus! Per altre banda, Sebas, et vull agrair moltíssim la confiança que em vas fer quan volies aplicar CFDs en MFCs. Ha estat un plaer treballar en un altre tipus de procés diferent al que estava acostumat, i del qual he après molt. A nivell personal m'he sentit super a gust treballant amb tu i compartir a més vivències de "papis".

Encara que la tesi s'ha desenvolupat molt bàsicament davant del PC, vull agrair també les persones amb qui he estat treballant dintre del procés Panammox, que hem passat un bon grapat d'hores al laboratori i a plantes pilot. Gràcies Xavi, Jordi G., Patri, Ramon G., Thiago, i com no a "gracias Helio, contigo empezó todo!", amb qui a més a més a nivell personal hem tingut una bona relació! A més gràcies també a un bon grapat d'estudiants que han anat passant per el lab per tot el suport que ens han donat (F. Padrés, Oscar, Mota, etc.). No em voldria deixar als membres del grup MFC amb qui encara que no tan intensament, també els he hagut d'emprenyar per demanar dades de disseny i a sobre van haver-me de patir en el congrés d'Alcalà: Narcís, Anna, Danielle, Pau, moltes gràcies. Crec que es mereixen moltíssim unes línies d'agraïment especial a la Montse Dalmau perquè en aquests últims moments m'ha donat un gran suport en el "formatting" de tesi i en mil-i-una ocasions ajudant a preparar presentacions o altres documents (va Héctor, tu també hi vas ajudar una mica!)

El camí ha estat molt llarg i entre màster, indecisió (treballant) i tesi, he tingut l'oportunitat de conèixer un bon grapat de persones, que és també

part de l'èxit: Laura Batche, Marta Coma, Carboneres team (Alba x 2, Esther V., Carla), MBRs team (Hector, Sara, Montse D., Ivan, Gaetan, Jordi Moreno, Sergi, Lluís G., Quim, Ignasi, J. Dalmau), Ramiro, Serni, Sara J., Sergio, la gent del Màster de l'Aigua (Marta B., Natlàlia, Ari, Marc, Anna, Ingrid), Teresa. A les "jefas" del labo Alba A., Ariadna, Rustu i Rossell que m'han hagut de "patir" al lab. A gent del Lequia i del Màster de Medi Ambient de qui d'alguna manera o altre he après molt, menció especial a Dr. Miquel Rigola, però també Manel Poch, Maria M., Clàudia Turón, Rafa Gonzalez, Lluís Corominas. I també un agraïment a tots als professors en general de IQS, però en particular al Sr. Molins, de qui mai m'hauria pensat que usaria tanta informació de les seves assignatures.

Dels que tampoc em vull oblidar és dels amics que sempre trobem moments per compartir dinars, algunes cerveses o el que calgui per compartir experiències i bones estones. Als Caballeros (al padrini Buket, Quim, Cesc, Jordi, Bertu, Miquel i Pepe) i respectives parelles/famílies, als que s'han anat dispersant però que encara tenim alguna estona per trobar-nos (Farra, Silvia, Anna S., Suárez, Xus). Tampoc em voldria oblidar de la gent de futbol, on sempre hi ha regnat el bon ambient i ha sigut una bona via de desconnexió. Jordi Ruiz, Carru i Patxi sou collunuts! També un bon record del presi Caste, Manel Carbó, en Toni & Ivan D. També la tantíssima gent que he conegut amb els Llobatons de Sant Dalmai (Xevi, Laura, Montse B., Ivan, Pep, Ingrid, Ferran, Ricard, Quim C., Jordi, Angel, Jesús, etc.) que també hem tingut molts bons moments per compartir.

Ja per acabar, vull agrair molt especialment als meus pares per tot el que han donat per mi tot aquest temps, perquè sempre m'han animat i ajudar a estudiar i formar-me encara més: moltíssimes gràcies. També voldria recordar en Pep i la Fina, i de tots els meus avis que segur estarien molt orgullosos de veure'm arribar fins aquí. A en Pau per haver estat casi com un

germà, i els altres doctors de la família Xavi i Quim P. que encara no us ho sembli sempre meu motivat a seguir endavant. També als qui sempre m'han fet sentir com la meva familia: els meus sogres, els meus cunyats i les "pekes". I per últim a les tres persones més importants de la meva vida: carinyo, moltes gràcies per tenir tanta paciència (ara sí que he acabat), per motivar-me, per fer-me feliç i ajudar-me a lluitar per el que vols. Sense tu al meu costat segurament no hauria estat possible, ho dic de veritat. Als petits, Jan i Abril, sou la meva felicitat i us estimo i us adoro, quan sigueu més grans us explicaré més bé però segur que estareu molt orgullosos.

Ths research has been financially supported by the Spanish Government (CTQ2014-53718-R) and the University of Girona (MPCUdG2016/137).

Universitat de Girona

CERTIFICAT DE DIRECCIÓ DE TESIS

El/la Dr Jesús Colprim Galceran, la Dra. Maria Dolors Balaguer Condom i el Dr. Maël Ruscalleda Beylier del Laboratori d'Enginyeria Química i Ambiental (LEQUIA) de la Universitat de Girona

DECLARO/DECLAREM:

Que el treball titulat "Integrating computational fluid dynamics and biological models to assess wastewater reactor design", que presenta Albert Vilà Rovira per a l'obtenció del títol de doctor/a, ha estat realitzat sota la nostra direcció.

I, perquè així consti i tingui els efectes oportuns, signem aquest document.

Dr. Jesús Colprim Galceran

Dr. Maël Ruscalleda Beylier

Dra. M. Dolors Balaguer Condom

Girona,

Index

SUMMARY

Resum

El disseny de plantes de tractaments d'aigües residuals té com a objectiu el desenvolupament de processos amb una elevada eficàcia de tractament amb els mínims costs (energia, reactius, entre altres) i el mínim impacte ambiental. La recerca de noves tecnologies d'eliminació biològica s'ha desenvolupat sota aquestes premisses. Tanmateix, es necessiten llargs períodes d'investigació per determinar els paràmetres de disseny més determinants per plantejar alternatives als processos de tractament convencionals. L´ús d'eines de simulació permeten agilitzar molt més aquest procés. En el tractament biològic d'aigües residuals, els models més àmpliament coneguts son els *Activated Sludge Models* (ASM), que són unes potents eines de disseny i optimització de reactors biològics.

La principal limitació en l'ús d'aquests models és que estan desenvolupats amb una sèrie de consideracions com assumir mescla complerta, tant de fangs com substrat, els quals no sempre són reals en segons quins tipus de disseny i d'operació de reactors. En aquest sentit, l'augment continu de les capacitats dels ordinadors, ha permet promoure l'ús de la Simulació de Fluids Computacional (CFDs) per fer més eficient el disseny de plantes i reactors de tractament d'aigües residuals (així com en altres indústries). En aquest context, la tesi que es presenta aquí té com a objectiu l'ús d'eines de simulació de fluids combinat amb l'ús de models biològics (ASM) per un disseny òptim de reactors d'eliminació biològica de nutrients.

S'ha realitzat la simulació de dos tipus diferents de reactors: reactor de piles biolectroquímiques (MFC) i de oxidació anaeròbica d'amoni (anammox). En quan al disseny del MFC, es van testar quatre tipus d'elèctrodes confinats en una cambra anòdica quadrada per tal d'avaluar la distribució de flux així com

l'eficiència d'eliminació: barra de grafit, barra de grafit amb grafit granular, barra de grafit amb malla d'acer inoxidable i una placa de grafit. Els resultats de la simulació van demostrar que la geometria del reactor i l'elevada corrent de recirculació van produir clars camins preferencials entre els dos corrents de recirculació (entrada i sortida), afectant la distribució de substrat dins de la cambra anòdica. Així mateix, es va veure que les reaccions biològiques tenien lloc només en una part del reactor, aconseguint la pràctica eliminació de nutrients L´ús de materials com la barra de grafit combinat amb grafit granular i malla d'acer inoxidable permeten una millor distribució de flux i de substrat a l'interior de la cambra anòdica, en comparació amb la resta de materials. Ambdós materials oferien una major superfície (per biomassa enganxada) i una millor conductivitat. Finalment, es va proposar l'ús d'una configuració amb malla d'acer inoxidable per les seves propietats elèctriques i el seu inferior cost.

En quant al disseny d'un reactor amb tecnologia anammox, es fa simular un reactor tipus columna amb plats interns i una corrent de recirculació de dalt a baix del reactor per mantenir els sòlids fluïditzats. Els resultats de la simulació van permetre observar un bon grau de mescla en l'interior del reactor per l'efecte de la recirculació externa. A més, la presència de plats interns produïen la formació de recirculacions internes que afavorien la transferència de massa de substrat a través del gránul de biomassa. En quan a l'eliminació biològica de nutrients, amb aquesta configuració s'obtenien elevats nivells d'eliminació d'amoni i de nitrit. Els resultats de la simulació van permetre localitzar a dins del reactor els punts de màxima i mínima eliminació biològica, una clara avantatge en comparació amb les eines de simulació convencionals. Basat en els resultats del model biològic al llarg del reactor, es proposa una alimentació del reactor distribuïda al llarg de l'alçada del reactor per d'incrementar la capacitat de tractament del reactor.

La tesi desenvolupada demostra el potencial d'una eina de simulació en el disseny de reactors biològics de tractament d'aigües residuals, que combina la simulació de fluids computacional amb models biològics. A partir d'aquí, la recerca s'ha d'adreçar a incorporar en models multi físics la variable que representi el fang biològic i que permeti obtenir la distribució de sòlids al llarg del reactor.

Resumen

El diseño de plantas de tratamiento de aguas residuales tiene como objetivo el desarrollo de procesos con una elevada eficiencia de tratamiento con los mínimos costes (energía, reactivos, entre otros) y un mínimo impacto ambiental. La investigación de nuevas tecnologías de tratamiento se ha desarrollado bajo estos requerimientos. Aún así, se necesitan largos períodos de experimentación para determinar los parámetros determinantes para considerar serias alternativas frente a los tratamientos convencionales de depuración. El uso de herramientas de simulación permite agilizar este proceso. Dentro del campo del tratamiento biológico de aguas residuales, los modelos más reconocidos y usados son los Activated Sludge Models (ASM), potentes herramientas para el diseño y optimización de reactores biológicos.

La principal limitación en el uso de dichos modelos es que incluyen asunciones como la de mezcla perfecta, tanto del fango como de nutrientes, lo que no siempre es aplicable en según qué tipos de reactores y diseño de reactores. En este sentido, el continuo aumento de las capacidades de los ordenadores, ha promovido el interés en el uso de la simulación de fluidos computacional (CFDs) para hacer más eficiente el diseño de plantas y reactores de tratamiento de aguas residuales (así como en el resto de industrias). En este sentido, la tesi que se presenta aquí tiene como objetivo el uso de herramientas de simulación de fluidos combinado con el uso de modelos biológicos (ASM) para un óptimo diseño de reactores de eliminación biológica de nutrientes.

Se realizó la simulación de dos tipos de reactores de tratamiento: reactores de pilas bioelectroquímicas (MFC) y de oxidación anaeróbica de amonio (anammox). En cuanto al diseño de MFCs, se testaron cuatro tipos distintos

de electrodos confinados en la mismo compartimiento anódico de geometría cuadrado por tal de evaluar la distribución de flujo así como la eficiencia de eliminación: barra de grafito, barra de grafito con grafito granular, barra de grafito con malla de acero inoxidable y una placa de grafito. Los resultados de la simulación demostraron que la geometría del reactor y un elevado caudal de recirculación producen la presencia de claros preferenciales entre las dos corrientes de recirculación (entrada y salida), afectando la distribución de sustrato en el interior del compartimiento anódico. Así mismo, se observó que las reacciones biológicas tienen lugar tan solo en una parte del reactor, consiguiendo prácticamente una total eliminación de nutrientes. El uso de materiales como la barra de grafito combinado con el grafito granular y la malla de acero inoxidable permiten una mejor distribución de flujo y sustrato el interior del compartimiento anódico, comparado con el resto de materiales. Ambos materiales ofrecían una mayor superficie (apego de biomasa) y una mejor conductividad. Finalmente, se propuso el uso de una configuración con malla de acero inoxidable por sus buenas propiedades eléctricas y su coste inferior.

En el caso del diseño de un reactor de tecnología anammox, se ha hecho la simulación de un reactor tipo columna con platos internos i una corriente elevada de recirculación des de arriba hacia debajo de la columna con la finalidad de mantener los sólidos en suspensión. Los resultados de dicha simulación permitieron observar una buena mezcla en el interior del reactor debido al cabal de recirculación externa. Además, la presencia de los platos internos generaban recirculaciones internas que garantizaban una buena transferencia de masa hacía los gránulos de biomasa. En cuanto a la eliminación biológica de nutrientes, con dicha configuración se obtienen elevados niveles de eliminación de amonio y nitrito. Los resultados de la simulación permitieron también localizar dentro del reactor los puntos de máxima y mínima eliminación biológica, una clara ventaja en comparación

con las herramientas de simulación ya existentes. A partir de los resultados de la simulación, se propone incrementar la capacidad de tratamiento del reactor introduciendo corrientes de alimentación distribuidas a lo largo de la altura del reactor para así conseguir incrementar la capacidad de tratamiento del reactor.

La tesis desarrollada demuestra el potencial de uso de la simulación de fluidos en el diseño de reactores biológicos de tratamiento de aguas residuales, combinando la simulación de fluidos con modelos biológicos. A partir de aquí, la investigación en este campo se de abordar incorporando modelos multifísicos que incorporen el fango biológico i obtener así el perfil de distribución de sólidos en el reactor.

Summary

The design of wastewater treatment plants is addressed to develop process with the maximum removal efficiency with the minimum costs (energy, reactants, among others) and the lower environmental impact. The research of novel biological treatment technologies is focused on achieving these results. However, long experimental periods are often necessary to determine the key parameters in order to validate alternatives in front conventional processes. The support of modelling tools facilitated this work. In biological wastewater technologies, the well-known Activated Sludge Models (ASM) is the powerful tool in the design and optimization of biological reactors.

However, these biological models has been developed with a set of assumptions which included ideal flux conditions (sludge and substrate), which are not often assumable in all the reactor operations. In this sense, the increase in the computer capacities has facilitated the use of the computational fluid dynamics (CFD) in the design of wastewater treatment facilities (and other industries). In this context, the present thesis is focused on the application of CFD combined with biological models for the design of novel biological nutrient removal reactors.

Two new reactor design configurations were simulated by the model integration: Microbial Fuel Cells (MFC) and anaerobic ammonium oxidation (anammox). Regarding the MFC four different electrode materials filling the squared anodic chamber were compared in terms flow distribution and efficiency: rod graphite, rod graphite plus granular graphite, rod graphite plus stainless steel mesh and graphite bar. The simulated results demonstrated that both, reactor geometry and high recirculation stream

clearly produced a preferable way of flow between influent and effluent recirculation, affecting the substrate distribution inside the anodic chamber. Moreover, biological reactions occurred basically at one half part of the reactor achieving practically full nitrogen removal. The granular graphite and stainless mesh permitted better flow and substrate distribution compared to the other materials. Both materials had a higher surface (for biomass attachment) and higher conductivity. Finally, stainless steel mesh was proposed as the better material for its electrical properties and low cost.

Regarding the novel anammox reactor design, it was based on column reactor with internal plates and a recirculation stream from top to bottom to maintain the biomass fluidized. Results of simulation indicated that a high mixing degree was achieved due to the external recirculation. Moreover, internal recirculation between plates was detected giving better conditions for mass transport of substrate to the biomass granules. Related to the biological nitrogen removal, practically complete nitrogen (amonium and nitrite) was achieved. Simulation permitted to allocate inside the reactor the zones of maximum and minimum removal rates, which is an advantage in front of conventional simulating tools. Analysing the removal rate profile along the column, a multi-feed through different column heights was proposed in order to increase the maximum removal rate within the overall reactor domain.

The present work demonstrated the power tool achieved in the biological reactor design field by the integration of computational fluid dynamics and biological models. Moreover, further research should be done to incorporate the sludge phase and simulate the biomass distribution in the reactors.

INTRODUCTION

Chapter 1. **Introduction**

1.1 Model application in biological wastewater treatment

During the last decades, modelling has gained interest as a support tool for the design of novel technologies and equipment on industrial applications, including engineered wastewater treatment facilities. The continuous increase in the computational power has facilitated the increase in model complexity (further processes and variables). The design and performance of the biological wastewater treatment has been assessed by using the well know Activated Sludge Models (ASM) (Henze et al., 2000). Moreover, these models has been extensively used and adapted to novel processes and technologies by incorporating new variables and rates. More concretely, the use of the ASM has been motivated by several factors (Corominas, 2006) such:

- ✓ Upgrade and design of activated sludge plants: The use of the model permits to improve the nutrient removal capacity of the treatment plant/reactor. It is also useful in the prediction of system behaviour in front several possible scenarios, as developed by Dalmau et al., 2013 and Yang et al., 2007.
- ✓ Definition and test of control strategies: it is feasible to test different control strategies of plant by the use of modelling tools. This could be in benchmark simulations - as in Jeppsson et al., 2007- and the control strategy in a real reactor operation (Ganigué et al., 2010).
- ✓ Model based control: It refers to stablish a system control based on a model working on line (in paralel) with the process (Kim et al., 2014b).

The advantages of using these models are directly related to system optimization and reducing time consuming in laboratory experimentation. However, the assumptions and preliminary considerations commonly applied

in ASM could derive to limit the accuracy of the results obtained when working with complex systems. The main limitations of this methodology result from the simplification of the model flux by considering ideal conditions in the reactor: two main approaches used in this sense are the Continuous Stirred Tank Reactor (CSTR) and Plug Flow Reactor (PFR) (Fogler, 2006). A wide range of studies related to modelling wastewater treatment technologies are based on this assumptions (Fan et al., 2009), and not considering system anomalies which not produced ideal conditions. The improvement of the simulation results could be achieved considering the hydrodynamic in the reactor such as flow and substrate distribution as well multiphase interactions in the system. Thereby, the influence of hydrodynamics has gained relevance in novel reactor configurations developed during the last decades where biomass is not homogeneously distributed, such as biofilm (Rochex et al., 2008), granular sludge (Dhenge et al., 2010), membrane reactors, among others.

Computational Fluid Dynamics (CFD) is the art of modelling fluid flow by numerically solving the mass, momentum and energy balances within any system involving fluid dynamics and discretizing both space and time scales (Versteeg and Malalasekera, 1995). This also requires including chemical processes, mass and heat transport, and additional processes occurring in systems (radiation, electricity, among others). The non-linear equations system may be solved numerically (by computer aided), which requires the proper definition of fluid properties and boundary conditions. First CFD-based studies were mainly addressed to improve aerodynamics (aeronautic and car sectors) and simulate motor engines combustions (Anon, 1980; Boni, 1978; Crider and Foss, 1966).

The exponential increase in processors capabilities and algorithms developed has expanded the applicability and uses of CFD simulation, reaching as well

the wastewater treatment field. The time evolution of the number of publications related to CFD applications to the wastewater treatment sector is analysed in Figure 1.1. A clear increasing tendency of the number of publications related to this field can be observed, illustrating the increasing interest in using CFD to improve these systems.

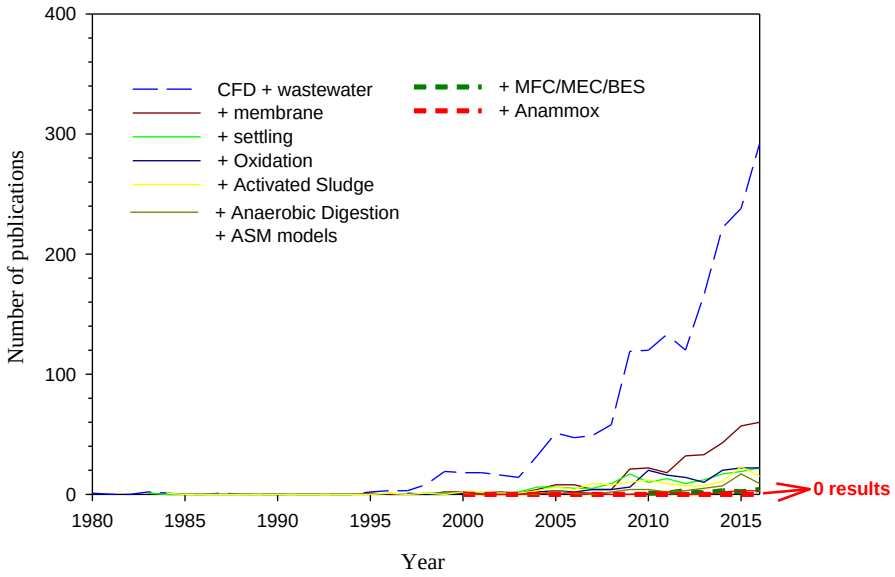

Figure 1.1 Time evolution of the number of publications involving CFD with wastewater and different technologies (membrane, settling, oxidation, activated sludge, anaerobic digestion, MFC or BES and anammox), using Scopus platform.

The use of the CFD tools in wastewater has been proved to be a powerful tool in the process scale-up. CFD has been recently applied to a variety of biological reactor configurations and other wastewater treatment processes units, including as well novel technologies in development: oxidation ditches (Lei and Ni, 2014; Karpinska and Bridgeman, 2015), membrane bio-reactors (Ratkovich and Bentzen, 2013), up-flow reactors, packed bed reactors (Lopes and Quinta-Ferreira, 2010a) stabilization ponds (Alvarado et al., 2012), settlers (De Clercq, 2003), activated sludge systems (Wang et al., 2009), or anaerobic digestion (Yu et al., 2013), as well as other related technologies to water treatment such as ultraviolet (Hijnen et al., 2006) or chemical

disinfection (Janex et al., 1998). Only few modelling works on biological nutrient removal systems developing biofilms introduced the effect of shear stress on biofilm development, such in a 2D dimensional model developed by Picioreanu and colleagues (2007). Related to the ASM with CFD simulations, only 17 publications have been found (Figure 1.1) so far.

The combination of CFD with the ASM became a new paradigm in the design (and scale-up) of novel reactors configurations. Additionally, it could be - in combination with optimization analysis - step forward on successfully achieving a good compromise between higher biological removal efficiencies and lower economic and environmental costs.

The present work is focused in the use of CFD combined with ASM model in the design assessment of two innovative biological nutrient removal technologies: Microbial Fuel Cells (MFC) and anammox (anaerobic ammonium oxidation). The tool will permit to analyse whether the reactor design and configuration will produce expected results for each case of application, and obtain further information about the flow and substrate distribution. In the following sections, a description of each technology (MFC, Anammox) is presented.

1.2 Novel reactor configurations

1.2.1 Microbial Fuel Cells

The term Bioelectrochemical Sytems (BES) englobes a group of technologies in which bioelectrogenic activity produces power and/or high added value chemical compounds treating a polluted fluid (Vilajeliu et al., 2016). The first BES technology developed was the MFC, which produced electricity from the oxidation of organic waste in the anode compartment. Alternatively, the microbial electrolysis cells (MEC) were developed which required energy (cell potential) to carry on the pollutant removal or to produce high valuable

products. Both systems (MFCs and MECs) consist of electrodes placed in anodic and cathodic chambers with an external electric circuit joining both compartments. In such cells, microorganisms are the responsible of catalyzing the oxidation or reduction in a single or both chambers. Figure 1.2 presents different configurations for MFC and MEC that can take place when wastewater is treated in the anode chamber.

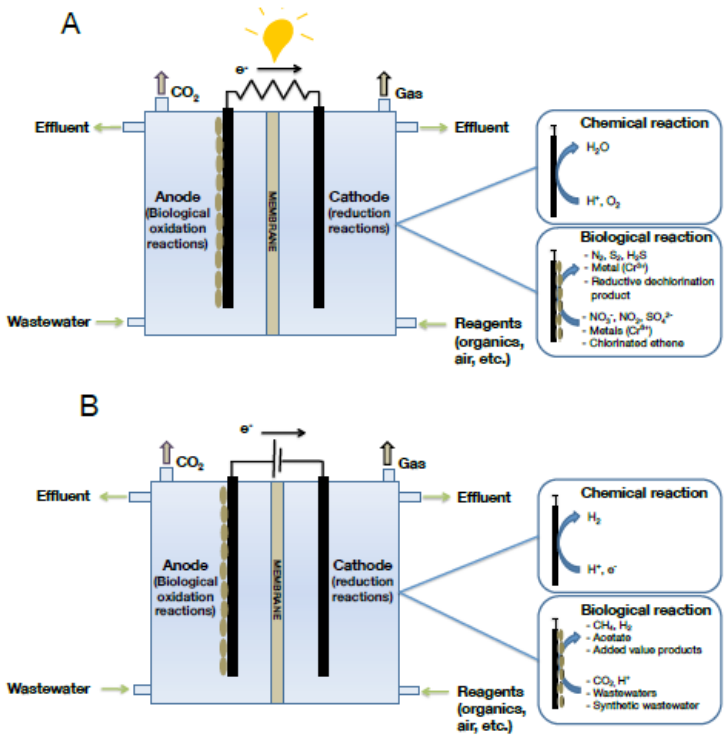

Figure 1.2 Scheme of two different configuration streams of biolectrochemical systems treating wastewater in the anode compartment: A) MFC, B) MEC. (Vilajeliu-Pons et al., 2016b).

Bacteria are the responsible of oxidizing the organic matter under anaerobic conditions in the anodic chamber, to generate electrons and protons. Both products migrate to the cathodic chamber through the external circuit and the internal ionic membrane, respectively. These electrons and protons remain in the anodic chamber and are directly used to produce biomass and oxidize organic matter to carbon dioxide. Inside the cathodic chamber, the

electrons and protons are used to electrochemically reduce oxygen to water. Alternatively, several biocathode configurations have been proposed focused on the reduction of different electron acceptors such as nitrate (Wrighton et al., 2010), sulfate (Coma et al., 2013), hydrogen (Batlle-Vilanova et al., 2014), among others.

Inside the chamber the microorganisms with the capacity of transferring electrons are mainly attached on the electrode surface forming a biofilm. To facilitate this electron transfer, proper electrode materials should be selected in order to have high conductivity and facilitate microorganisms' attachment. In this sense, the most used material to date is the granular graphite, due to its good electrical conductivity and lower cost, compared with other materials. Research has been addressed to study and develop new electrode materials (Wei et al., 2011) in order to enhance conductivity as well as biomass attachment.

MFC technology has the challenge of changing the present paradigm and turn the current high energy-demanding wastewater treatment processes into energy balanced facilities by biologically producing energy (electricity) from the resources contained in wastewater (organic matter). The proof of concept of the technology has been proved in several studies demonstrating that electricity production from wastewater is possible in MFC. However, enough energy production to supply a whole wastewater treatment facility is still far to be achieved and several issues regarding materials, design and construction cost must be overpassed to successfully scale-up the technology (achievement of higher MFC power densities at large scales).

During the last years, several studies have been developed to assess the key parameters for the process scale-up. So far, the main issues to be addressed by research for the successful MFC scale-up can be summarized as: i) the response to increase electrode surface are and disclaim whether is related

with the energy production (Dewan et al., 2008); ii) the increase of volume reactor or connecting single units (i.e. stacks) in a continuous flow (Ieropoulos et al., 2010); iii) selection of low-cost, simple construction and easy maintenance to operate at large scale (Ter Heijne et al., 2011).

The operation conditions and critical parameter values in MFC have been widely investigated, but there are still important issues to be addressed: pH, Temperature, OLR, and the flow rate and shear stress. The last parameters are related to the system hydrodynamics and are a key parameter on the biofilm formation. Generally, increasing the inflow of the compartments positively affects the power density (Aelterman et al., 2008), but could result in a lower nutrient removal efficiency since the hydraulic retention time is decreased and microorganisms are not capable of assimilating all the substrate. Regarding the shear stress, the application of high shear during the enrichment phase results in thicker and denser biofilms as well as higher power density and intensity, compared to biofilms enriched at low shear (Pham et al., 2008). However, biofilm can support a maximum shear rate above which the biofilm detachment processes is induced.

Definitely, CFD became a powerful tool in the support of the design of novel MFC configurations, since it describe internal flow and substrate distribution. As far as we know, only few works were performed applying CFD for the development and optimization of MFC. These studies include the development of innovative designs of anodes (such as helical geometry; (Michie et al., 2014) or different anode configurations (Kim et al., 2014b). However, CFD has so far not been used to assess the hydrodynamics and species distribution in MFC, which has an important impact on the overall efficiency of the system.

1.2.2 Anammox process

The anammox process is an efficient alternative to the conventional (nitrification/denitrification) process for biological nitrogen removal. In this process, anaerobic ammonium-oxidizing bacteria are able to remove ammonium under anoxic conditions using nitrite as electron acceptor and producing nitrogen gas. Figure 1.3 presented and scheme reflecting the advantages of anammox (autotrophic nitrogen removal) process in front a conventional nitrification-denitrification processes, inside the nitrogen cycle.

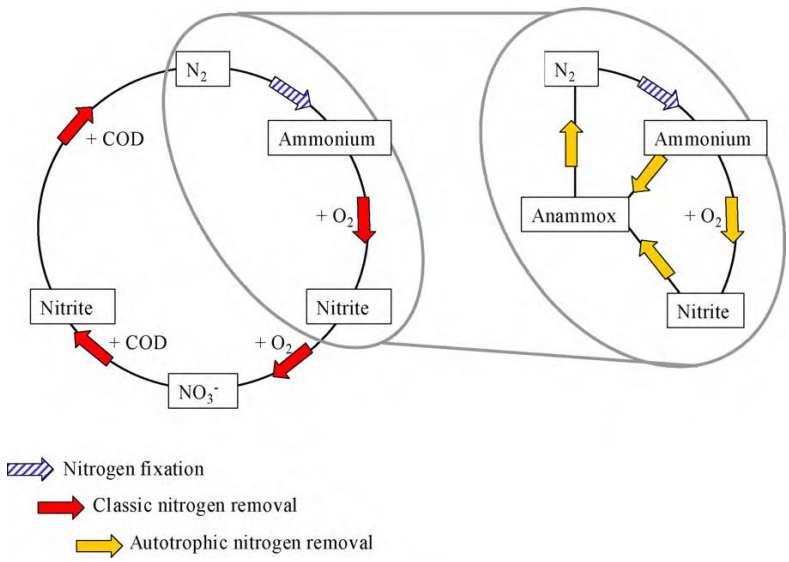

Figure 1.3 Scheme of the nitrogen cycle including the anammox process (autotrophic) (Van Hulle et al., 2010)

As proposed (Strous et al., 1998) from mass balances in enrichment of the anammox cultures, the overall stoichiometry of the process is defined by Equation 1.1:

$$1\,NH_4^+ + 1.32\,NO_2^- + 0.066\,HCO_3^- + 0.13\,H^+ \rightarrow \\ \rightarrow 1.02\,N_2 + 0.26\,NO_3^- + 0.066\,CH_2O_{0.5}N_{0.15} + 2.03\,H_2O \qquad (1.1)$$

Despite Equation 1.1 is a commonly accepted stoichiometry, Takács et al., 2007 proposed a revised stoichiometry (Equation 1.2) in order to account for the balance of bicarbonate considering as well the nitrogen used for synthesis in the nitrogen balance, which caused small unbalance in Equation 1.1:

$$1\,NH_3 + 1.37\,HNO_2 + 0.047\,CO_2 + 1\,H_3PO_4 \rightarrow \\ \rightarrow 1.05\,N_2 + 0.26\,HNO_3 + 0.0011\,C_{41.3}H_{64.6}O_{18.8}N_{7.04}P + 2.03\,H_2O \quad (1.2)$$

Anammox bacteria are autotrophic microorganisms, characterized by its reddish colour (Figure 1.4) and a low doubling time (Strous et al., 1997). Specific anammox activity can be inhibited mainly by high nitrite concentrations (above 50 mg $N\text{-}NO_2^-$ L^{-1} and depending on exposure time; reversible inhibition) and dissolved oxygen levels above 0.5 mg O_2 L^{-1} (reversible inhibition). The anammox microorganisms tend to form granules spontaneously, which favoured its retention inside the reactor. The influent stream to the anammox process should present an equimolar ratio of ammonium and nitrite species. For this reason, the ammonium content in wastewater is partially oxidized to nitrite, in a previous partial nitritation (PN) process. The advantages of the overall process are the reduction of oxygen consumption (compared to conventional nitrification/denitrification), the suppression of organic matter supply for efficient N removal (since anammox are autotrophic bacteria) and the low sludge production, resulting in reduced treatment costs.

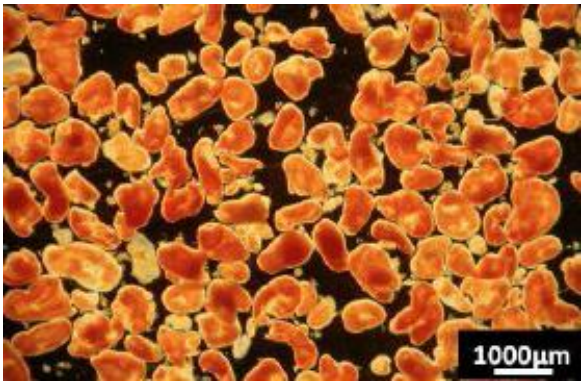

Figure 1.4 Image of granules operating an SBR Anammox reactor, obtained with stereomicroscope (Ruscalleda, 2011)

Anammox process has been widely applied to treat nitrogen (N) rich streams (above 500 mg $N \cdot L^{-1}$), with low Chemical Oxygen Demand (COD) ratio. Examples of this kind of streams are landfill leachate (Ruscalleda, 2011), piggery manure (Scaglione et al., 2015) or reject wàter (Galí et al., 2007), among a variety of industrial wastewaters. More recently, this process has been used for the treatment of lower N content, such municipal wastewater (Lotti et al., 2014). The slow doubling time of anammox bacteria remains a break on the fast implementation of novel anammox reactors, which involves long start-up periods and obliges to preserve biomass inside the reactor.

As mentioned above, the anammox process is combined with a PN to supply the necessary nitrite. This global process can be performed in a single reactor or in two separated reactors. Single reactor involves less capital costs and processes foot print and a proper DO control. However, presents limitations related to process instability when treating wastewater with some biodegradable organic matter content, due to a in parallel heterotrophic growth in the system (Ruscalleda et al., 2010) which made necessary to ensure constant conditions in the influent.

When a two stage PN-Anammox process is used, each stage becomes more flexible and stable since optimal conditions can be separately applied for both PN and anammox processes. This configuration has a special value when treating streams with organic matter content and complex matrix presenting some substances affecting the maximum specific anammox activity. Moreover, a special design can be proposed for anammox process to improve the biomass retention. In this sense, several reactor designs and configurations have been developed to perform anammox process (Lackner et al., 2014): Sequencing Batch Reactors (SBR), fixed bed, fluidized bed, UASB Reactor, Upflow Reactors, Airlift reactors, Membrane Bioreactors (MBR), Continuous Stirred Tank Reactors (CSTR), among others. Accepted widely used configuration for the anammox process is the SBR, due to its good biomass retention capacity, its homogeneous mixing conditions, its stability and reliability for long periods. There are different parameters to control the granulation of anammox microorganisms: salinity (Dapena-Mora et al., 2004a), shear rate (Arrojo et al., 2008, 2006) and the settling time (López et al., 2008). Another configuration which ensures the maximum biomass retention is the MBR (van der Star et al., 2008), alone or combined with an SBR (Wyffels et al., 2004). However, the risk for membrane fouling and too high operational costs (related to backwashing and chemicals to clean membranes) made it not well-competitive.

Since all these parameters are influenced by the flow distribution, it is necessary the use of CFD tools in order to gain knowledge about the improvement in the design of anammox reactors. As far as we know, any study used this computational tool in the design of anammox reactors.

OBJECTIVES

Chapter 2. **General objectives**

2.1 Problem definition

The design and optimization of novel technologies in biological wastewater treatment has been historically managed with biokinetic models that allowed testing different configurations and operating conditions. In the field of biological wastewater engineering, the most widely used models are the Activated Sludge Models (ASM). These models describe the chemical/biological processes occurring in the reactor and allow evaluating the system response to parameters such as influent conditions (flow and reagents concentration), volume or temperature, among others. However, these conventional models are assuming ideal mixing conditions which is not always representative of real scenario, particularly for systems with complex internal configurations. For this reason, such cases require including hydrodynamic information into the model definition. In this sense, the use of Computational Fluid Dynamics (CFD) is a powerful tool to model the hydrodynamic behavior in complex designs. Historically, the use of these numerical tools has been linked to dangerous and economically expensive processes to be carried experimentally. Due the continuous increase in computer capacities, the use of CFDs has been extended to a wide range of industries. CFD simulations in wastewater engineering became a challenge for the design and optimization of wastewater equipment (settlers, reactors, among others). Moreover, the combination of CFD and ASM models facilitated the design and optimization of novel reactors configurations.

2.1 Objectives

The main objective of this thesis is to evaluate the capability of integrating CFDs and biological models (ASM) for the design and optimization of novel bioreactors for nutrient removal from wastewater. Two novel reactor designs are assessed with this combined tool: microbial fuel cells (MFC) and

anammox reactors. In order to achieve this overall goal, a set of sub-objectives are proposed:

- To define the methodology to use the combination of CFD and biological models (ASM) to simulate a biological reactor.
- To integrate the biological reactions kinetics in the hydrodynamic model
- To simulate the internal flux distribution inside each of the novel reactor configurations assessed.
- To map the internal species distribution produced by the flow and biological reactions defined by the integrated model.
- To obtain the internal distribution of reactor removal performance in order to optimize it.
- To test the suitability of several electrodes design for a specific MFC reactor configuration and its influence on the reactor performance.
- To evaluate the performance of a novel anammox reactor configuration with internal plates distribution and mixing by recirculation.
- Based on the CFD results, propose improvements on reactors designs.

The outline of this Thesis to attain the mentioned objectives is as following:

- Chapter 4: Integration of CFD and biological reactions and the numerical methods to resolve it;
- Chapter 5: Application of these methods in the simulation of the anodic chamber of a MFC; and
- Chapter 6: Simulation of a novel anammox reactor configuration.

METHODOLOGY

Chapter 3. **Methodology**

3.1 CFD tools

The mass, momentum and energy balances involved the resolution of a large number of differential equations which involves the use of computer assisted numerical methods. This section described the software and utilities used for the simulation of novel wastewater reactors.

3.1.1 Ansys Fluent platform

Ansys is launching almost yearly a new version of its Fluent's software, and the last version was the 17 (Figure 3.1). The renewed versions includes further models and sub-models, numerical methods among others simulations properties. This solver includes a wide range of models and sub-models, all of them prepared to resolve a wide range of simulations cases. Additionally the solver includes a wide range of numerical methods (solvers and solution controls) to resolve each simulation case. The next picture shows the typical image (it could change depending on the software's version) when starting Ansys Fluent software. Details of the models and sub-models, boundary conditions and solution methods used in this thesis will be found in the Model development chapter. Despite the existence of specific software to do it, the Ansys Fluent software is also designed for the results processing (Figure 3.1 – Results). A wide range of tools are included to process the contours profiles, velocity vectors or streamlines included presented within this thesis.

3.1.1.1 User defined funcions

It is often necessary to create user-defined models, new materials properties, boundary conditions or variables, such in the simulation cases presented in this thesis. The integration of biological reactions was necessary

to be defined as a user defined source term, and also to define special boundary conditions, such recirculation streams. Ansys Fluent includes the option of developing user defined functions (UDF) and developed an own code (developed in C++ programming code) which the user should know properly in order to adapt its own functions with the code and include them in the simulations. The Appendix section (Appendix section 9.7.7) presented the code developed for the simulations developed in this study.

3.1.1.2 Biological models

The simulations of this thesis included modelling of species and biological reactions. The biological models used in this Thesis were based on the models developed by Henze and colleagues (2000). Further details about the application of these models will be found in the Chapter 4 of this thesis.

3.1.2 Ansys Workbench: pre and post processing utilities

Since the simulation process involves geometry treatment, meshing development, simulation and post processing, Ansys offer a set of utilities addressed to carry on these tasks. All these tools are included in the Workbench software, which is software created to start a Project, which included all the above mentioned steps (Figure 3.2).

The geometry of the simulation cases was developed by the use of Solidworks 3D software, which has a connection plug in to the Geometry step (Figure 3-2). Since the geometry is imported from the 3D software, it is necessary in the Geometry utility to define the fill the geometry with the fluid of interest in order to define the simulation domain. After it, the next step is to create a discretization (mesh) of the geometry to be able to resolve the case numerically. The Workbench software also includes different softwares to do it, and the one used in this thesis was the Meshing tool

(Figure 3.3) After it, the mesh is directly read in Ansys Fluent to resolve the simulation case.

Regarding the post-processing, it could be done or by Ansys Fluent or with another Workbench tool called CFD-Post (Figure 3.4). This is another powerful tool for the treatment of simulation results. This option was the selected for the results development in this thesis, except for the treatment of user defined variables and functions which are necessary to be processed in Ansys Fluent Results tool.

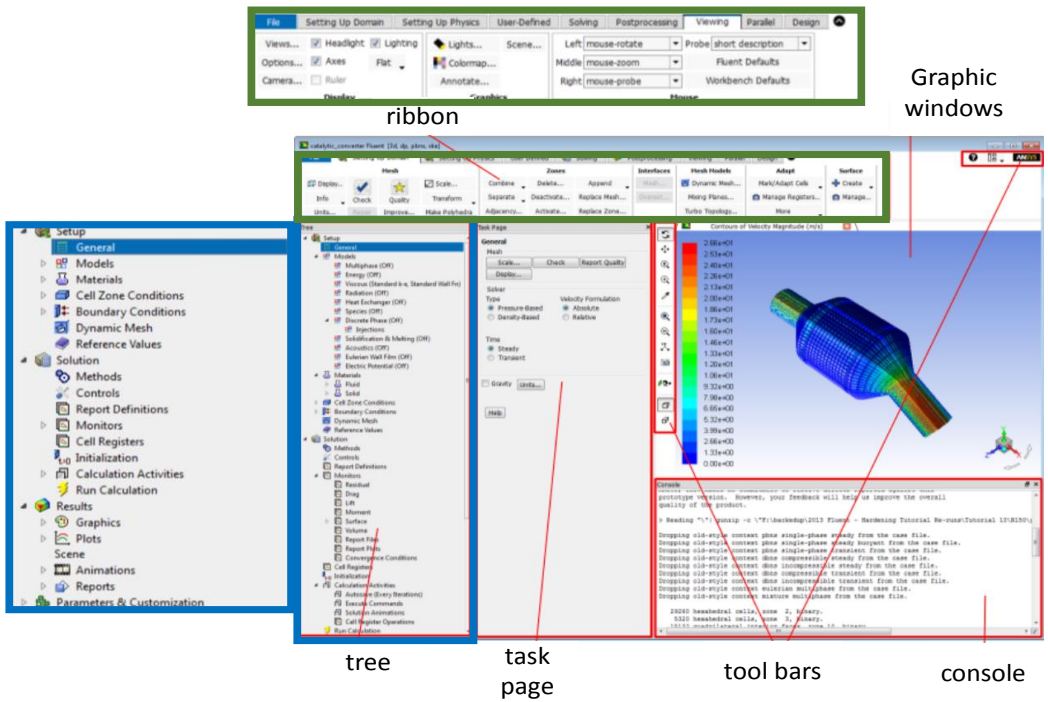

Figure 3.1**. Graphical User Interface of Ansys Fluent simulator**.

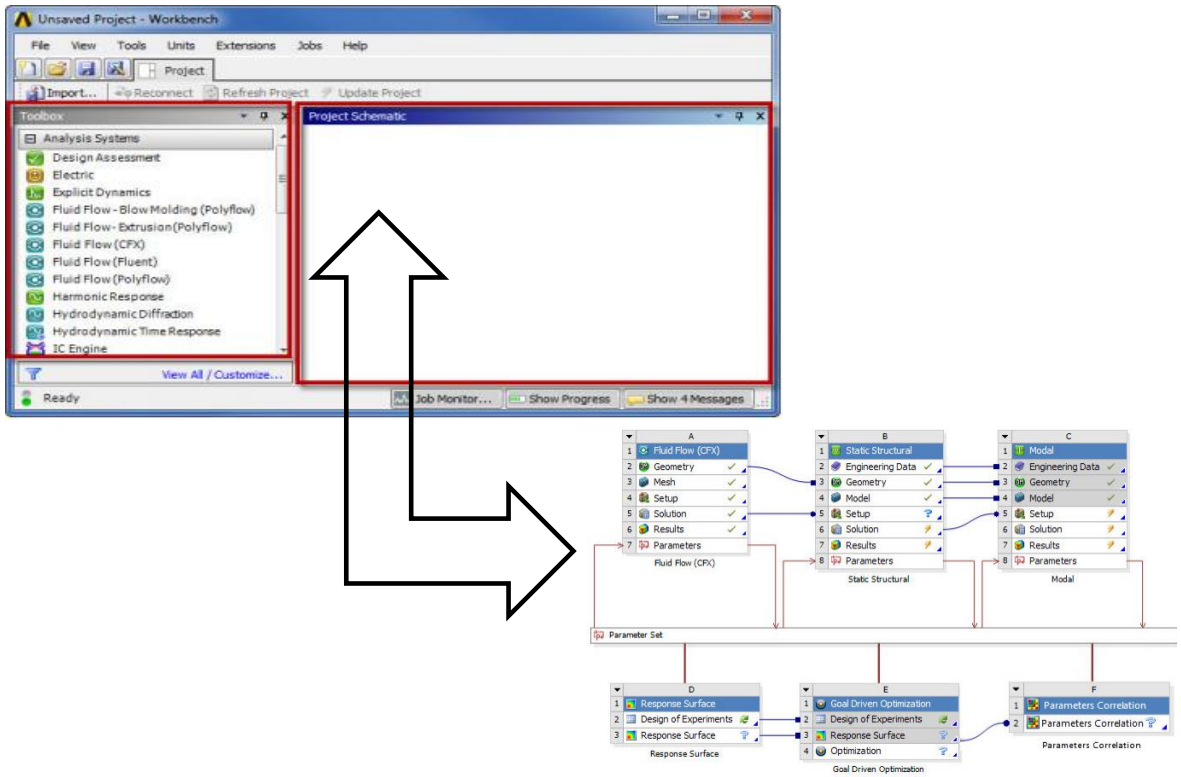

Figure 3.2 **Workbench platform graphical interface**

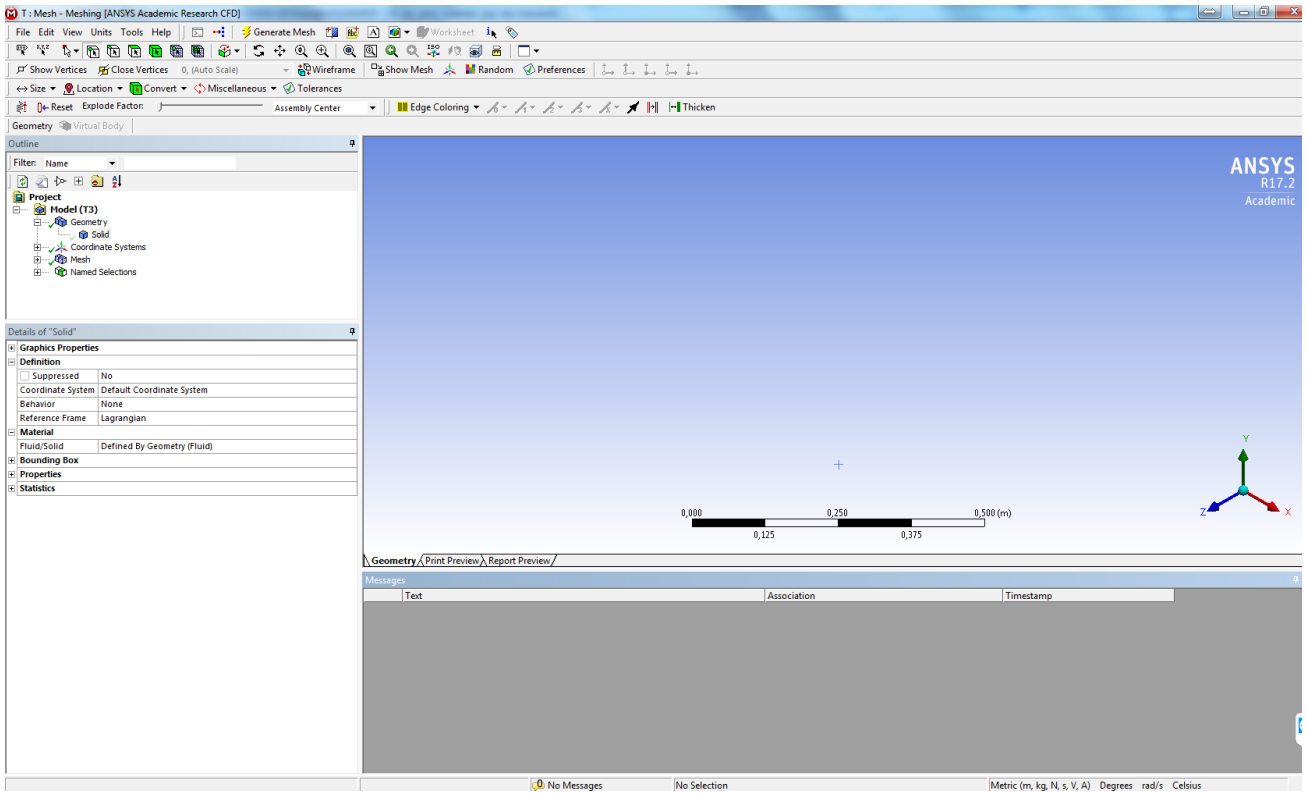

Figure 3.3. **Meshing software graphical interface**

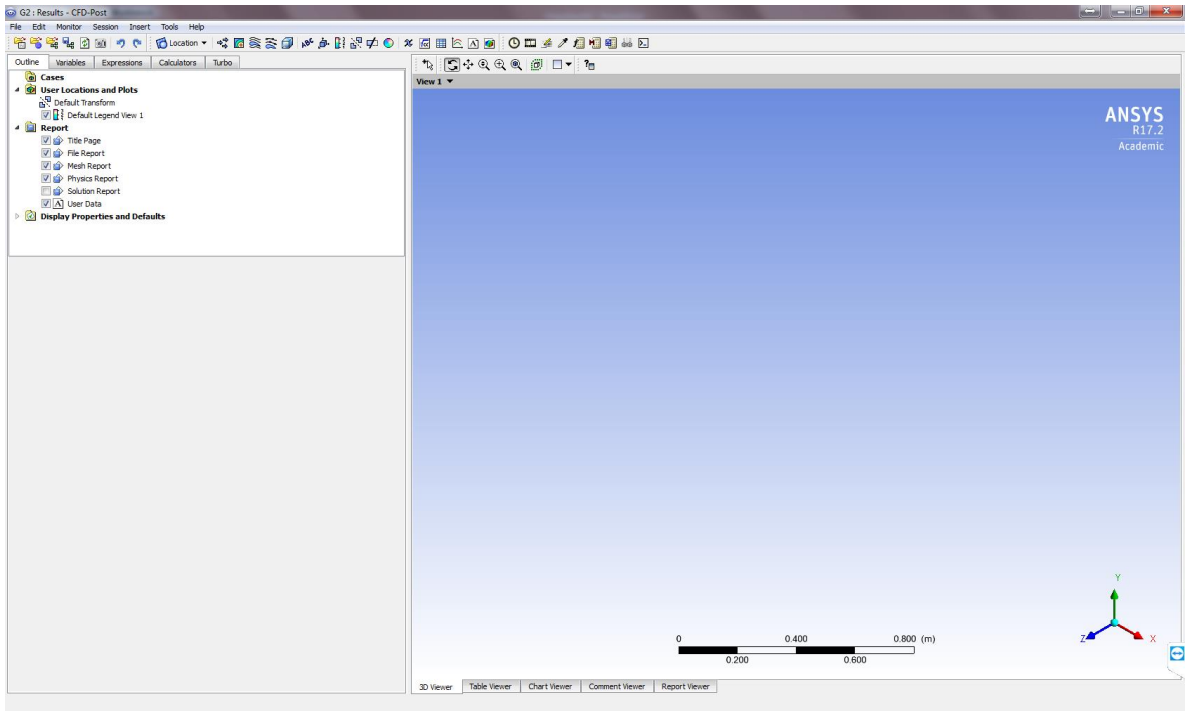

Figure 3.4. **CFD-post software graphical interface**

3.2 Reactors design

3.2.1 Microbial Fuel Cells

The MFC configuration was originally designed for organic matter and nitrate removal from wastewaters (Puig et al., 2012). Granular graphite and graphite rods were historically used in this research as an electrode material in the anodic chamber. However, novel electrode material alternatives wanted to be investigated to up-grade the anodic chamber performance, focussing on their characteristics and properties, such as electrical conductivity, geometry, bed porosity and price.

Four different anode materials (Figure 3.5) were compared in this study: a graphite rod, a graphite rod plus granular graphite, a graphite rod plus a stainless steel mesh, and a graphite bar, with each one in a separate reactor. All the reactors operated at a temperature of 25 °C and a pressure of 1 atm with the same configuration of the anodic chamber, which included an inflow and outflow of 1.5 $L \cdot d^{-1}$ and a recirculation stream (from/to inflow/outflow) of 150 $L \cdot d^{-1}$. The main design characteristics of each simulated case are defined in Table 3.1.

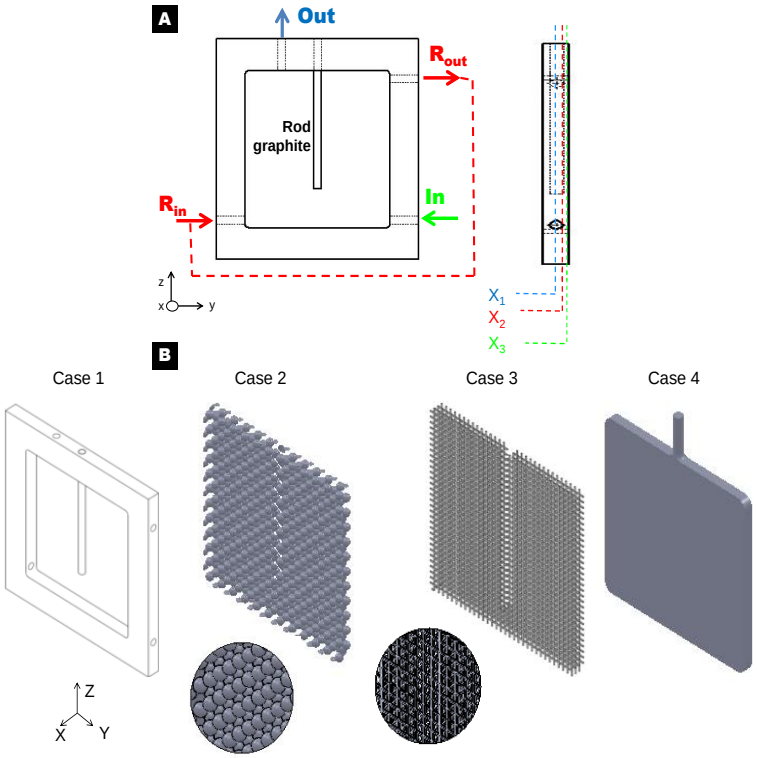

Figure 3.5. Reactor flowchart and selected planes (x_1, x_2 and x_3) for the plotted results (A) and various electrode materials used in the study (B) Various electrode materials: case 1: graphite rod; case 2: granular graphite plus graphite rod; case 3: stainless steel mesh and graphite rod and case 4: graphite.

Table 3.1 Main characteristics of the electrode materials analysed for the anodic MFC.

Case	Electrode Material	Characteristic size	Distribution
1	graphite rod (control)	ϕ = 10 mm Height = 17,5 cm	Centre
2	graphite rod plus granular graphite	$\phi_{granule\ particle}$= 9 mm	Two layers of spheres separated 3 mm each other Separation between spheres 11 mm (centre to centre)
3	graphite rod plus stainless steel mesh	ϕ_{mesh}=1 mm	Three layers of mesh, separated 4 mm each other Mesh light path: 5 mm x 5 mm
4	graphite plate	180 x 180 x 10 mm	

3.2.2 The anammox process

The anammox reactor configuration (Figure 3.6) proposed was a column reactor with a height of 2.6 m, an internal diameter of 0.5 m (resulting in a total volume of 434 L) and a complex internal geometry. Several internal plates were horizontally placed along the reactor height in a pattern such that each level of plates (four plates per level and oriented at ±45°) had a perpendicular orientation with respect to the lower and upper levels. The aim of this geometry was to produce proper local mixing conditions inside the reactor and enhance biomass retention.

The reactor was fed from the bottom with a 1:100 mixture of influent wastewater (Q_{in}^{0}) and a recirculation flow (Q_R). The effluent stream (Q_{out}) was separated from the recirculation stream (Figure 3.6). The temperature of

the reactor was kept constant by an electrical resistance that was implemented in the recirculation flow, and the reactor was isolated to avoid heat loss. The reactor was sealed and pressurized (operating pressure of 1 bar) to maintain total anoxic conditions. The nitrogen gas that was generated by the anammox microorganism's activity was conducted to a gas container (used for plant service).

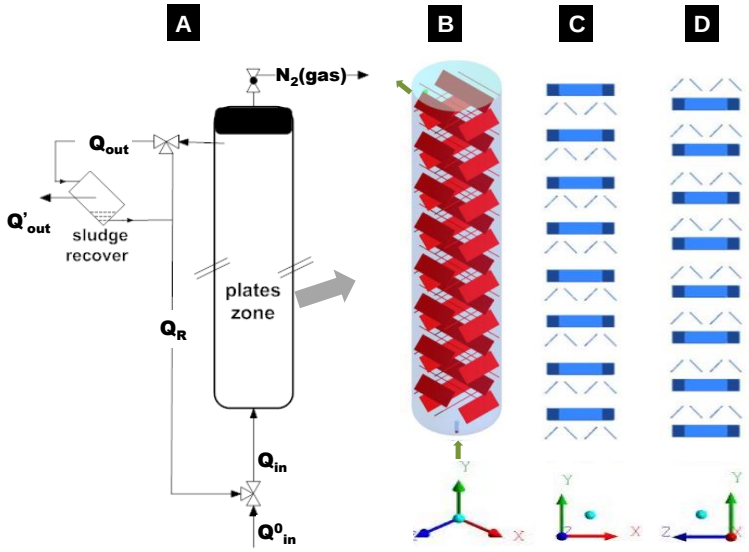

Figure 3.6 Scheme of the anammox reactor used in this study: A) flow diagram, B) isometric view of the internal plate distribution, C) view of plane XY and D) view at plane YZ.


RESULTS

Chapter 4. **Model development**

4.1 Overview

Global challenges in wastewater engineering have been addressed to improve process performance with minimum cost (Hreiz et al., 2015). Current investigations are focused on the highest operational cost processes for wastewater treatment: solids handling and aeration processing (Karpinska and Bridgeman, 2015; Samstag et al., 2016). Moreover, research has concentrated on finding alternatives to conventional processes in order to reduce costs and the economic impact (use of chemicals and energy) of wastewater treatment processes.

Activated sludge models (ASM) (Henze, M. et al., 2000) are the most widely utilized models in biological wastewater treatment. These models describe the kinetics and stoichiometry of biological reactions and physio-chemical processes (hydrolysis, acid-base equilibrium, etc.), which include an estimation of the global mass transfer (Ganigué et al., 2010). This tool is clearly meant to be used for process control, to anticipate phenomena and to ensure proper system efficiencies.

However, the abovementioned modelling tools have limitations that rely on a wide range of formulated hypothesis and assumptions, which were specifically addressed to eliminate the influence of physical-hydrodynamic processes. These assumptions include completely mixed conditions, and an overall estimation of mass transference processes in aeration or other gas/liquid applications. These models do not consider physical parameters, such as system geometry and flow distribution, which have an impact to the overall process efficiency. Additionally, the ASM are not fully applicable to multiphase simulations because of assumptions in the solids distribution or gas/liquid interactions. In this sense, the use of computational fluid dynamics (CFD) modelling tools coupled to biological models may solve these limitations and further optimize the system.

CFD is widely used in many industrial processes and can be applied to optimize the design and configuration of individual units (Gimbun et al., 2009). Related to wastewater, Karpinska and co-workers (2015) stated that CFD is a powerful and necessary tool for the optimization of activated sludge systems. With a prominent increase in the use of CFD in this field, two studies (Laurent et al., 2014; Wicklein et al., 2016) were conducted to define protocols for good modelling practices and ensure the proper use of this technique for wastewater modelling.

However, the use of CFD, as a computer -assisted modelling tool has its own limitations. A large number of variables require a large computational effort in time, computational power and related price. For this reason the user should clearly define the target using CFD. The models must be constructed so that useful information can be obtained with appropriate simplifications to avoid larger and difficult simulations. The correct application of such models could be a powerful tool to improve and test novel designs and system configurations.

This chapter presents the methodology for combining CFD with biological process modelling (ASM) for the assessment of two cutting edge wastewater treatment technologies: Microbial Fuel Cells (MFC) and the anammox process.

The art of CFD modelling requires a systematic routine to perform the simulations. The process modelling phases are summarized in Figure 4.1.

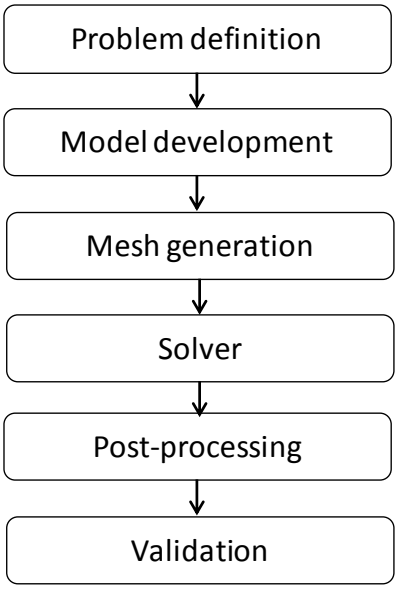

Figure 4.1. **Scheme of the CFD modelling process.**

These steps are followed sequentially and are strictly interrelated. Any modification in a previous step requires a review of the following steps. The steps applied to each of the technologies studies are described in the following sections.

4.2 CFD modelling process

4.2.1 Problem definition: reactors design

In the design and scale-up of biological reactors with complex internal geometries, the proper flow conditions and substrate distribution must be ensured for good performance. There are a wide range of parameters that can affect or compromise this goal, including mixing typology (agitation, recirculation), the stream distribution in the reactor, temperature and multiphase interactions. CFD was applied to evaluate the new design of two different biological technologies, in terms of hydrodynamic performance and its influence on biological processes.

The two simulated reactors – Microbial Fuel Cells and anammox reactors – were described in the Methodology chapter (Chapter 3). This chapter is describing the balances and numerical methods developed in this Thesis to resolve the simulation of both biological reactors.

4.2.2 Model development

CFD is a powerful numerical tool that provides the fluid flow distribution inside a predefined system by simultaneously computing mass, momentum and energy conservation equations. The general balance of a property (mass, momentum or energy) in a fluid element can be defined by Equation 4.1.

$$\begin{Bmatrix} acumulation \\ rate \end{Bmatrix} + \begin{Bmatrix} transport\ by \\ convection \end{Bmatrix} = \begin{Bmatrix} transport\ by \\ diffusion \end{Bmatrix} + \begin{Bmatrix} source \\ terms \end{Bmatrix} \quad (4.1)$$

This balance is the basic principle of conservation and must be respected either for a particular point of fluid or the total fluid domain. The numerical resolution of these mathematical equations for the overall fluid domain requires discretising the domain into smaller parts (meshing) and defining the boundary conditions.

4.2.2.1 Mass conservation equation

When applied to a small portion of the fluid domain, the mass balance should be consistent for the mass entering and leaving that region of fluid (mass conservation is detailed in the Appendix, Section 9.1). The mass conservation equation for a three-dimensional unsteady state is presented in Equation 4.2.

$$\frac{\partial \rho}{\partial t} + div(\rho \mathbf{u}) = 0 \tag{4.2}$$

where ρ refers to the fluid density and **u** refers to its velocity (vector). The term **div** refers to the divergence of a vector, which is defined in Equation 4.3 (Cartesian form).

$$div(\mathbf{u}) = \nabla \cdot (\boldsymbol{u}) = \frac{\partial u_x}{\partial x} + \frac{\partial u_y}{\partial y} + \frac{\partial u_z}{\partial z} = \sum_{i=1}^{3} \frac{\partial u_i}{\partial x_i} \tag{4.3}$$

In the two simulated cases,

In the two studied cases steady state conditions were simulated and the main fluid of the system as an incompressible fluid (water). Therefore, the assumptions made in Equation 4.4 can also be made with Equation 4.2.

$$div\ \boldsymbol{u} = 0;\ \rho = ct, \tag{4.4}$$

These assumptions facilitated the resolution of the overall fluid domain since a simplified equation was obtained for each cell in the computational domain (mesh).

4.2.2.2 Momentum conservation balance

The momentum conservation equation was based on Newton's second law, which postulates that the momentum rate of a fluid particle is equal to the sum of forces on this fluid particle. Further information regarding the equations developed for the momentum balance is presented in the Appendix (Section 9.1.2). In both cases studied (MFC and anammox simulations), the liquid (wastewater) was defined with a Newtonian rheological behaviour. Assuming this, the mathematical description for the liquid phase is presented in Equation 4.5 to 4.7 for each spatial direction.

$$\rho\frac{\partial u}{\partial x}+\rho div(u\boldsymbol{u})=-\frac{\partial P}{\partial x}+div\big(\mu\ grad(\boldsymbol{u})\big)+\ S_{Mx} \tag{4.5}$$

$$\rho\frac{\partial v}{\partial y}+\rho div(v\boldsymbol{u})=-\frac{\partial P}{\partial y}+div\big(\mu\ grad(\boldsymbol{u})\big)+\ S_{My} \tag{4.6}$$

$$\rho\frac{\partial w}{\partial z}+\rho div(w\boldsymbol{u})=-\frac{\partial P}{\partial z}+div\big(\mu\ grad(\boldsymbol{u})\big)+\ S_{Mz} \tag{4.7}$$

where the parameters u, v and w are the spatial components of the abovementioned velocity vector ***u*** (Equation 4.2) and *P* is the pressure. The S_{Mi} parameters correspond to the source momentum term, which can include a wide range of external forces, such as buoyancy and lift or drag forces, depending on the simulated case. For the simulated cases, the gravity momentum source was defined as ρg *(*buoyancy force). Equations 4.5 to 4.7 also included a mathematical operator (*grad*), which means the gradient of a vector and is defined in the Equation 4.8.

$$grad(\mathbf{u}) = \nabla(\boldsymbol{u}) = \left(\frac{\partial u_x}{\partial x}, \frac{\partial u_y}{\partial y}, \frac{\partial u_z}{\partial z}\right) \quad (4.8)$$

4.2.2.3 Energy equation

The energy balance of the system was also developed for both simulated cases. The full development of the energy balance can be found in the Appendix chapter (Section 9.1.3). The energy balance was obtained by taking into account the stress forces and the energy flux due to heat conduction (Versteeg and Malalasekera, 1995). The final equation of the energy balance applied for an incompressible fluid is presented in Equation 4.9.

$$\frac{\partial(\rho E_I)}{\partial t} + div(\rho E_I \boldsymbol{u}) = -p \cdot div\ \mathbf{u} + \mathrm{div}(kgrad\ T) + \Phi + S_{E_I} \quad (4.9)$$

where T is the temperature, E_I represents the internal energy, Φ is a parameter that includes viscous stress terms in the energy equation (See Appendix 9.1.3), and S_{EI} refers to any source of internal energy. The internal energy is denominated by thermal energy and is directly proportional to the fluid temperature by means of the heat capacity.

4.2.2.4 Additional equations integrated in the computational fluid dynamics model

4.2.2.4.1 Modelling Turbulence

When the fluid in a system exhibits turbulent behaviour (Reynolds number up to 2300), the effects of the turbulent eddies in the hydrodynamics equations (in terms of viscous stress and energy) may be considered. The CFD platforms propose a wide range of turbulent models, and the selection depends on the final goal and system conditions to be modelled. Various turbulence models included in the Ansys Fluent® platform are listed and briefly described in the Appendix (Section 9.1.4).

In the present work, a turbulence model was applied in the case study of the anammox reactor since turbulent flow was expected due to the internal geometry and operation conditions in this reactor. The turbulence model selected in this case was the k-ε model, more precisely the *RNG k-ε model* (Ansys, 2009). The selection and use of this model offered two main advantages: i) it included additional terms for the ε-equation (see Appendix 9.1.4) that improved the model accuracy in rapid strained flows and ii) it enhanced the model accuracy in swirling flows. The main disadvantage of the RNG k-ε model was the lack of calibrated values for the equations used in the model (Andersson, 2012) compared with the standard k-ε model. Otherwise, the model has predefined (and properly calibrated) values when applied in systems with water or water/air mixtures.

4.2.2.4.2 Species mass balance

The study of bioprocesses implies the consideration of different species, which include substrates, products and biomass. The mass balance for species *i* can be formulated by Equation 4.10.

$$\frac{\partial}{\partial t}(\rho Y_i) + div(\rho \boldsymbol{u} Y_i) = -\mathrm{div}(J_i) + R_i + S_i \qquad (4.10)$$

where Y_i represents the mass fraction of species *i* and J_i is the diffusion flow rate vector for species *i*. R_i represents a source term due to a elemental chemical reaction (with elemental kinetic laws) and S_i is the term used for reactions with no elemental kinetic laws (such as biological reactions in ASM). The lecturer should be aware that R and S terms from Equation 4.10 are conceptually equal, but usually CFD softwares seperate it to remark that R term is a elemental kinetic law (preconfigured reactions) and S is performed to introduce biological reactions (such in this thesis) or other mass source terms.

Special attention must be paid to the diffusion term, since it varies depending on the nature of the flow (laminar or turbulent). Hence, two alternatives can be selected. For laminar flow, the diffusion term is defined by Equation 4.11, which is based on Fick's law (assuming a dilute approximation and constant temperature).

$$\vec{J_i} = -\rho \cdot D_{i,m} \cdot \mathrm{grad}\,(Y_i) \qquad (4.11)$$

where $D_{i,m}$ is the mass diffusion coefficient ($m^2 \cdot s^{-1}$).

In case of a turbulent flow, the diffusion term is expressed as Equation 4.12 (assuming constant temperature).

$$\vec{J_i} = -\left(\rho D_{i,m} + \frac{\mu_t}{Sc_t}\right)\text{grad}\,(Y_i) \quad (4.12)$$

where μ_t is the turbulent viscosity ($kg \cdot m^{-1} \cdot s^{-1}$) and Sc_t the turbulent Schmidt Number. Note that in systems with variable temperature between the different points of the systems, Equations 4.11 and 4.12 incorporate the thermos-diffusion coefficient, which was not the case of the present study.

Moreover, the biological mode was introduced within the source term (S_i) of Equation 4.10. The Ansys Fluent® platform proposes defined functions to incorporate such a source term. The most common form of biological models is the well-known ASM, which is described in the next section.

4.2.2.4.3 Biological model

ASM1 (Henze, M. et al., 2000) was the first approach that was developed to model the biological removal of organic matter and nitrogen in wastewater treatment systems. The developed model considered two microbial populations (autotrophs and heterotrophs) and described the growth and decay processes of these microorganisms and the ammonification and hydrolysis processes. The original model was further improved with models ASM2 and ASM3, which incorporate more processes and variables that are mainly related to biological nutrient removal. In both simulation cases in this work, the proposed biological model was based on ASM1.

4.2.2.4.3.1 Microbial Fuel Cells

Regarding the MFC system, the biological model implemented in the CFD simulations was based on the model developed by Pinto et al., 2010 included two microbial populations – anodophilic and methanogenic – which were computed using the same substrate (acetate). Since the simulations were

performed at steady state, this model assumed a constant microorganism concentration, with biomass concentrations fixed at 500 and 250 mg $COD_x \cdot L^{-1}$ (determined experimentally) for the anodophilic and methanogenic bacteria, respectively. The rates of substrate (acetate) consumption introduced in Ansys Fluent® through user-defined functions are presented in Equations 4.13 to 4.15.

$$\frac{dS}{dt} = -q_a X_a - q_m X_m \tag{4.13}$$

$$q_a = q_a^{max} \cdot \frac{S}{K_{Sa} + S} \cdot \frac{M_{ox}}{M_{ox} + K_M} \tag{4.14}$$

$$q_m = q_m^{max} \cdot \frac{S}{K_{Sm} + S} \tag{4.15}$$

where S is the substrate concentration (mg $COD \cdot L^{-1}$), X_a and X_m are the anodophilic and methanogenic microorganism concentrations (mg $COD_x \cdot L^{-1}$), respectively, q_a and q_m are the substrate consumption rates for the anodophilic and methanogenic microorganisms (mg $S \cdot mg^{-1}$ X d^{-1}), respectively, and M_{ox} is the oxidized fraction of mediator per anodophilic microorganism (mg $M \cdot mg^{-1}$ X). The q_a^{max} (8.48 mg-$S \cdot mg^{-1}$ $x \cdot d^{-1}$) and q_m^{max} (8.20 mg-$S \cdot mg^{-1}$ $x \cdot d^{-1}$) are the màximum substrate consumption rates. Finally, K_{sa} (20 mg $S \cdot L^{-1}$) and K_{sm} (80 mg $S \cdot L^{-1}$) are the half saturation (Monod kinetic) constants for the anodophilic and methanogenic microorganisms, respectively. The S, X and M terms are refered to COD units. The values of the kinetic parameters were taken from the orginial model (Pinto et al., 2010).

4.2.2.4.3.2 Anammox process

Regarding the anammox process, an extension of ASM1 was developed that incorporates anammox bacteria growth and decay. Several studies on anammox process modelling can be found in the literature (Dapena-Mora et al., 2004; Ni et al., 2009; among others), , which reported different values for the stoichiometric coefficients and kinetic parameters of anammox growth and decay processes. In this Thesis, the stoichiometry developed by Tákacks ((2007) was chosen because a detailed stoichiometric balance was done for each component, which permitted a perfectly defined stoichiometry. Since anammox bacteria are slow growing microorganisms, the concentration of anammox microorganisms was assumed to be constant during the simulations. Thus, the processes introduced in the hydrodynamics equation were the substrate (ammonium and nitrite) consumption rates and nitrogen and nitrate generation rates. The anammox process stoichiometry and kinetic parameters that were considered in this study are presented in Tables 4.1 and 4.2, respectively.

Table 4.1 **Simplified kinetic model coupled to the CFD model.**

Process	SN-NH4+	SN-NO2-	SN-NO3-	SN-N2	RATE
Growth	$-\left(\frac{1}{Y_{AMX}}+i_{NBM}\right)$	$-\left(\frac{1}{Y_{AMX}}+\frac{5}{3}\cdot 1.52+\frac{4}{3}\right)$	1.52	$\left(\frac{2}{Y_{AMX}}+\frac{2}{3}\cdot 1.52+\frac{4}{3}\cdot\frac{14}{32}\right)$	ρ_{growth}^{AMX}

$$\rho_{grwoth}^{AMX}=\mu_{AMX}^{growth}\cdot\frac{S_{NH4}}{S_{NH4}+K_{NH4}^{AMX}}\cdot\frac{S_{NO2}}{S_{NO2}+K_{NO2}^{AMX}}\cdot X_{AMX}$$

Table 4.2 **Kinetic and stoichiometric parameters used in this study.**

Parameter	Value	Unit	Source	Definition
μ_{AMX}^{max}	0.072	d^{-1}	Ni et al., 2009	Anammox maximum growth rate
K_{AMX}^{NO2-}	0.55	g N·m^{-3}	Ni et al., 2009	Affinity constant for NH4+ of X_{AMX}
K_{AMX}^{NH4}	0.73	g N·m^{-3}	Ni et al., 2009	Affinity constant of NO2- of X_{AMX}
Y_{AMX}	0.164	g COD·g^{-1} N	Ni et al., 2009	Yield coefficient for X_{AMX} growth
i_{NBM}	0.07	g COD·g^{-1} N^{-1}	Gujer et al., 1999	Nitrogen content of X_{AMX}

4.2.2.4.4 Multiphase models

Both cases presented in this thesis generated gas phase as a product. However, in case of MFC reactor, the generated gas (methane and carbon dioxide) has been considered negligible and has no effect on the hydrodynamics of the system. The modelling of an anammox reactor by CFD was a special and challenging case due to the generation of nitrogen gas by the anammox biomass. This case involved the use of multiphase simulations, which added complexity to the CFD study. To determine the multiphase CFD system resolution, an optimal methodology was selected that depended on the number and type of phases to be considered (liquid, gas and solid) and the desired level of accuracy. The selection of the most appropriate multiphase model represented a significant part of the modelling study itself. Further information regarding the available multiphase models can be found in the Appendix (Section 9.1.5) section.

From various alternatives, the model selected in this study for the anammox reactor simulations was the Euler-Euler approach since the gas phase had a large number of bubbles and it was necessary to account for the overall bubble momentum (Lopes and Quinta-Ferreira, 2009), (instead of measuring the movement of each bubble (Lagrangian approach)). The Euler-Euler model is commonly used in multiphase bubble reactors (Garcia-Ochoa and Gomez, 2009) , airlift (Huang et al., 2010), and other types of aerated reactors. Other approaches that are similar to the Lagrangian approach accounted for the exact interphase of each bubble.

The main parameter to be defined in a multiphase CFD simulation is the volume fraction for each phase, which is a measure of the volume occupied by each of the respective phases over the total fluid volume. The volume fraction of a phase was calculated using Equation 4.16.

$$\alpha = \frac{\sum_{i=1}^{N} V_i}{V} \tag{4.16}$$

In the present case, the gas phase was a consequence of nitrogen gas, which was generated as a product of the anammox reaction. In studies found in the literature that combined CFD with biological reactions for the simulation of wastewater treatment processes, multiphase models were used to simulate aeration process (Lei and Ni, 2014) from gas (air supplied) to liquid (water) phases (optimization studies of the aeration system in bioreactors). In this study, the mass transfer of nitrogen was in the opposite direction from liquid to gas. Taking into account the configuration of the anammox reactor simulated in this study with a large recirculation flow with respect to the influent flow, the liquid phase that was considered saturated with dissolved nitrogen gas (generated by the anammox metabolism). Hence, it was assumed that all the nitrogen gas produced by the anammox reaction was instantaneously transferred to the gas phase.

4.2.3 Mesh generation

CFD software numerically solves a single equation or a set of partial differential equations, which requires time and space discretization (Mavriplis, 1996). To accomplish the discretization, the simulation fluid domain is discretized into a set of grid cells, which is called a meshing process. The optimal meshing for a specific CFD study is the best compromise among the accuracy of the obtained results, desired precision and required computational effort.

Although there are several meshing techniques, the results (meshes) can be classified in two categories: structured (nodes regularly located) and unstructured meshes (nodes not regularly located) (Andersson, 2012). Tetrahedrons or hexahedrons are commonly utilized as meshing elements in 3D simulations. As a general rule, hexahedral meshes provide results, particularly when the flow and grid lines are perfectly aligned. The density of the mesh must be adapted along the simulation domain, which depends on the required level of detail. Hence, the density of cells is increased in critical zones, such as the fluid adjacent to the reactor walls, to properly capture the boundary layer. Several parameters are used to evaluate the quality of the mesh: i) the skewness, which is how close or far a face or a cell is to the ideal condition (equilateral or equiangular), with values ranging from 0 (best situation) to 1 (worst situation); ii) the smoothness, which is the gradual change in mesh size; and iii) the aspect ratio, which is the ratio between the largest and shortest edge of the mesh (the ideal value of aspect ratio is 1, the equilateral condition).

Considering the abovementioned indications, the meshing methodology applied in each simulation is explained below.

4.2.3.1 Microbial Fuel Cells

As mentioned above, the CFD study of the MFC reactor was used to assess four different electrode materials (anode chamber material) and determine which one favours the flow and substrate distribution. Thus, four configurations were tested depending of the electrode material (a graphite rod, a graphite rod plus granular graphite, a graphite rod plus a stainless steel mesh and a graphite bar). Since these electrode materials in the anode chamber provides different hydraulic properties, the mesh for the simulation domain must be specifically defined for each case.

4.2.3.1.1 Meshing case 1 – MFC reactor plus rod graphite

The graphite rod case was the simplest to mesh (Figure 3.5B, case 1). A mix of tetrahedral and triangular cells was applied to grid the fluid and wall boundary conditions. Figure 4.2 presents a set of cross-section images of the mesh used in this study (dimensions of 200 x 200 x 20 mm).

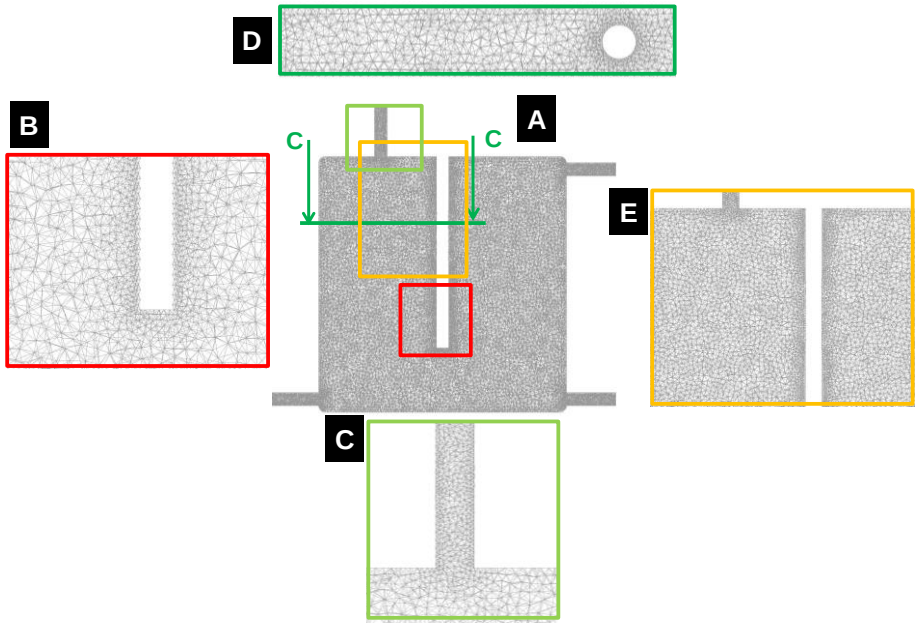

Figure 4.2 Mesh development for the graphite rod case. A) full view of the mesh, B) enlarged view of the graphite rod surface, C) enlarged view of the outflow stream, D) cross-section of the graphite rod and E) enlarged view of the graphite rod close to the wall surface.

Meshing inflation algorithms were applied to the inlet/outflow streams to refine (increase the density of cells) the mesh in these critical zones. Additionally, the mesh was refined close to the graphite rod position to evaluate the wall effect of this element on the hydrodynamic.

4.2.3.1.2 Meshing case 2 – MFC reactor with graphite rod plus granular graphite electrode

This configuration had a graphite rod and granular graphite spheres as the electrode material (Figure 3.5B, case 2). In the simulations, the granular spheres were regularly distributed within the fluid domain and were larger (9 mm) than the real spheres to avoid a high computational effort. The resulting mesh is shown in Figure 4.3.

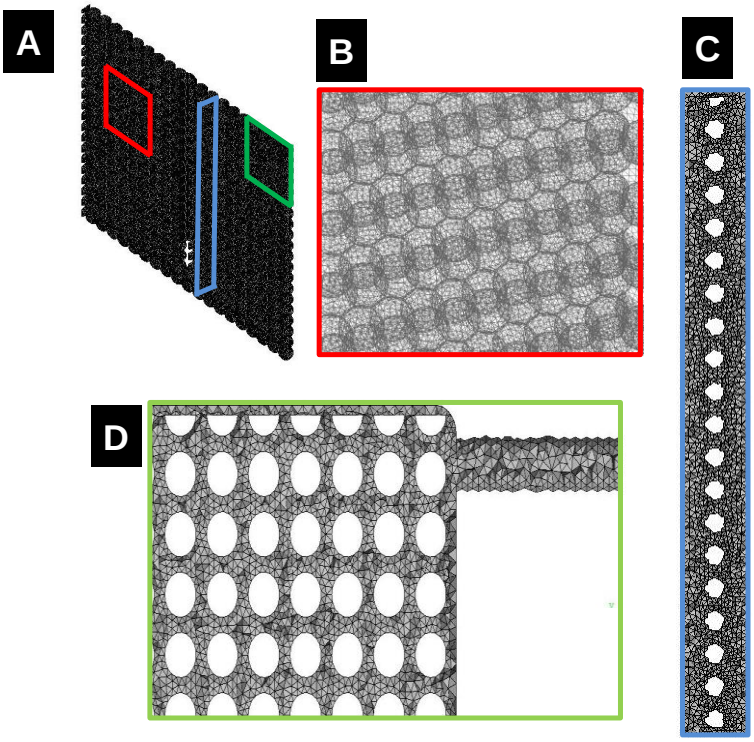

Figure 4.3 Mesh development for the case of the graphite rod plus granular graphite: A) full view, B) detail of the red section of the mesh, C) longitudinal section of the mesh and D) magnified view of the effluent recirculation (including the recirculation stream).

In this case, a higher meshing degree was required where the graphite rod and granular graphite acted as the electrode. The presence of a large number of granular spheres within the domain caused difficulty in attaining a refined mesh around the spherical granule wall. A dense mesh was

necessary, which made the calculation of the solution complicated. Despite this limitation, a denser mesh was defined in the area between granular graphite, whereas larger elements were defined between the plates and sphere area. The resulting mesh was a combination of tetrahedral and hexahedral meshing cells. As in the previous case, a mesh refinement was also implemented for the inlet/outlet streams.

4.2.3.1.3 *Meshing case 3* – MFC reactor with a graphite rod plus a stainless steel mesh

The third simulated case consisted of two electrode materials: a graphite rod and a stainless steel mesh (Figure 3.5B, case 3). As in the previous case, the number of steel meshes was reduced to avoid large computational memory usage. Three regularly distributed meshes were used, which were separated by a 4 mm distance from the other meshes and anode walls. The meshes had a square light path of 5 mm (Figure 4.4).

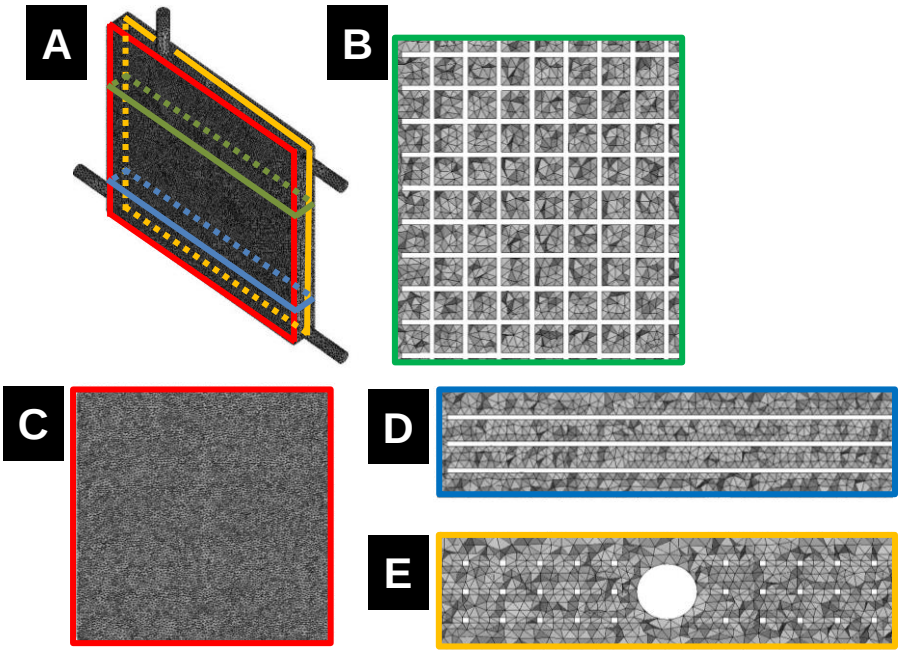

Figure 4.4. Mesh development for a graphite rod and a stainless steel mesh: A) full view, B) enlarged size of a cross-section in the position of the stainless steel mesh, C) cross-section of the position close to the chamber wall, D) cross-section of the positon crossing the meshes and E) cross-section of the domain at the point of the graphite rod and stainless steel.

Similar to the case of granular graphite, the presence of stainless steel made it difficult to obtain an ideal situation close to the wireless mesh. However, a deep refinement was applied in close proximity to these elements and the anode chamber walls, whereas the mesh was maintained as simple as possible in the non-critical zones (Figure 4.6).

4.2.3.1.4 *Meshing case 4* – MFC reactor with a graphite plate

The last case was based on a graphite plate, which almost filled the entire anode chamber domain (Figure 3.5B, case 4). The dimensions of the plate were 180 x 180 x 10 mm. The resulting mesh is presented in Figure 4.5.

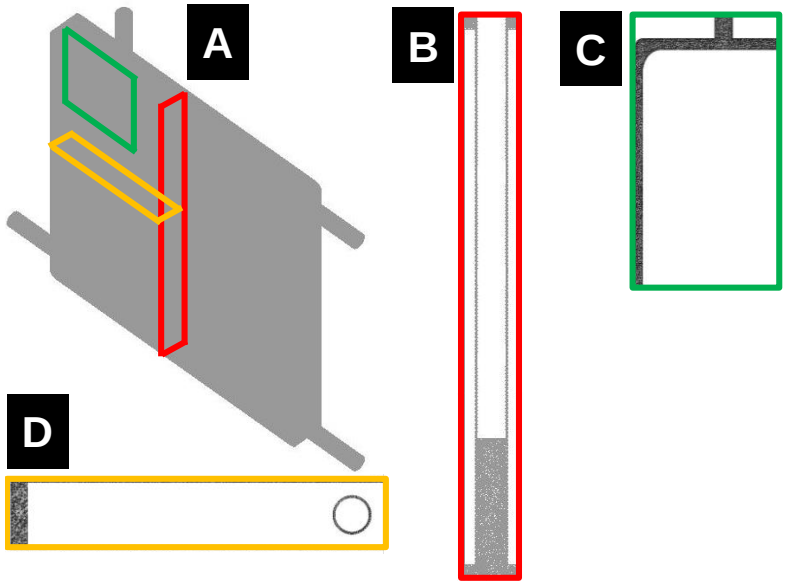

Figure 4.5 Section plots of the resulting mesh for the graphite plate simulation case.

As observed, a denser mesh was possible since the fluid zone occupied less volume in comparison with the previous two cases. The volume between the bar and wall anode chamber was defined as a set of tetrahedral cells and triangular cells (for the wall boundary condition).

Overall, a larger presence of physical components inside the simulation domain required an increase in the elements and cell density of the mesh. Hence, the first case demonstrated a lower number of mesh elements because only a refinement around the graphite rod was necessary. In contrast, the fourth case (the graphite bar), had a larger quantity of triangular elements because of the considerable presence of wall surfaces (internal surfaces). The optimal mesh was obtained by testing different mesh sizes (from larger to smaller elements) and determining the minimum size that did not produce a change in the results (velocity flow).

4.2.3.2 Anammox reactor

The anammox reactor meshing (Figure 4.6) followed the same methodology and criteria as the MFC cases. The mesh refinement was close to the internal plates of the reactor was applied and a reasonable number of elements throughout the overall mesh was maintained. Additionally, the inlet and outlet streams were refined to obtain the proper flux distribution in these critical zones. Again, the meshing degree for the optimal mesh was the one which produced acceptable velocity profile results with the fewest elements.

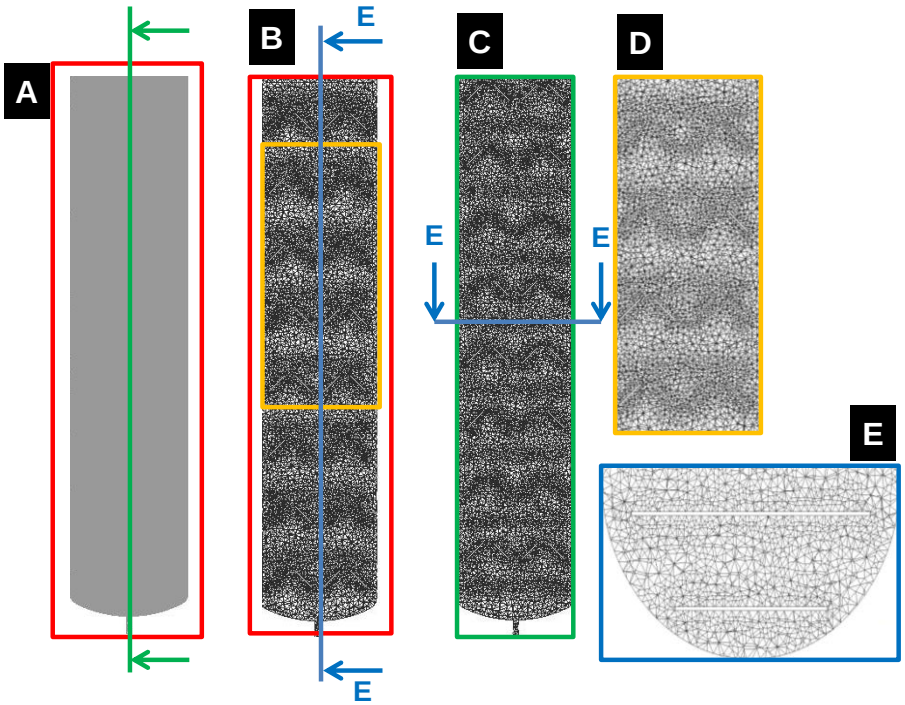

Figure 4.6. Section plots of the resulting mesh for the anammox reactor simulation case. A) two sections of the fluid domain, B) extended view of the first plots of A, C) mesh for the external wall and D) cross-section of the reactor in a zone with internal plates.

Table 4.3 provides a summary of mesh characteristics for each anodic chamber configuration simulation and for anammox reactor, which includes

the number of elements, number of nodes and number of faces that were generated.

Table 4.3 Mesh characterization for the simulation cases in Microbial Fuel Cells.

Case	N elements (tetrahedrons)	N nodes	Face Elements
MFC + rod graphite	800855	145322	1623732
MFC granular graphite + rod graphite	1670591	335118	3466144
MFC stainless steel + rod graphite	979657	197631	2054447
MFC graphite plate	1928137	495845	4200587
Anammox reactor	850717	160361	1741760-

4.2.4 Solver

From the wide range of commercial platforms (licensed or open source) available in the CFD industry, Ansys Fluent® software was selected for the development of this Thesis.

Since the program must be able to read the mesh, a preliminary check was necessary to ensure the readiness of its domain, geometry and size. All the information need to be properly transferred from the meshing platform to the solver, with special attention to the correct definition of the dimensions, domain boundaries and boundary condition profiles.

4.2.4.1 Solver definition

Both simulated cases were developed under steady-state conditions. These conditions were utilized to analyse the flow and species distribution while maintaining the continuous and stable operation of the reactor. However, for the anammox case, the gas generation was modelled using a transient simulation until the gas generation was stabilized within the overall fluid domain. This strategy ensured simulation convergence.

4.2.4.2 Fluid/solid properties

The specific properties for each fluid/solid, which comprised the simulation domain, must be properly defined. The Ansys Fluent® solver contains pre-defined libraries of materials and fluids including a wide range of properties (density, specific heat, electrical conductivity, etc.). The number and accuracy of the properties used in the simulations depend on the number of solver models selected for the simulated case. In the simulated cases that were developed, the fluid was assimilated to pure water. Additionally, in the anammox case – multiphase simulations – the nitrogen gas was set as a secondary phase. For the reactor wall and internal surfaces, solid materials were defined. For the external walls of the MFC reactors, methacrylate was introduced as a new material, and the graphite and stainless steel properties for the anodes were taken from the software library. In the anammox case, the external walls and internal plates were made of stainless steel, and their properties are defined in the software library.

For the resolution of MFC and anammox processes, a mixture of species was outlined. In the first case (MFC), a mixture of acetate in a water solution was specified. In the second case, a mixture of nitrogenous species (ammonium, nitrite, nitrate and dissolved nitrogen) in a water solution was defined. The

definition of this mixture was necessary to calculate the mixture properties, and the molecular weight for each component was introduced by the user.

4.2.4.3 Fluid zones

The fluid zone in Ansys Fluent® is the section of the geometry that was occupied by a fluid or fluids. In the simulations presented in this study, a unique fluid occupied the overall reactor domain, independently of if it was a mixture of species or if it was a multiphase simulation.

In the fluid zone, equations of mass, momentum and energy balances were solved (discretization of fluid). Moreover, operation conditions (pressure, temperature of fluid) and set of mass, momentum and energy sources were defined.

Biological reactions were included in the CFD model included as a source terms (S_i Equation 4.10) into the fluid zone, one for each of the species. This was done by user-defined functions (UDF), which are fully developed in the Appendix, section 9.1.6.

Finally, the anammox process simulations involved two different phases (liquid and gas), which required implementations of a drag coefficients model based on the Schieller-Neumann model (Ansys, 2009). No other forces were considered in the boundary condition model.

4.2.4.4 Boundary conditions

Special attention was paid to setting the boundary conditions of the fluid zone and computational domain. The correct definition of initial and boundary conditions is essential to correctly solve the set of governing equations in CFD (Andersson, 2012). The boundary conditions used in these studies are described as follows.

- Velocity inlet: For incompressible fluids, the velocity and scalar values for inlet boundaries were defined. Velocity was used to define inlet/outlet and recirculation streams for both simulation cases. The inflow velocity vector and species concentrations (in mass fractions) were fixed by this boundary condition. The outflows were implemented as an equivalent of the velocity inlet in an opposite direction to the fluid zone to define the outflow from the fluid domain (although specific outflow boundary conditions definition is possible, this ensured setting the exact flow).
- Degassing boundary condition: This particular boundary condition was implemented in the anammox multiphase simulations to model a free surface where only the dispersed gas bubbles were allowed to escape from the domain (the continuous phase was kept inside the domain). The condition was implemented using an Eulerian multiphase model.
- Wall boundary conditions: This boundary condition was used as a connection between the fluid and solid regions and a model for reactor walls and other internal elements that were introduced in the fluid zone (rod / electrode materials for the MFC or internal plates in case of the anammox reactor). Additionally, this boundary condition requires specifications related to the material and wall temperature. When modelling turbulent conditions, the wall roughness can also be specified.

More details regarding the boundary conditions used in each case (with the exact values) are given in Section 4.3 (simulation cases). Since both processes are isothermal (no heat exchange), the fluid temperatures in the boundary conditions of both simulation cases were set.

4.2.4.5 Solution methods

The next task in the simulation process was the methodology selection to solve the balance equations. These methods are distinguished between spatial and temporary discretization. A full description of the CFD solution can be obtained in the literature (Versteeg and Malalasekera, 1995), , as well the specific methods employed in Ansys Fluent® (2009). In this Thesis, a SIMPLE scheme and a Phase-Coupled SIMPLE scheme were selected for pressure-velocity coupling in the MFC and anammox simulation cases, respectively. Regarding the flow solution and species variables, a second-order upwind method was selected. Furthermore, the QUICK method was used to determine the volume fraction in the anammox multiphase case.

Solution controls are necessary to control the convergence of the solution methods. Further information can be obtained in the Appendix of the Thesis (9.3). From the default values of solution controls in Fluent, slightly reduced values were used for all the variables to get converged solution.

4.2.5 Post Processing

Ansys Fluent® allows a representation of the variable values in different forms. The software also presents contours of the cross-section planes of the geometry, plots at specific points or lines of the geometry and often averages or ranges the values of variables within the fluid. Additionally, the user is able to calculate user-defined variables from the original model variables (i.e., biological removal rates from species concentrations). These variables, which are calculated at each computational cell of the domain, can be read and plotted like any other variable. In this investigation, both the contour profiles at various sections of the domain and the average value of the entire domain were presented. Finally, the modelling processes ended with the validation process. However, the cases developed in this Thesis

were used to support the design, and it was not possible to perform a validation process: only the experimental knowledge about the performance of both systems was useful (biological performance) to validate the simulations.

4.3 Simulated cases

4.3.1 MFC reactor

Table 4.4 presented a summary of the model development for each of the four simulated scenarios for the anode chamber design. All the simulations shared the model methodology and the boundary conditions definition. The model development was based on single phase and laminar simulations. The specific model definitions are detailed in the table.

Regarding the acetate concentration, the MFC configuration had two recirculation streams (inlet and outlet), which had the same flow, but the acetate concentration was adapted based on its distribution within the chamber. For this reason, a double UDF was employed to read the acetate concentration at the outflow recirculation stream (DEFINE_ADJUST) at the end of iteration. Then, the read value was used as the acetate concentration in the influent concentration using the DEFINE_PROFILE routine. Both UDF routines are fully developed in the Appendix section 9.3.

Table 4.4 **MFC simulation definition**

MFC Reactor		
Solver	Pressure Based	
	Time	Steady state
	Gravity	On {0,-9.81,0}
Materials	Mixture	AcO-, H_2O [*1]
	Solid	Graphite
		Methacrylate
		Stainless steel
Models	Energy	Isothermal (298.15 K)
	Turbulence	Laminar
	Species transport	On
Cell conditions	Acetate source terms	Biological model [*2]
Boundary conditions	Inlet (velocity inlet)	1.5 $L \cdot d^{-1}$, 293.15 K, 500 $mg \cdot L^{-1}$ AcO
	Outlet (velocity inlet)	1.5 $L \cdot d^{-1}$, 293.15 K, adapted concentration
	Recirculation in (velocity inlet)	150 $L \cdot d^{-1}$, 293.15 K, adapted concentration
	Recirculation out (velocity inlet)	150 $L \cdot d^{-1}$, 293.15 K, adapted concentration
	Wall	298.15 K, no species diffusion
Solution Methods	Pressure Velocity Coupling	*SIMPLE*
	Spatial Discretization	Gradient: Least Squares Cell Based Pressure: Second Order Momentum: Second Order AcO- : Second Order Upwind Energy: Second Order Upwind

The kinetic rate of acetate consumption, by means of biological activity, was formulated with substrate dependence terms (and constant microorganism population). This formulation was conducted using the DEFINE_SOURCE (see Appendix 9.3 routine and was introduced within the fluid zone definition as a source term.

In order to analyse the mixing degree of the systems, a tracer step input was simulated to obtain the residence time distribution (RTD) of the system. This analysis was made for granular graphite plus graphite rod and stainless steel plus graphite rod. The output data of tracer concentration at the outflow stream was collected until the concentration of the tracer was stable and homogeneous. After it, the RTD determination was done.

4.3.2 Anammox reactor

Regarding the anammox process (modelling a column reactor with internal plates), multiphase simulations were performed at a pressure of 101325 Pa and a temperature of 308.15 K. Table 4.5 shows the simulation settings for the anammox cases: A) solver settings (solver and models), B) solver settings (boundary conditions) and C) solution methods.

The anammox model involved multiphase simulations in turbulent flow and considered a variety of species. The equations were solved using the following sequence. First, the fluid flow at each computational point of the domain was resolved by solving the continuity, momentum and energy equations under steady-state conditions and incorporating biological reactions as a source terms (S_i Equation 4.10). Finally, the generation of gas was switched on (volume fraction), and the equations were solved for the unsteady state. For the turbulence model, the k-ε model was selected due to fluid characteristics that are similar to water-air simulations, as reported in the literature (Ansys, 2009).

Table 4.5 **Anammox simulation definitions**

Anammox Reactor		
Solver	Pressure Based	
	Time	Steady state/Transient
	Gravity	On {0,-9.81,0}
Materials	Fluid Primary Phase	Mixture: N-NH_4^+, N-NO_2^-, N-NO_3^-, N-N_2 (d), H_2O
	Fluid: Second. Phase	N-N_2 gas
	Solid	Stainless Steel
Models	Energy	Isothermal (308.15)
	Turbulence	k-Ɛ model
	Species transport	On
Cell conditions	Dissolved nitrogen species and gas	Biological model[*2]
Boundary conditions	Inlet (velocity inlet)	36 $m^3 \cdot d^{-1}$, 308.15 K NH_4^+: 5,5 mg $N \cdot L^{-1}$, N-NO_2^-: 7,4 mg $N \cdot L^-1$, N-NO_3^-: 1 mg $N \cdot L^-1$, N_2: 28,5 mg $N \cdot L^{-1}$
	Outlet (degassing)	(-)
	R_{out} (velocity inlet)	36 $m^3 \cdot d^{-1}$, 308.15 K , Concentration of species adapted from the zone close to the BC
	Wall	308.15 K, no species diffusion
Solution Methods	Pressure Velocity Coupling	*Phase Coupled SIMPLE*
	Spatial Discretization	Gradient: Least Squares Cell Based Pressure: Second Order Momentum + Vol Fraction: QUICK N species : Second Order Upwind Energy: Second Order Upwind

The consumption and production of species were based on Monod's substrate dependence terms, which considered a constant biomass

concentration. Similar to MFC reactors, the model was defined by a UDF DEFINE_SOURCE routine (included in the Appendix Section 9.3).

The RTD distribution was simulated, as in MFC case, by adding a tracer pulse in the influent concentration and measuring the tracer concentration until the concentration in the outflow reached zero concentration.

Chapter 5. **Anode hydrodynamics in Bioelectrochemical Systems**

The results obtained in ths chapter were published in the following paper:

Vilà-Rovira, A., Puig, S., Balaguer, M.D., Colprim, J., 2015. Anode hydrodynamics in bioelectrochemical systems. RSC Adv. 5, 78994–79000.

5.1 Overview

Bioelectrochemical systems (BES) is a sustainable technology used in groundwater (Pous et al., 2013) and wastewater (Lim et al., 2012) treatments. A wide range of products, such as methane(Batlle-Vilanova et al., 2015), acetate (Nevin et al., 2011), butyrate (Ganigué et al., 2015), and hydrogen (Jeremiasse et al., 2010) can also be produced from contaminated water or polluted gaseous streams using BES. The performance of BES is influenced by many factors such as: substrate characteristics and availability (Torres et al., 2008), microbial community (Vilar-Sanz et al., 2013), electrode characteristics (Park and Zeikus, 2003) and reactor design (Ahn et al., 2014), among others. Some of these key factors are directly linked to the hydrodynamics inside the BES.

Computational Fluid Dynamics (CFD) modelling uses numerical methods and algorithms to analyse fluid flows. CFD is a powerful tool for investigating fluid flow by computer software and it complements the limitations of field and laboratory experiments with minimal cost. CFD are widely used to optimise processes and equipment's design in wastewater treatment plants (Andersson et al., 2004) such as: aeration systems operation (Le Moullec et al., 2010), membrane reactor designs (Bentzen et al., 2012), anaerobic digesters performance (Wu, 2012), mass transfer in airlift reactors (Huang et al., 2010) or reaction parameters in packed bed reactors (Lopes and Quinta-Ferreira, 2010b). The use of CFD could be also a powerful tool in MFC (and other BES configurations) to optimise scaling-up BES design or select the suitable electrode material, among others. Unfortunately, CFDs have been hardly applied to BES. Recently, Kim et al., 2014 investigated for the first time the fluid flow and estimated the electricity generation in the anodes of 12 different BES configurations with different internal structures (shape - triangular and rectangular type-, number, length, and angle) (Kim et al.,

2014). Michie et al., 2014 applied CFD modelling within three novel helical geometries anodes within an anodic BES chamber. They linked COD (Chemical Oxygen Demand) removal and power production to the fluid flow distribution.

One of the key parameters in designing BES is the identification of suitable conductive materials to ensure proper electron transfer distribution and an appropriate surface for biofilm attachment(Logan et al., 2006). In the current state of the art, anode configurations are mainly composed of graphite-based electrode collectors and additional conductive material which favours biomass attachment (Logan et al., 2006). Since a plethora of conductive materials have been reported in literature (graphite rod, granular graphite, carbon felt, among others) (Zhang et al., 2012; Zhou et al., 2011), it is necessary to gain a mechanistic insight on how these materials affects the hydrodynamic behaviour, and consequently the substrate distribution, within the bioanodes. Up to date, further research on fluid distribution and hydrodynamics within the anode compartment in common anode electrodes is still missing. This study determines the fluid flow and substrate distributions in the anode compartments of different conductive materials (graphite rod, granular graphite, stainless steel mesh and graphite plate) commonly used in the literature.

5.2 Materials and methods

5.2.1 Bioelectrochemical System

The MFC considered for the modelling was a rectangular methacrylate reactor (Puig et al., 2012), with a squared internal chamber of 200 mm x 200 mm x 10 mm (Figure 5.1). It consisted of an anode and a cathode chambers separated by a cation exchange membrane (CEM, Nafion 117, DuPont, USA). Both anode and cathode chambers contained a graphite rod as collector

electrodes (107 × 6 mm [anode] and 130 × 6 mm [cathode], Sofacel, Spain). The cathode chamber was filled with granular graphite (model 00514, EnViro-cell, Germany). This design was successfully applied for treating contaminated groundwater (Pous et al., 2015).

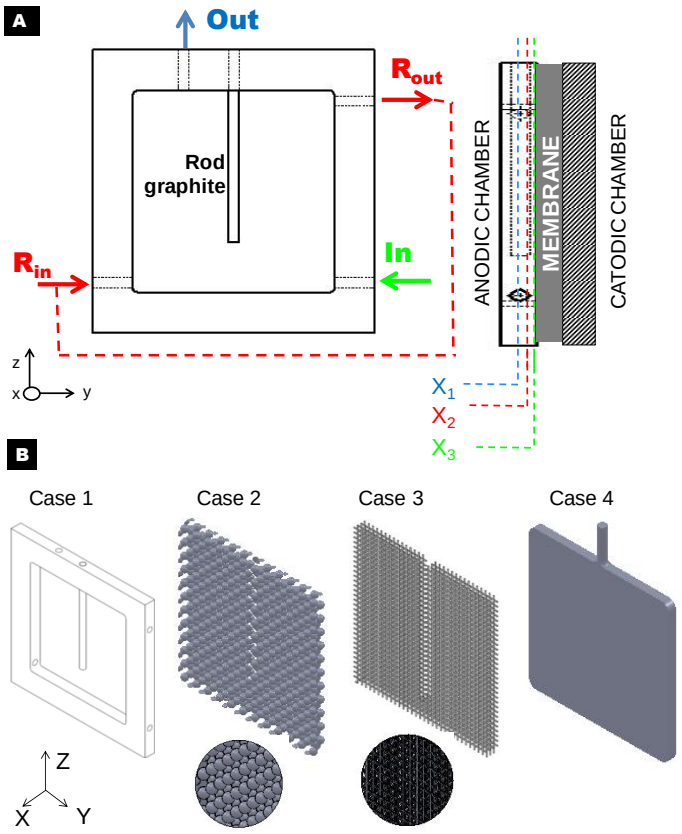

Figure 5.1. Representation of the reactor design: a) reactor flowchart and the selected planes for results plotting (x_1, x_2 and x_3), b) different electrode materials used: graphite rod (Case 1), granular graphite (case 2), stainless steel (case 3) and graphite plate (case 4). Rin and Rout represented inlet and outlet recirculation's streams, respectively.

Figure 5.1 shows a scheme of each anode compartment configuration (Figure 5.1A) and the different additional conductive material assessed (Figure 5.1B). Four different anode electrodes were considered for evaluating the anode hydrodynamics, as they have been widely reported in the literature. Table 5.1 presents the main characteristics of the materials assessed, which were:

- Case 1: Graphite rod (as the control and the collector electrode).

- Case 2: Graphite rod (collector electrode) plus granular graphite particles filling the total anode chamber domain.

- Case 3: Graphite rod plus stainless steel meshes (three different meshes separated by 4 mm).

- Case 4: Graphite plate.

The anode compartment was fed with 1.5 $L \cdot d^{-1}$ of an enriched acetate medium (containing 500 $mg \cdot L^{-1}$ of acetate). A recirculation loop ratio of 1:100 was applied to homogenise the anode compartment. The operating temperature and pressure were kept at 293.15 K and 101325 Pa, respectively.

5.2.2 Computational fluid dynamics modelling

The fluid hydrodynamics were modelled using Ansys Fluent platform (ANSYS® Academic Research, Release 12.1). The momentum, continuity and energy equations were resolved for each case (Appendix Chapter 9, Equations 9.59 – 9.62). The low velocities streams of made feasible to work in a laminar state. Proprieties values of aqueous solution were considered at 298.15 K and 101325 Pa. Gravity forces were also accounted within the simulations. To solve the hydrodynamic equations, velocity inlet boundary conditions were set for the inlet and outlet streams and recirculation loop streams (inlet and outlet), adapting in each case the velocities magnitudes and directions. All of them were fixed as a constant flux: the recirculation streams were fixed at 80 $m \cdot h^{-1}$ (150 $L \cdot d^{-1}$) and the inlet/outlet streams at 0.80 $m \cdot h^{-1}$ (1.5 $L \cdot d^{-1}$). Wall boundary conditions were set for the collector graphite rod electrode and the anode walls, as well for the rest of the electrode materials (granular graphite, stainless steel and graphite plate). All these wall boundary conditions were defined as non-slip. The low water permeability

through biofilm made the water velocity negligible (Picioreanu et al., 2009). The planes were defined as a middle section of anode chamber (Figure 5.1A - x_1), the section between those two planes (Figure 5.1A - x_2) and near the anode wall (membrane) (Figure 5.1A - x_3). The experimental low Reynolds number (Appendix Chapter, Figure 9.3) resulted in a laminar flow, which is characterised by smooth and constant fluid motion.

5.2.3 Biological model

A simplification of the biological model proposed by Pinto et al., 2010 was considered for acetate oxidation in the anode compartment. The biological model proposed two main microbial populations (anodophilic and methanogenic) competing for a common substrate (acetate). The kinetic equations are presented within the Appendix (Section 9.1.4). The concentrations of these microorganisms within the anode compartment were considered to be constant at steady state run, and homogeneous through overall anode domain; and fixed at 500 mg $COD_x \cdot L^{-1}$ and 250 mg $COD_x \cdot L^{-1}$, respectively, as assumed by Pinto et al., 2010. Acetate concentration was introduced as solubilised specie within aqueous solution. The acetate biological consumption was introduced as source term in the mass conservation equation (Appendix Chapter, Equation 9.59), by means of user defined functions. The anode was fed with an influent acetate concentration of 500 $mg \cdot L^{-1}$. The Void fraction of the anòdic chamber was determined with the NAC / TAN (Net Anode volume Compartment / Total Anode volume Compartment) ratio. Current generation and methane production rates were calculated according to Equations 9.67 and 9.68, respectively, from the Appendix Chapter.

Table 5.1 Main characteristics of the electrode materials used in this study

Case	Electrode Material	Characteristic size	Distribution
1	graphite rod (control)	ϕ = 10 mm Height = 17,5 cm	Centre
2	graphite rod plus granular graphite	$\phi_{granule\ particle}$= 9 mm	Two layers of spheres separated 3 mm each other Separation between spheres 11 mm (centre to centre)
3	graphite rod plus stainless steel mesh	ϕ_{mesh}=1 mm	Three layers of mesh, separated 4 mm each other Mesh light path: 5 mm x 5 mm
4	graphite plate	180 x 180 x 10 mm	

Power generation ($W \cdot m^{-2}$) was calculated using Equation 5.1 (Logan et al., 2008):

$$P = \frac{\mu_{max} X b_{es} F C_E E}{Y_{x/c}} \quad (5.1)$$

Where maximum specific growth rate (μ_{max}) was fixed at 8.3 d^{-1}, cell yield ($Y_{X/C}$) of $4.1 \cdot 10^3$ cells$\cdot mol^{-1}$-Ac, b_{es} of 8 mol $e^- \cdot mol^{-1}$-Ac, being F the Faraday's constant ($C \cdot mol^{-1}$), C_E the coulombic efficiency (-) and E the redox potential (V), and *X* is the fraction of anode surface occupied by the cell biofilm. C_E (Equation 5. 2) was calculated as (Logan et al., 2006):

$$C_E = \frac{MI}{Fbq\Delta COD} \quad (5.2)$$

From which q is the inlet flow ($L \cdot s^{-1}$) and ΔCOD is the total substrate removal (mg COD$\cdot L^{-1}$), M is the molecular weight ($g \cdot mol^{-1}$) and I is the corrent intensity (mA).

Shear rate ($\dot{\gamma}$, Equation 5.3 - Ansys, 2009) was analyzed within the different configurations to determine if the hydrodynamics conditions reinforced biomass attachment. Pham et al., 2008 stated a value of 120 s^{-1} as optimal value during the enrichment period to obtain high MFC performance:

$$\dot{\gamma} = \sqrt{\frac{1}{2} \cdot \overline{\overline{D}} : \overline{\overline{D}}} \tag{5.3}$$

The shear rate is defined as the second order deformation tensor, where D (Equation 5.4) represents the rate of deformation tensor, defined as:

$$\overline{\overline{D}} = \left(\frac{du_j}{dx_i} + \frac{du_i}{dxj}\right) \tag{5.4}$$

u represents the velocity vector, and *x* the distance or position vector, with *i* and *j* representing each of its components.

5.3 Results and discussions

5.3.1 Anodic fluid dynamics

Anodic fluid flow was analysed for different selected electrode materials. Figure 5.2 presents the fluid velocities contours and vectors profiles for each anode compartment configuration (A: graphite rod, B: granular graphite, C: stainless steel mesh and D: graphite plate). Graphite rod was considered as the control configuration and the collector electrode (Figure 5.2A). The low surface availability (14.76 $m^2 \cdot m^{-3}$ NAC– Table 5.2) conducted to a clear preferential way caused by the recycling flow. The fastest velocity, ranging from 10-50 $m \cdot h^{-1}$, was reached in the preferable way from inlet to outlet recirculation (Figure 5.2A). In contrast, the slowest velocities (0-1 $m \cdot h^{-1}$) were found at the opposite sides corresponding to both inlet and outlet streams.

Velocity ranges between 0 – 10 $m \cdot h^{-1}$ represented 78 %, 83 % and 92 % of all the flow distributions for the x_1, x_2, x_3 planes, respectively (Figure 5.3). The highest velocities range (10-20 $m \cdot h^{-1}$) represented only 10 % of the total area (averaged from the three different planes). The wide range of velocities indicated a poor flux distribution influenced by the electrode used, the chamber architecture (square design) and the recirculation flow (100 times higher than the influent flow).

Table 5.2 Comparison of the ratio between electrode surface and liquid volume, void fraction, hydraulic retention time, power generation, columbic efficiency, and methane production for each case studied.

Case	Electrode Material	$m^2 \cdot m^{-3}$ NAC	Void fraction	HRT (h)	Power ($W \cdot m^{-2}$)	I ($A \cdot m^{-2}$)	C.E (%)	CH_4 prod. ($mL \cdot d^{-1}$)
1	Graphite rod	14.76	0.98	12	-	-	-	-
2	Graphite rod plus granular graphite	225.44	0.75	9.55	0.02	0.40	52	26.9
3	Graphite rod plus stainless steel mesh	213.81	0.94	12.08	0.14	0.36	58	28.6
4	Graphite plate	208.7	0.50	6.41	-	-	-	-

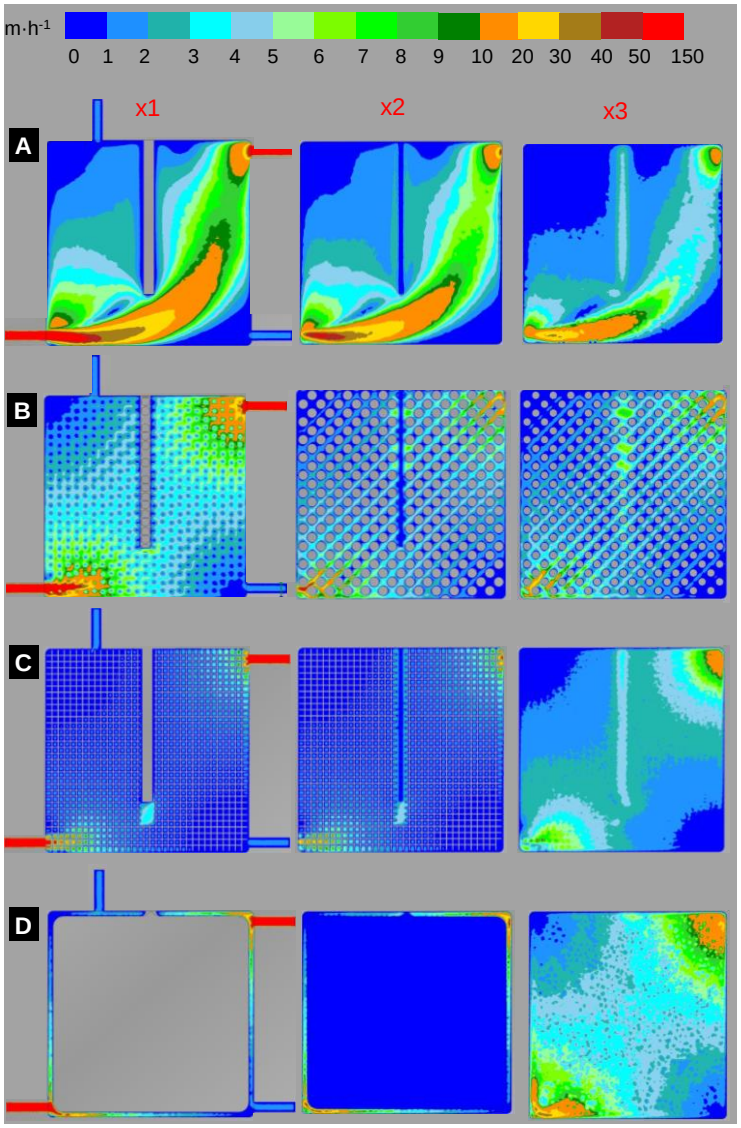

Figure 5.2. Velocity contours and vectors at three different planes (x1, x2, x3) from the centre to the anode wall, for each simulated case (inlet/outlet flow: 1.5 $L \cdot d^{-1}$, recirculation flow: 150 $L \cdot d^{-1}$) : a) graphite rod (14.76 $m^2 \cdot m^{-3}$ NAC, HRT 12 h), b) graphite rod + granular graphite (225.44 $m^2 \cdot m^{-3}$ NAC, HRT 9.55 h) , c) graphite rod + stainless steel meshes (213.81 $m^2 \cdot m^{-3}$ NAC, HRT 12.08 h), d) graphite plate (208.7 $m^2 \cdot m^{-3}$ NAC, HRT 6.41 h).

When granular graphite was introduced in the anode compartment (Figure 5.2B), the available electrode surface considerably increased 225.44 $m^2 \cdot m^{-3}$ NAC decreasing the void fraction to 0.75 (Table 5.2). Granular graphite favoured the flow dispersion in the inlet zones with a better velocity

distribution within the domain. Velocity ranges were between 2 and 5 $m \cdot h^{-1}$. The lowest velocities zones were found closer to the both inlet and outlet streams (0-1 $m \cdot h^{-1}$) influenced by the anode architecture. When moving towards the anode chamber wall (x_2, x_3), the maximum velocities at the recirculation streams were reduced. The range of velocities was more homogeneous. Velocities between 0 and 10 $m \cdot h^{-1}$ occupied an average area of 96 % (93%, 98% and 98 % to x_1, x_2 and x_3 respectively).

The third electrode assessed was stainless steel mesh (Figure 5.2C). Three meshes were introduced inside the compartment (Figure 5.1). This resulted in an available surface of 213.18 $m^2 \cdot m^{-3}$ NAC and a void fraction of 0.94. The flow inside the chamber was regularly distributed by the presence of stainless steel meshes. An average of 95 % of the total liquid relative area relied on velocities range between 0-5 $m \cdot h^{-1}$. Only a predominant flux between inlet and outlet recirculation streams was observed in x_3 (Figure 5.2C, Figure 5.3) because of the no presence of electrode material near ~~to~~ the membrane wall. The average percentage of the total area at velocity range 0-5 $m \cdot h^{-1}$ was 96 %, with the smallest value close the membrane wall (x_3 – 93 %).

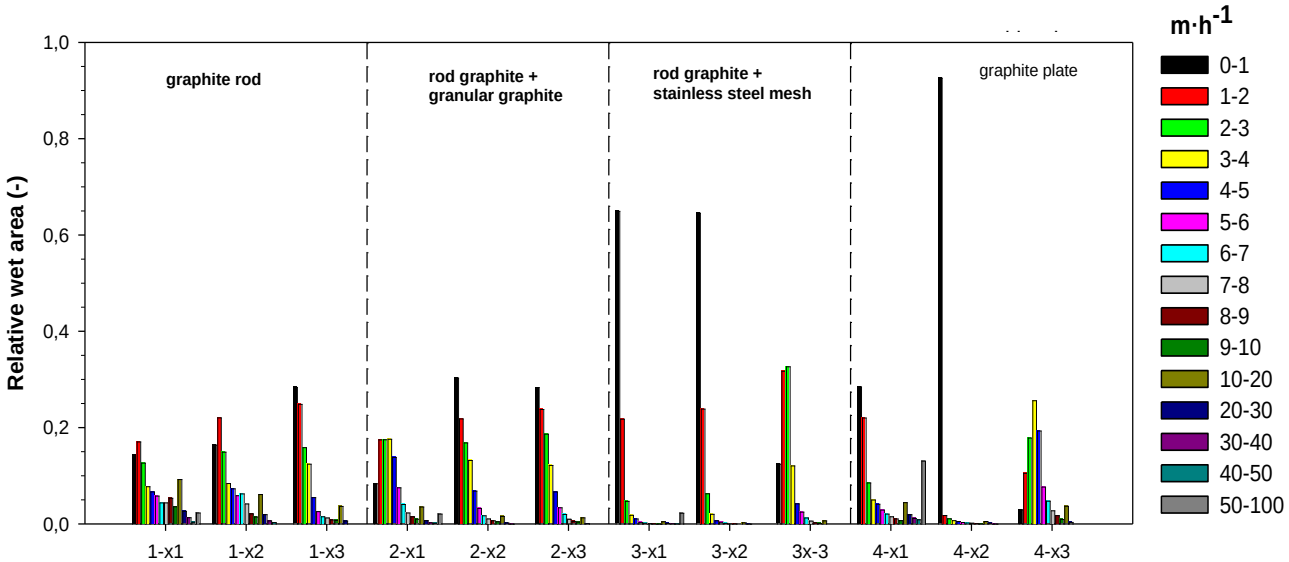

Figure 5.3 Relatives areas as a function of velocity ranges for the different longitudinal planes of the anode chamber (x1, x2 and x3). Operational conditions: inlet/outlet velocities: 0.80 $m \cdot h^{-1}$, recirculation velocities: 80 $m \cdot h^{-1}$. Parameters: a) graphite rod: 14.76 $m^2 \cdot m^{-3}$ NAC, HRT 12 h, b graphite rod + granular graphite (225.44 $m^2 \cdot m^{-3}$ NAC, HRT 9.55 h) , c) graphite rod + stainless steel meshes (213.81 $m^2 \cdot m^{-3}$ NAC, HRT 12.08 h), d) graphite plate (208.7 $m^2 \cdot m^{-3}$ NAC, HRT 6.41 h).

The fourth case of study used a 10 mm thickness graphite plate (Figure 5.2D). The plate covered the majority of the anode chamber domain (a surface area of 208.7 $m^2 \cdot m^{-3}$ NAC and a void fraction of 0.50). The inlet recirculation was configured with the fluid stream flowing through the space between the anode chamber wall and graphite plate surface. The friction of the water in contact with the plate caused a drop of the velocity to 0-1 $m \cdot h^{-1}$ close to the graphite plate wall (x_2). The fastest velocities were found near the membrane wall in plane x_3 in the zone connecting both recirculation streams (ranging from 5 to 30 $m \cdot h^{-1}$).

5.3.2 Dynamics of substrate within the anode compartment

The different hydrodynamics may influence the substrate distribution within the anode compartment. In order to assess hydrodynamics effects on substrate distribution, the two cases with a better flow distribution were considered (Cases B and C). The biological model considered the acetate oxidation and its competition between anodophilic and methanogenic bacteria. Figure 5.4 depicts the simulated acetate concentration profiles at steady state conditions for Cases 2 and 3. The anodes were fed with an acetate enriched solution of 500 $mg \cdot L^{-1}$. The low daily flow (1.5 $L \cdot d^{-1}$) favoured the fast consumption of substrate at the inlet zone. In both cases, the anode initially worked as a plug flow system with circular development, since the concentration gradients occurred in the direction of the influent flow. When the inlet flow reached the recirculation stream, substrate was completely homogenized.

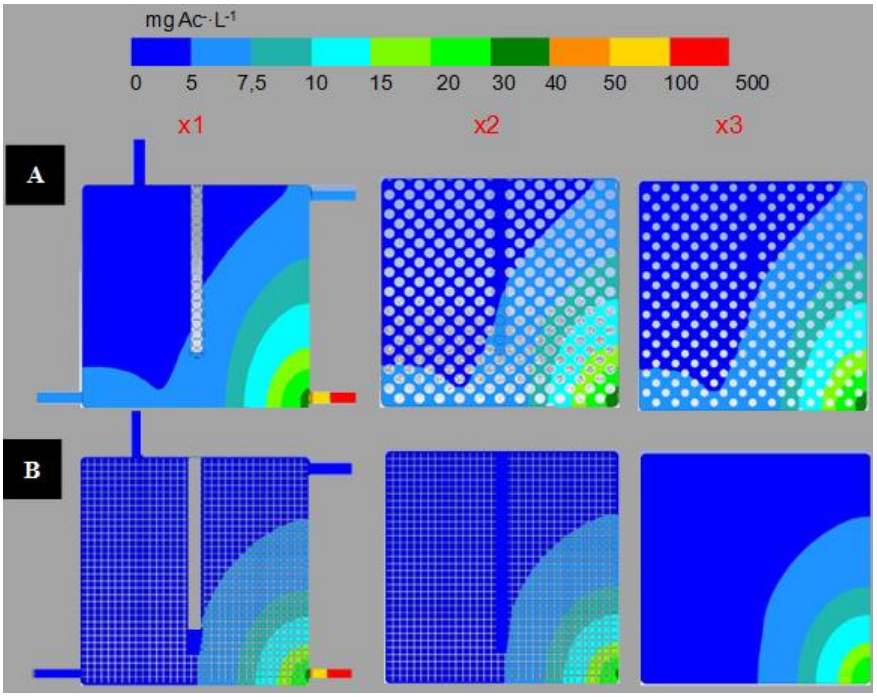

Figure 5.4 Acetate concentration profiles using a) rod graphite + granular graphite (225.44 $m^2 \cdot m^{-3}$ NAC, HRT 9.55 h) and rod graphite + stainless steel meshes b) (13.81 $m^2 \cdot m^{-3}$ NAC, HRT 12.08 h) as electrode materials.

The main differences in both concentration profiles were found due to the different void fractions which influenced the HRT value (Table 5.2). The lower HRT (9.55 h) of the granular graphite anode (Case B, Figure 5.4A) involved lower substrate removal efficiency, causing higher substrate gradient within the anode compartment. The higher HRT (12.08 h) of the stainless steel meshes anode (Case 4, Figure 5.4B) maximized substrate removal efficiency. The substrate was mainly removed in one quarter of the anode and no acetate was recirculated. This result suggested that an increment of the daily flow was hydrodynamically feasible.

This computational fluid dynamics study demonstrated that spatial heterogeneity existed. This result was validated by Pous et al., 2015, who took inoculums from three different sampling ports of the cathode volume of an identical MFC with granular graphite as the electrode. The highest nitrate

removal and current production were observed close to the feed stream, where according to Figure 5.A more substrate was available.

5.3.3 Selection of the electrode material

The selection of the electrode material affects the hydrodynamic behaviour within the chamber, influencing the substrate distribution and biomass attachment. The use of CFD enables the selection of the proper conductive material shape in terms of regular flow distribution within the anode compartment minimising preferential flow ways. The choice of the optimal configuration should be done based on three parameters: available surface, shear rate and power performance.

At larger conductive surface areas, more biomass can be attached and consequently, power production can be reinforced. Both granular graphite and stainless steel anodic materials ensure these conditions. Stainless steel had slightly higher surface (0.16 m^2 of electrode) and a void fraction (0.94) than granular graphite (0.13 m^2 and 0.75, respectively).

Moreover, both stainless steel and granular graphite had better flow homogenization within the system. To assess the homogeneity of the systems, residence time distribution curves by CFD were determined. A constant concentration of a tracer at the inlet stream was applied, measuring the response at the outflow stream. To simulate the recirculation stream, and especial user defined function was developed to adapt the tracer concentration at the outflow recirculation stream to the concentration at the influent recirculation. The essay was done for the two more representative electrode materials (granular graphite and stainless steel mesh). The average time (t_m, Equation 5.5) for each distribution was calculated, for a step input as:

$$t_m = \frac{1}{C_{max}} \int_0^{Cmax} t dC \qquad (5.5)$$

Figure 5.5 presents the residence time distribution curves. The average times of each distribution were 14.5 and 11.6 d for granular and stainless steel, respectively. These values compared to the HRT values confirmed the heterogeneity of the anode flow (dead zones, preferential flows). This reinforces the information given by the velocity contours from Figure 5.2.

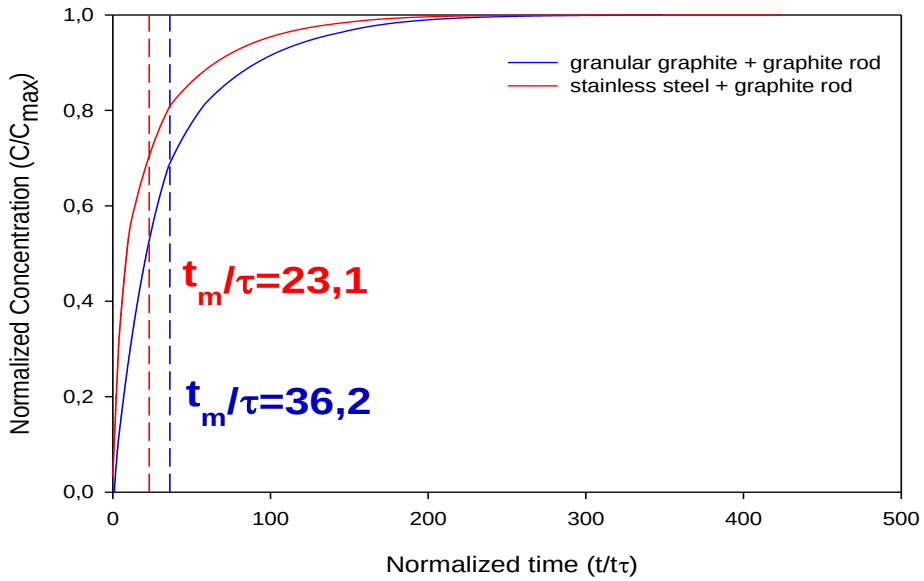

Figure 5.5 Computational Residence Time Distribution using two different electrode materials: rod graphite + granular graphite (225.44 $m^2 \cdot m^{-3}$ NAC, HRT 9.55 h) and rod graphite + stainless steel meshes (13.81 $m^2 \cdot m^{-3}$ NAC, HRT 12.08 h) as electrode materials. Value τ means Hydraulyc Residence Time.

The larger void fraction and larger HRT favoured the better homogenization within the configuration using stainless steel mesh. Additionally better substrate distribution was achieved when using both materials (Figure 5 4), and the long HRT favoured better acetate removal when using rod graphite plus stainless steel mesh.

Shear rate represents the velocity gradient produced by the movement between a fluid in movement and other in stationary movement or a wall influencing biomass attachment. Figure 9.4 (Appendix Chapter) presents the shear rate across the anodic chamber using both materials. The maximum shear reached was 20 s^{-1}, far below the 120 s^{-1} suggested by Pham et al., 2008. At such low values, the biomass got attached. Moreover, despite the model presented in this study was not developed a multiphase model, dimensionless values were useful to balance the substrate convection and mass transfer through the biofilm. To determine the mass transference from the liquid to the solid surface the Peclet number at each computational cell was determined. Peclet number (Peis a balance ratio between the advection processes over the diffusion processes (Equation 5.6). The Pe profiles (Figure 9.5, Appendix Chapter) obtained showed that mass transfer was achieved by dispersion or diffusion, rather than convection.

$$Pe = \frac{Lu}{D} \tag{5.6}$$

From which L is the characteristic length, u the fluid velocity and D the mass diffusivity.

Moreover, the biomass attached on the electrodes could be either exoelectrogenic bacteria or methanogenic archaea. The highest power production was obtained using stainless steel material (0.14 $W \cdot m^{-2}$, Table 5.2) instead of granular graphite (0.02 $W \cdot m^{-2}$). The coulombic efficiency was slightly higher for stainless steel mesh and less methane was produced.

The choice of the anode material is crucial for every bio-anode microbial fuel cell (MFC) setup. Several types of catalysts, such as platinum, manganese

oxides, and iron complexes have been investigated as catalysts to enhance electricity production (decrease the overpotential) in MFCs. Unfortunately, these catalysts are often expensive, unsustainable or time-consuming in preparation, might be subject to poisoning or secondary pollution, and difficult biofilm formation on the surface of the electrode. Carbon materials with various structures, shapes and properties are widely used as electrodes for MFC applications due to their high conductivity, good chemical stability and relatively low cost but constrained by low current density mainly resulting from the low rate of extracellular electron transfer between bacteria and electrode (Fiset and Puig, 2015). Granular graphite is one of the most used carbon based electrode. It is advised to do chemical cleanings to remove possible metal and biomass contamination which could inhibit electrogenic population (Bond and Lovley, 2003). The negatives impacts of using granular graphite particles is related to the biofilm builds up through the granular graphite particles, blocking the fluid flow path, and producing clogging, which would affect directly the electrogenic microbial activity (Aelterman et al., 2008; Di Lorenzo et al., 2010).

Biofilms on electrode surfaces play a key role in current generation or transformation in MFC. By modifying the electrode properties the electronic conductivity, electron transfer and biofilm adhesion can be enhanced. The surface properties, which include the chemistry and charges present at the electrode surface, have been found to affect bacterial adhesion, biofilm formation and electron transfer significantly (Fiset and Puig, 2015). When having biofilms, the material composition should only be accounted if it is influencing rheological surfaces properties of the material. The rheological and physical properties of surface materials should be taken in account in the art of numerical methods. The definition of the material properties (i.e. surface rugosity) had a particular interest when modelling turbulent flow motions. Computational fluid dynamics is able to model systems including

specific wall properties (even reacting, moving or heating walls). However, a logical equilibrium by proper modelling results and computational effort should be taking into account. In this study, the material composition was not selected as a key parameter since the operational conditions made the flow to be in a laminar flow (Figure 9.3, Appendix Chapter), and the motivation of this work is to test specific operational conditions with different anode materials.

Considering all these parameters and flow distribution, the stainless steel anodic material was selected as the best configuration. These results are in agreement with Pocaznoi et al., 2012 who proposed stainless steel as an alternative material for MFC electrodes, due to lower costs and higher electronic conductivity and higher current densities (up to 35 A m^{-2}, while graphite did not exceed 11 A m^{-2}). This was the first demonstration that stainless steel offers a very promising ability to form microbial anodes. Recently, Ledezma et al., 2015 proposed oxidised stainless steel as a very effective electrode material besides its high risk of corrosion and the low material porosity.

5.4 Conclusions

Inside knowledge about the behaviour of bioanodes was obtained by combining flow hydrodynamics and biological process modelling. This computational fluid dynamics study demonstrated that spatial heterogeneity existed. Some configurations (graphite rod or plate) favour the occurrence of preferential flow ways which decreases the anode performance. The use of granular graphite or stainless steel meshes as anode material ensures a better flow distribution within the anode chamber and offers high surface available for biomass attachment and consequently, higher treatment capacity and electricity production.

Chapter 6. **Hydrodynamic and biological modelling of an anammox reactor**

6.1 Overview

The anammox process is an efficient alternative for biological nitrogen removal from wastewaters with low C/N ratio (Strous et al., 1997). The process consists of ammonium oxidation under anoxic conditions using nitrite as the electron acceptor, which is previously generated in a partial nitritation (PN) process. The main advantages of the PN-anammox process over the conventional activated sludge process (nitrification-denitrification) are lower oxygen consumption, no extra organic carbon addition, and reduction of nitrous oxide emissions (Van Hulle et al., 2010). In addition, the slow growth rate of chemolithotrophic anammox microorganisms (van der Star et al., 2007) results in a very low excess sludge production, but it does require using systems that can ensure biomass retention.

Different reactor configurations based on both biofilm (Fernández et al., 2014) and granular technologies (Dapena-Mora et al., 2004a) devised for optimal sludge retention and proper removal efficiencies have been reported. Both studies claimed that operational conditions such as mixing, shear stress and salinity affected the anammox sludge retention and activity. The main parameter analysed was the shear stress over the granule, considering the mechanical mixing (Arrojo et al., 2006), gas upflow velocity (Arrojo et al., 2008) and recirculation ratio (Jin et al., 2012) as well as the substrate loading rate (Tang et al., 2011). Additionally, another study (Tang et al., 2013) developed a larger model linking a larger number of parameters (packaging density, sludge concentration, the hydraulic retention time and volumetric loading rate) to process performance. These studies all revealed the influence of hydrodynamics on process performance and underscored the need to develop tools accounting for hydrodynamic effects to complement the well-established models that are currently used in bioreactor design.

Activated sludge models (ASMs) (Henze et al., 2000) are the most widely used mathematical models for biological processes in wastewater treatment systems. An extension of ASM that includes the anammox kinetic rates was proposed by Takács et al. 2007. To date, only a few studies have linked ASM models to simple hydrodynamic models focusing on different studies: the effect of anammox granular size distributions (Volcke et al., 2012), the mass transfer from bulk liquid to the granule (Ni et al., 2009) and its correlation with the kinetic removal rate (Vangsgaard et al., 2012). All of the studies mentioned above assume ideal mixing conditions in the bioreactor. However, a complete homogenization is not often feasible, and it is necessary to consider heterogeneous distributions that can contribute to the biomass distribution and substrate availability. In this sense, the development of computational fluid dynamics (CFD) is a powerful solution for wastewater reactor design.

The increase in computer capacity over the last decade has favoured the use of CFDs within a wide range of applications, although few works have addressed wastewater treatment systems (Cockx et al., 1999). The first application of CFD to bioreactors was the design of oxidation ditches, which focused primarily on optimizing the aeration configuration (Gresch et al., 2011) or stabilization ponds (Alvarado et al., 2012), membrane bioreactor (Ratkovich and Bentzen, 2013) and anaerobic digesters (Wu, 2012). Only a couple studies combined biological models and CFDs (Le Moullec et al., 2010; Lei and Ni, 2014). Both studies also considered the oxygen liquid-gas mass transference effects, including oxygen consumption via biological activity. Moreover, both studies considered the sludge as a pseudo-solid phase with a constant concentration.

Considering the results of the previous works mentioned above, the aim of this study is to develop the first modelling approach that integrates an

anammox biological model into a hydrodynamic model by means of CFD. Such a model would be used to evaluate how the internal geometry of an anammox reactor influences the flow and substrate distribution and its impact on the process efficiency.

6.2 Materials and methods

6.2.1 Model development

6.2.1.1 Anammox reactor configuration

The anammox reactor configuration used in this study was a cylindrical stainless steel reactor with an internal diameter of 0.50 m and a height of 2.60 m (total volume 430 L). The reactor design (Figure 6.1) was based on the UASB configuration, which is widely used in the anammox process (Tang et al., 2011). The internal plates were fixed at a slope of ±45 degrees with respect to the *y*-axis and were equally distributed along the reactor height. Each level had four plates perpendicularly oriented relative to the previous level. This design was developed with three objectives: i) to enhance biomass retention in the reactor, ii) to favour turbulent conditions and thereby ensure better mass transfer between liquid and biomass granules, and iii) to improve the flow distribution inside the system.

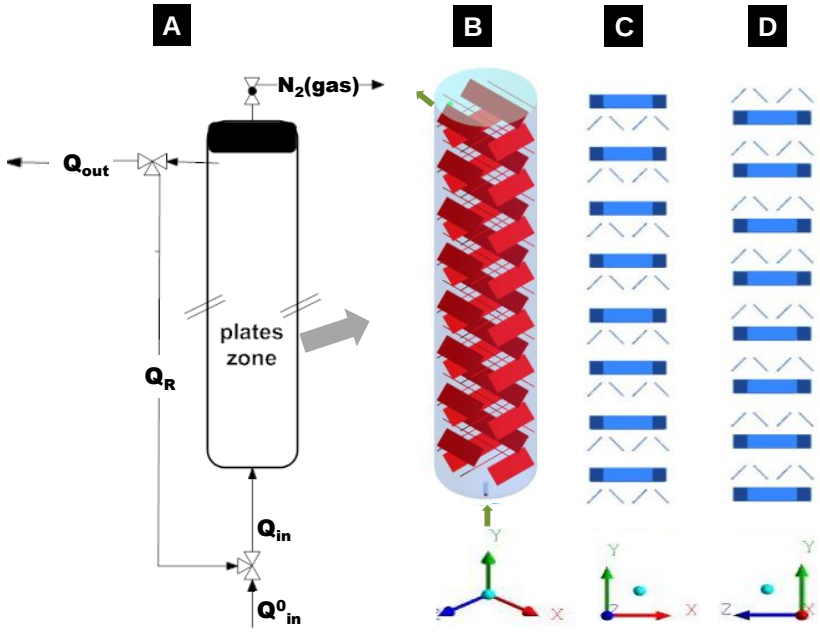

Figure 6.1 Scheme of the anammox reactor simulated in this study: A) flow diagram, B) isometric view of the internal plate distribution, C) view of plane XY, D) view at plane YZ

The system simulated in this study is presented in Figure 6.1. The reactor was continuously fed from the bottom part (Q_{in}^{0} in the column). An internal recirculation stream (Q_R) was applied from a lateral valve (close to the column head) and connected to the feeding line. The outflow stream (Q_{out}) was derived from the recirculation stream. The nitrogen gas generated in the anammox process was accumulated in the head space at the top of the column until the valve was opened due to overpressure (Figure 6.1).

Additionally, system was sealed and pressurized to work at 1 bar over the atmospheric pressure, and was isolated to keep the temperature at 35 ºC, which was controlled by means of an electric resistance connected to the recirculation stream.

6.2.1.2 Hydrodynamic model

The hydrodynamic behaviour of the system was modelled considering the mass, momentum and energy balance equations and solved by means of the Ansys Fluent® CFD solver (Ansys, 2009). The solution for such a system using non-linear equations involved sub-model closure and boundary condition definitions, which are defined below. The turbulence phenomenon was formulated by the RNG k-ε model (Andersson, 2012; Ansys, 2009), since the presence of internal plates in the reactor involved swirling flows.

Regarding the multiphase definition, a water based primary phase containing dissolved species was considered. For model simplification, the reactor was considered to have sludge occupying the space between the bottom part of the reactor to the recirculation stream. Moreover, all the sludge particles were considered to have the same diameter, and the anammox microorganisms' concentration was considered to be constant (this later condition was reasonable formulated due to the low duplication rate of anammox bacteria). Additionally, the activated sludge phase was considered to be totally soluble in water phase, as proposed by Le Moullec (2010b), in order to reduce model complexity. The secondary phase was set as nitrogen gas dispersed in the liquid phase with the assumption of a constant bubble diameter. The governing equations for the multiphase flow were solved using the Euler-Euler approach (Versteeg and Malalasekera, 1995). In the case of the momentum conservation equations, the drag forces between the gas and liquid phases were modelled by the Schiller-Neumann model (Ansys, 2009).

The computer used to perform the hydrodynamic simulations was an Intel Xenon CPU, with a processor of 2.27 GHz and 23.9 GB of RAM. Since the solution of the hydrodynamic equations (mass and momentum) should be accomplished numerically (no analytical solution), the simulated geometry

should be discretized (meshing) at each point of the domain. For this reason, a mesh dependence test considering only water (without dissolved species) had previously been developed. The model response to different mesh grids was analysed to determine the optimal mesh, which was composed of 850717 elements.

To consider the chemical species involved in the anammox process, the CFD model included the species mass balance described by Equation 6.1:

$$\frac{\partial}{\partial t}\left(\alpha_k \rho_k Y_{i,k}\right) + \sum_{j=1}^{3} \frac{\partial\left(\alpha_k \rho_k \overrightarrow{u_j} Y_i\right)}{\partial x_j} = \sum_{j=1}^{3} \frac{\partial}{\partial x_j}\left(\alpha_k \overrightarrow{J_i}\right) + R_i \qquad (6.1)$$

where ρ_k is the density of the liquid phase (*k*); u_j is the velocity vector component; $Y_{i,k}$ is the mass fraction of species *i* (in a phase k); $\overrightarrow{J_i}$ is the diffusion flux of species *i*; and α_k refers to a multiphase volume fraction. Finally, R_i means the production or consumption rate of species *i* relative to the anammox activity described by the biological model.

6.2.1.3 Biological model

The biological model implemented in this study was based on ASM (Henze, M., Gujer, W., Mino, T. and Van Loosdrecht, 2000). The anammox process was defined by the kinetics of ammonium and nitrite substrate consumption, as well as the nitrate and nitrogen gas generation from the model developed by Takács et al. 2007, where the generation and consumption of the nitrogen species were described by Monod's substrate dependence terms for nitrite and ammonium (Table 6.1). The model did not include nitrite inhibition

terms because the maximum concentration did not reach inhibitory values (Scaglione et al., 2012). The kinetic and stoichiometric parameters, based on the literature, are summarized in Table 6.2.

6.2.2 Simulated scenario

The 0.43 m^3 reactor was designed to operate at 1 kg $N \cdot m^{-3} \cdot d^{-1}$, treating 0.34 $m^3 \cdot d^{-1}$ (Q_{in}^0 HRT = 1.3 d) of wastewater with a total nitrogen (TN) influent of 1300 mg $N \cdot L^{-1}$ (556 and 744 mg $N \cdot L^{-1}$ of ammonium and nitrite, respectively), which is in the range of a mature landfill leachate(López et al., 2008). The recirculation ratio (Q_R, Figure 6.1) was set experimentally by the minimum fluidization rate to guarantee granular biomass suspension.

The solids concentration of the anammox biomass was considered constant at 1 kg $VSS \cdot m^{-3}$. The model also assumed that the sludge outflowing within the outflow recirculation stream was negligible. Moreover, heterotrophic activity was neglected in the model because the influent was free of organic matter (Ruscalleda et al., 2010).

The liquid phase was assumed to be saturated with dissolved nitrogen due to the high recirculation ratio (Q_R/Q_{in}) applied to the system. This implies that the generated nitrogen by means of the anammox activity was directly released to the gas phase.

Three types of boundary conditions were defined to solve the set of hydrodynamic equations: velocity inlet, degassing and wall boundary conditions. The specifications for each boundary condition developed in this study are summarized in Table 6.3.

.

Table 6.1 **Simplified kinetic model coupled to the CFD model**

Process	SN-NH4+	SN-NO2-	SN-NO3-	SN-N2	RATE
Growth	$-\left(\frac{1}{Y_{AMX}}+i_{NBM}\right)$	$-\left(\frac{1}{Y_{AMX}}+\frac{5}{3}\cdot 1.52+\frac{4}{3}\right)$	1.52	$\left(\frac{2}{Y_{AMX}}+\frac{2}{3}\cdot 1.52+\frac{4}{3}\cdot\frac{14}{32}\right)$	ρ_{growth}^{AMX}

$$\rho_{grwoth}^{AMX}=\mu_{AMX}^{growth}\cdot\frac{S_{NH4}}{S_{NH4}+K_{NH4}^{AMX}}\cdot\frac{S_{NO2}}{S_{NO2}+K_{NO2}^{AMX}}\cdot X_{AMX}$$

Table 6.2 List of kinetic rate parameters and stoichiometric coefficients used in this study.

Parameter	Value	Unit	Source	Definition
μ_{AMX}^{max}	0.072	d^{-1}	Ni et al., 2009	Anammox maximum growth rate
K_{AMX}^{NO2-}	0.55	g N·m^{-3}	Ni et al., 2009	Affinity constant for NH4+ of X_{AMX}
K_{AMX}^{NH4}	0.73	g N·m^{-3}	Ni et al., 2009	Affinity constant of NO2- of X_{AMX}
Y_{AMX}	0.164	g COD·g N^{-1}	Ni et al., 2009	Yield coefficient for X_{AMX} growth
i_{NBM}	0.07	g COD·gN^{-1}	Gujer et al., 1999	Nitrogen content of X_{AMX}

Table 6.3 **Boundary conditions (BC) definition**

Stream	***Type of BC***	***Definition***
Inlet (Qin – Figure 6.1)	*Velocity inlet*	Loading Rate: 1 kg $N \cdot m^{-3} \cdot d^{-1}$.
		Temperature: 308.15 K
		Species concentration: The result of mixing influent stream (Q_{in}^{0}: 556 mg $N\text{-}NH_4^+ \cdot L^{-1}$ and 744 mg $N\text{-}NO_2^- \cdot L^{-1}$) and recirculation.
		VF_{gas}: = 0
Recirculation stream	*Velocity inlet*	Discharge rate: ~1 kg $N \cdot m^{-3} \cdot d^{-1}$ (depends on species concentration)
		Temperature: 308.15 K
		Species concentration: Obtained from the interior cells adjacent to the recirculation stream (special user defined function)
		VF_{gas}: 0
Liquid-Gas top interphase	*Degassing*	For the liquid this boundary is a non-slip wall and for the gas is an outflow stream. (Fayolle et al., 2007)
Reactor walls/internal plates	*Non-slip walls*	Temperature: 308.15 K

6.2.3 Residence Time Distribution Function

The use of CFD also permitted the simulation of the tracer concentration evolution to obtain information about residence time distribution function (*E*) (Equation 6.2) (Fogler, 2006):

$$E(t) = \frac{C(t)}{\int_0^\infty C(t)dt} \tag{6.2}$$

The mean residence time (t_m) was calculated by Equation 6.3:

$$t_m = \int_0^\infty tE(t)dt \tag{6.3}$$

where E(t) is the function of residence time distribution (RTD) and t is the analysis time.

The variance (σ^2) is an additional parameter that is useful for evaluating the spread of the local distribution times (Equation 6.4):

$$\sigma^2 = \int_0^\infty (t - t_m)^2 E(t)dt \tag{6.4}$$

The model of Tanks in Series (Fogler, 2006) is able to discriminate whether the non-ideal reactor is approaching a tanks in series configuration. The number of tanks in series (*n*) is calculated by Equation 6.5 (Fogler, 2006):

$$n = \frac{\tau^2}{\sigma^2} \tag{6.5}$$

where τ (d) is the space time (volume to flow ratio). Additionally, the residence number (also called quality number) is a measure for determining the closeness to plug flow occurring inside the reactor. The quality number (α) is defined by Equation 6.6:

$$\alpha = \int_0^1 \theta \cdot E(\theta) d\theta + \int_1^\infty E(\theta) d\theta \quad (6.6)$$

where θ is the normalized time (ratio of time to reactor hydraulic or space time, t), and $E(\theta)$ is the normalized RTD. Fractions of fluid volume with a residence time greater than the space time (hydraulic retention time) have a residence number of 1, whereas fractions of fluid volume with a residence time lower than the space time are linearly weighted with time (Brannock, 2003). Hence, the residence number indicates whether the reactor is well mixed or has the presence of short-circuiting or preferable ways of flow. For a perfectly mixed reactor, the quality number is 0.6250, and in the case of two perfectly mixed reactors in series, the quality number is 0.77 (Brannock et al., 2009).

6.2.4 Fluidization assay of anammox biomass granules

Fluidization tests were experimentally performed to determine the minimum fluidization velocity of biomass granules. Experiments were carried out in a water-jacketed tubular glass reactor ($3 \cdot 10^{-2}$ m diameter and $5 \cdot 10^{-1}$ m height), which was fed from the bottom and discharged from the top. The temperature was set to 35 °C for all experiments. A peristaltic pump with a variable frequency drive was used to adjust the up-flow velocity. The system was also equipped with a manometer to measure the pressure decrease in the water column. Granular anammox biomass was obtained from a lab-scale SBR that treated synthetic wastewater at an NLR of approximately 1 kg N m^{-3} d^{-1}. Due to the wide range of anammox granule sizes measured by laser diffraction (Beckman-Coulter laser light scattering instrument LS 13 320 SW), sieves were used to discretize the particles into two separate diameter

ranges: from 63 to 400 µm and from 400 to 1000 µm. Then, fluidization was tested separately for each particle diameter range.

The fluidization test was performed by leaving the particles initially settled and measuring both the pressure drop and the bed height at different up-flow velocities. The minimum up-flow velocity was achieved when the drop in pressure remained constant, despite an increase in the up-flow velocity.

6.3 Results and Discussion

A new reactor design was previously developed (Figure 6.1) to favour the retention of biomass and promote turbulent conditions to enhance liquid-solid mass transport during the anammox process. To evaluate this design, a mathematical model was proposed by integrating the biological model (ASM + anammox model (Takács et al., 2007)) with the hydrodynamic model by using CFD tools. Prior to the modelling work, the minimum up-flow velocity was experimentally determined for maintaining the biomass fluidized in the reactor.

6.3.1 Determination of the recirculation flow

The recirculation flow in the anammox column was based on the minimum fluidized up-flow velocity determined experimentally for the granular anammox biomass.

In the fluidization test (Table 6.4), a minimum fluidization velocity of 5 $m \cdot h^{-1}$ were need for diameters between 63 and 400 µm well fluidized, whereas the largest particles (close to 1000 µm in diameter) required velocities of 10 $m \cdot h^{-1}$. Hence, a mean up-flow velocity of 7.5 $m \cdot h^{-1}$ was considered for an average particle diameter of 500 µm, which gave a recirculation flow of 35 $m^3 \cdot d^{-1}$.

Table 6.4 Experimental fluidization velocities as a function of particle size.

Particle size (mm)	Fluidization velocity ($m \cdot h^{-1}$)
63	5
400	5
1000	10

6.3.2 Hydrodynamic simulation results

A CFD simulation was carried out for the reactor configuration presented in Figure 6.1 to determine the internal hydrodynamic conditions and predict the flow distribution inside the reactor.

The reactor was fed with 0.34 $m^3 \cdot d^{-1}$ (Qin^0) of wastewater containing 504 mg $N \cdot L^{-1}$ of ammonium and 743 mg $N \cdot L^{-1}$ of nitrite. The recirculation flow (Q_R) was set based on the experimental minimum fluidization velocity for a mean particle diameter of 500 µm and resulted in a $Q_R/Q_{in}^{\ 0}$ ratio of 101.

The results obtained from the hydrodynamic analysis are presented in Figure 6.2, which shows the flow streamlines in the reactor. The CFD results allow a differentiation between the up flow velocities (in red), down-flow velocities (in blue), zones with velocities ranging between 0 and 20 $m \cdot h^{-1}$ (grey streamlines) and completely quiet zones (0 $m \cdot h^{-1}$, black). As a general trend, the fluid circulated upwards between the plates and downwards near the reactor wall and towards the central axis of the reactor. This provided an internal recirculation between plates, which favoured the fluid distribution within the overall reactor domain. However, a clear impact of the influent stream (recirculation plus inflow) was observed at the bottom of the column, with faster flow streamlines in the centre and slower flow streamlines moving to the column bottom (black streamlines). This may cause a dead zone in which particles of fluid would be kept completely quiet.

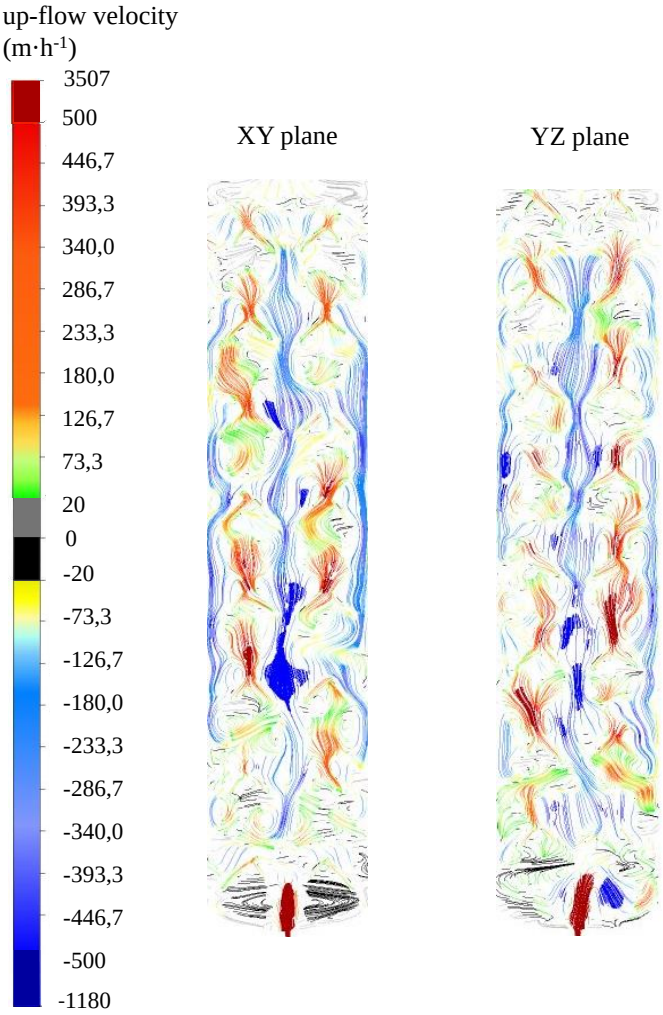

Figure 6.2 Up-flow velocity contours and the projected area vectors for two perpendicular longitudinal sections of the column reactor (XY and YZ planes).

Regarding the fluid velocity along the entire liquid domain, it was interesting to analyse the positive (upwards) and negative (downwards) velocities, which represented 53% and 43% of the total volume, respectively. This indicated the presence of bidirectional flow inside the reactor, which could favour liquid mixing. Only a very low percentage (2.7%) of the domain points

had velocities ranging between 0 and 5 $m \cdot h^{-1}$, indicating the presence of a low number of quiet zones.

To thoroughly analyse the reactor behaviour in terms of the mixing conditions, the RTD was calculated using a CFD simulation by adding a pulse peak through the bottom of the reactor. For this specific simulation, an additional input was defined at the bottom of the reactor in order to directly add the tracer pulse. Figure 6.3 presents the normalized RTD function ($E(\theta)$) versus the normalized time (θ) and the ideal RTD for a perfectly mixed tank reactor (dashed lines) to compare the ideal and real conditions of the system. As shown, the real distribution curve is characterized by an initial concentration peak corresponding to the tracer crossing the column, after which both the simulated and ideal (theoretical) curve profiles are similar. The presence of plates caused a time delay from the instant of the tracer injection to the time that it reached the outflow stream. Then, the high recirculation stream distributed the tracer within the overall domain and the curve profiles approach ideal mixing conditions.

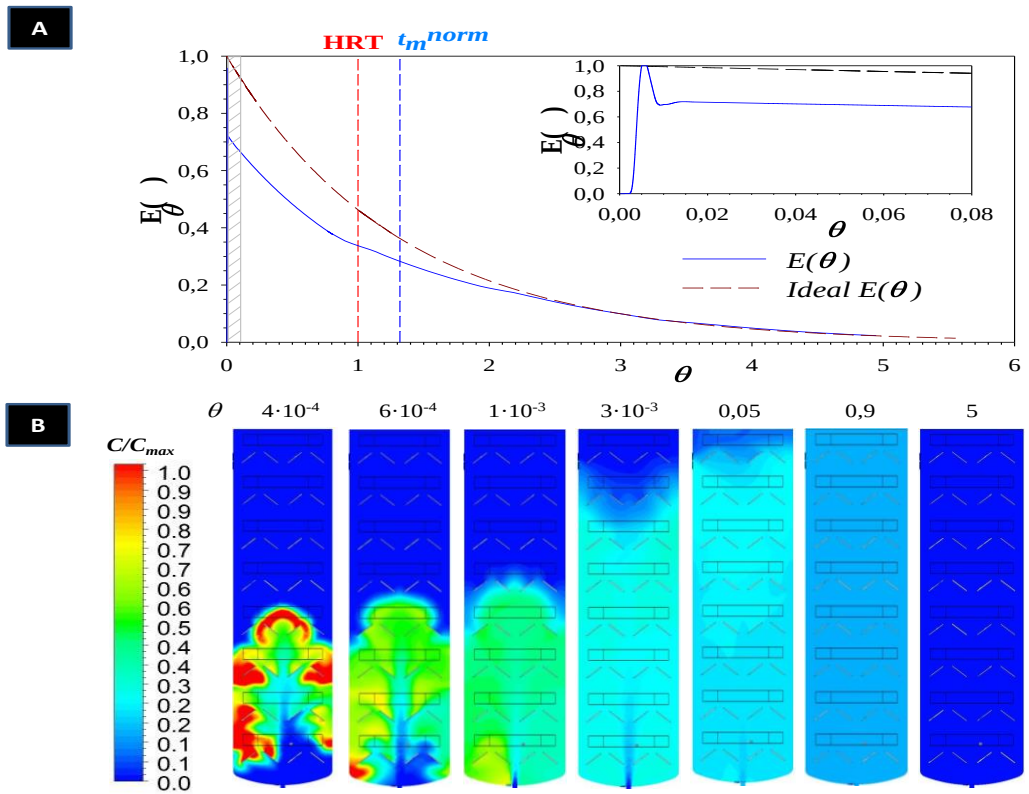

Figure 6.3 A) Residence time distribution of the system simulated (continuous line) and of an ideally mixed tank (dashed line), B) relative tracer concentration contours at different normalized times.(Please note that $\theta = t/\tau$, the same as in Figure 5.5)

From the RTD, a set of parameters were calculated to determine the closeness of the system to ideal mixing conditions (Table 6.5). The calculated mean residence time (t_m) value was 1.72 d, which was slightly higher to the space time (volume to flow ratio) of the system (1.3 d). The calculated value was slightly higher than the theoretical one due to the presence of internal recirculation streams (Figure 6.1). This factor is also highlighted in the variance of the distribution (1.83 d^2, whereas the ideal mixing conditions correspond to 1.64 d^2), indicating that the fluid spent more time in the reactor than what the space time permitted as a result of the internal recirculation produced by the presence of the plates.

Table 6.5 **Results obtained from the RTD function.**

Parameter	Value	Unit
t_m	1.72	d
σ^2	2.1	d
n (tanks in serie)	0.9	-
α (quality number)	0.72	

The result obtained from the tanks-in-series (*n*) model analysis was 0.9, which indicated that the simulated reactor behaviour was close to a perfectly mixed tank. On the other hand, the residence number (α) indicates the closeness of the analysed system to a plug flow system (Equation 6.3). Under ideal mixing conditions, the residence number has a value of 0.625 and 0.737 when there are one and two ideal tanks in series, respectively. The increase in the number of tanks in series results in a logarithmic increase of the residence number up to 1 (plug flow at a high number of tanks in series). The value calculated for the distribution from the simulations of our reactor was

0.72, which again confirmed the closeness of the system to the ideal mixing conditions.

6.3.3 Coupling biological model

A biological model describing the anammox stoichiometry was coupled to the hydrodynamic model. This biological model accounts for the consumption of ammonium and nitrite (substrates) and the generation of nitrogen and nitrate species by the anammox activity. The species concentration contours obtained from the integrated model were presented in Figure 6.4A.

The influent species (ammonium and nitrite) followed a predominant pathway producing a plume of higher ammonium and nitrite concentrations. For the remaining reactor domain, the ammonium concentration was practically fully depleted and remains in low concentrations in the rest of the domain Nitrite followed the same behaviour, although its concentration was slightly higher due to the influent NO_2^-/NH_4^+ ratio.

The ammonium and nitrite removal rates were also analysed (Figure 6.4B). The higher removal rates (approximately 0.4 kg $N \cdot m^{-3} \cdot d^{-1}$) were located in the inlet plume at the bottom of the column due to a greater substrate availability. The rest of the reactor domain, with lower substrate concentrations, presented removal rates between 0.15 and 0.25 kg $N \cdot m^{-3} \cdot d^{-1.}$

Based on the substrate affinity constants of microorganisms, the CFD simulation allows the calculation of the biological reaction rate (anammox) at each point of the reactor domain (Figure 6.4 C) with respect to the maximum specific reaction rate (Equation 6.7). This determines whether the biomass activity is limited by substrate availability along the reactor domain. In this case, since ammonium was the limiting substrate, only the ammonium concentration was considered.

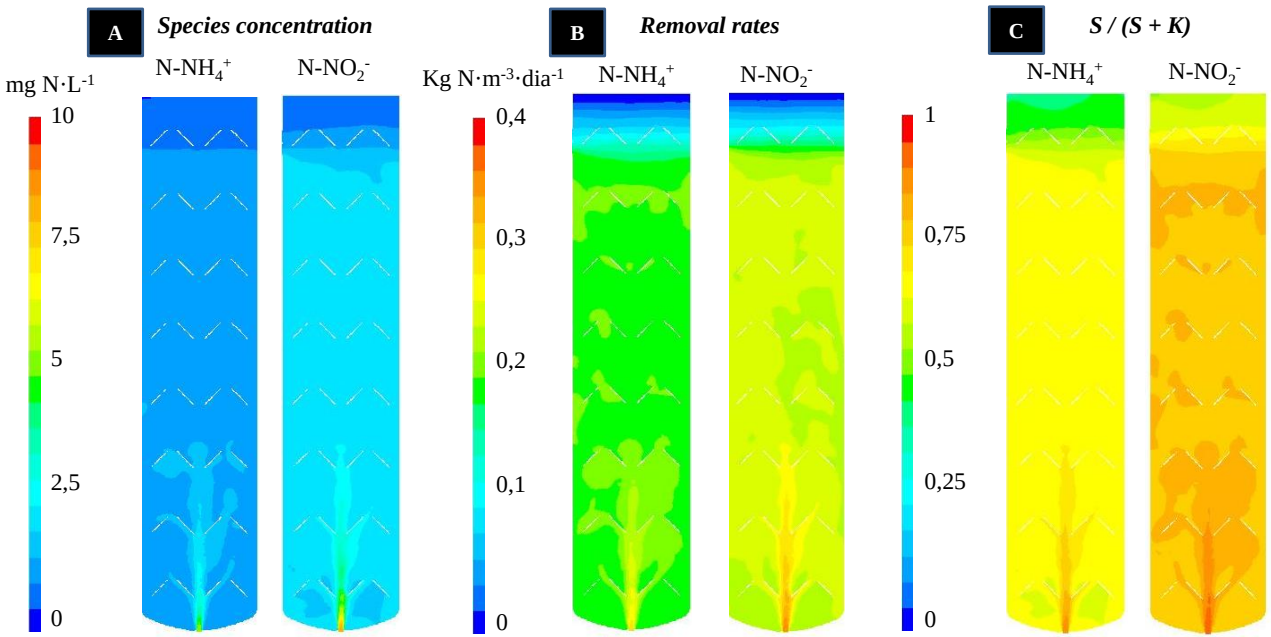

Figure 6.4 A) Ammonium and nitrite concentration profiles; B) Ammonium and nitrite removal rates; C) Substrate dependence terms for ammonium and nitrite species.

$$\frac{\mu}{\mu_{max}} = \frac{S_{N-NH4}}{K_{N-NH4} + S_{N-NH4}} \quad (6.7)$$

Equation 6.7 is the ratio between the rate at a specific point and the maximum rate. For points with ammonium concentrations (S_{N-NH4}) that are twice the semi-saturation constant (K_{N-NH4}), the kinetic term can be considered zero-order (close to the maximum activity value of the microorganisms). However, if the concentration is at least half of the semi-saturation constant value, the reaction rate can be considered first-order; thus, the system is not operating at the maximum rate and depends on the concentration.

Figure 6.4C shows the μ/μ_{max} ratio for the different points of the domain. From this calculation, it is possible to identify the zones of maximum and minimum reaction rates: at the zone of influent stream, the ratio was near 1, and for the rest of the domain, the ratio was close to 0.6. From the biological model it is also possible to determine the order of reaction at each point of the domain. The reaction order based on substrate is calculated by the substrate Monod term of the equation 6.6, which is determined for the ammonium substrate (nitrite in excess). The order of reaction is based on the difference between substrate concentration and substrate assimilation constant (semi-saturation constant, K_{N-NH4} in equation 6.6). The first order reaction is obtained when substrate concentration is clearly lower in comparison to the saturation constant (numerically calculated to be lower than the half of K_{N-NH4}). In such case, the Monod term of equation 6.6 is practically equal to (S_{N-NH4} / K_{N-NH4}). The zero order reaction resulted at large substrate concentration: above twice the constant value, from which the Monod term is practically equal to one. One could assume that the ideal

situation for the biological reaction is to have large number of points of zero order reaction. It was calculated for the overall reactor volume, resulting in a 45% of the entire volume had a zero-order reaction rate for ammonium. It must be noted that part of the reactor domain exhibited a first-order reaction rate. These results are useful for assessing the treatment capacity. In this case, the nitrogen loading rate could be increased without negatively impacting the effluent quality.

In reference to the N_2 gas generated, Figure 6.5 presented the contour profiles of gas volume fraction (VF). The gas generation was linked to microbial activity (nitrogen removal rates) within the overall domain. In this sense, the maximum gas production rate was at the bottom of the reactor. The low gas volumetric ratio was related to the large volume of the reactor compared to the nitrogen generated by microorganism activity.

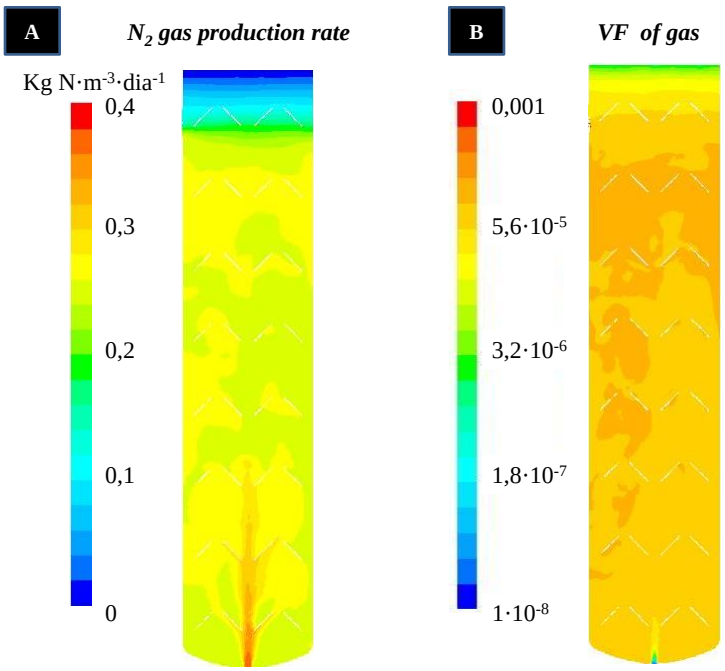

Figure 6.5 Nitrogen production rate (A) and volume fraction profiles (B) through the *xy* and *yz* section planes, respectively.

6.4 Conclusions

This study coupled for the first time an anammox process biological model to the hydrodynamic model by means of CFD. A multiphase model was developed to test the influence of hydrodynamics on a biological process in a reactor with complex internal geometry. The combination of the CFD with the biological model reveals how substrate is distributed and how this affects substrate availability and biomass activity along the reactor domain. The identification of potential dead zones (no substrate available and biomass entrapped due to the hydrodynamics) is of special interest for reactor design optimization. The modelling of the anammox process in this study imposed the simulation of N_2 gas generation and its subsequent behaviour in a multiphase CFD. The Euler-Euler approach was the most suitable solution alternative for this scenario.

The integration of both models was useful for obtaining knowledge about the hydrodynamics inside a novel reactor configuration with internal plates. The CFD simulations demonstrated that the presence of internal plates favoured the generation of internal recirculation points, which ensured mass transference between liquid and granular sludge. The use of CFD facilitated obtaining the RTD distribution curve, indicating ideal mixing conditions. Based on the species results, the substrate was readily removed from the overall domain, and was able to treat a higher nitrogen loading rate. Moreover, the reactor efficiency could be improved by feeding the influent simultaneously at different height points of the reactor (lateral feeding). Additionally, related to this improvement, further research should be done by including the solid phase in the simulations to obtain granule distributions within the reactor. This will produce a better estimation of the solids

distribution and further details about the removal rate distributions within the reactor domain.

DISCUSSION

Chapter 7. **General Discussion**

The design of biological wastewater treatment plants has been always addressed to achieve high efficiency at a low cost and environmental impact, linked with a better use of energy and raw materials. In this sense, the legislation concerning spills of pollutants to the environment is getting more restrictive and pushes engineers to redesign and optimize wastewater treatment facilities to fulfil these objectives. Modelling has been demonstrated to be a useful supporting tool for these purposes.

Activated Sludge Models (ASM) are the most widely used model to describe biochemical reactions occurring in the wastewater biological reactors. It includes several variables and parameters mainly related to the biological performance and removal efficiency, and enables testing the influence of operating conditions (such as influent loading rate, reactor volume, temperature) over the reactor performance. However, assuming homogeneous flow and reactions rates over the reactor domain can turn out to obtain deceptive results, especially in reactors with complex internal design, where perfect mixing conditions could not be considered.

Computational Fluid Dynamics (CFD) coupled to the ASM model is the integrated platform proposed and evaluated in the present thesis for design and optimization of wastewater treatment processes' engineering. The new integrated platform is a proper tool to simultaneously simulate hydrodynamics and biological activity in bioreactors, and including as well the different fluid phases (sludge, liquid and gas phases) existing in such systems.

The Laboratory of Chemical and Environmental Engineering (LEQUIA) from the University of Girona has been working on the development of novel and promising alternatives to the conventional biological wastewater treatments. Among the innovative technologies being developed, two of them were chosen to evaluate the potential of this coupled modelling tool to support

the design and scale up of the processes: Microbial Fuel Cell (MFC) and the anaerobic ammonium oxidation (anammox). Both technologies presented particularities that could be addressed by the integrated platform.

A MFC anodic chamber of 800 mL of capacity was simulated in order to evaluate to assess the suitability of different electrode materials by analyzing substrate distribution as well the current generation. The characteristics of the selected electrode's material (mainly geometry and electrical conductivity) affect the flow, species distribution and reaction rates and the mass transport, as the most relevant. Such impacts have strong influence on the overall performance.

The results obtained claimed that the chamber configuration and operation produced preferable ways of flow, resulting in inhomogeneous substrate distribution. CFD simulations were crucial in determining that the configurations with granular graphite and stainless steel conducted to a better substrate distribution. However the streams distribution profiles demonstrated that flow inside the anode chamber was heterogeneous, with a half of the anode chamber exposed to really low substrate concentration. In spite that biomass was not incorporated as individual solid phase in the model, the high velocities entering the anodic chamber may produce low concentration of attached biomass in this particular zone of the reactor, as reported in Vilageliu-Pons (2016b). Further research should be done using integrated-platform tools to analyze the cause of the microbial community heterogeneity in the anodic chamber. The coupled hydrodynamic and biological study made possible determining that stainless steel mesh is preferable in terms of substrate distribution, electrical conductivity and material costs. The modeling research should be continued by incorporating sludge as a new phase to analyze the effect of shear forces on biofilm distribution, characteristics (thickness, density, shape and microbial

structure) and its biological performance. Additionally, a more complete biological model should be developed including as well the generated gas (carbon dioxide) in a new gas phase and analyze its the effect on the flow distribution.

Regarding the anammox process, reactors design is generally focused on obtaining maximum biomass retention in the reactor, attending the low duplication rate of anammox microorganisms commonly reported for real wastewater application. Moreover, anammox process is usually used in high loading rate facilities but a relatively low substrate concentration should be kept in the reactor domain to prevent inhibition, particularly for nitrite.

The anammox reactor configuration assessed was a 434 L column-shape reactor characterized by the presence of internal plates regularly distributed along the reactor column to promote turbulence (mass transference) and biomass retention. An external recirculation was implemented to maintain the granular biomass fluidized. A multiphase (gas-liquid) hydrodynamic model coupled to the biological model was used to simulate the new design. Simulation results gave information about the flow and species distribution. The gas generated by means of biological activity represented less than 1% of the total liquid volume, resulting in a very limited influence to the flow distribution.

With the analysis of the simulation results it was possible to demonstrate that practically perfect mixing conditions were achieved through the system. In this case, the presence of the internal plates produced a large number of internal recirculation streams which favoured the substrate distribution and mass transference (from bulk liquid to sludge, this should be tested by incorporating a sludge phase in the model), which was the main reason for their implementation. Additionally, the inflow to the reactor produced a clear preferable way of flow at the lowest part of the reactor. From the

biological model, it was observed that nutrient removal was practically obtained at the lower part of the reactor, and really low concentrations were circulated through the upper part of the column reactor. The model permitted to analyse the reaction rates distribution inside the reactor, from which close to the 45 % of the total volume is close to the maximum removal rate respect the ammonium substrate. This kind of information obtained with the integrated platform tool is of special interest and can be very helpful in the design assessment, allowing optimization of compact and high rate solutions.

The main limitation of this model was that anammox microorganism's concentration was considered to be homogeneous and totally dissolved in the water phase. The simulations results demonstrated that the system is able to treat higher nitrogen loading rates. Moreover, the kinetic rate could be increases by distributing the feeding along the reactor height (lateral feeding streams).

The application of the coupled model – CFD and biological – has been demonstrated to be a useful tool to analyse new designs. The main advantages of this modelling technique are summarized in obtaining deep information about the flux (velocities), mixing (residence time distribution), species and removal rates distribution at each point of the reactor domain. This allows determining exactly what is the process performance at each point of the reactor in order to help improving better treatment capacity along the reactor volume and optimal sizing of reactors. The obtained results have implications in several other design aspects, such parameter calibration (Arnaldos et al., 2015) and also in the sensor location (Rehman et al., 2015).

The improvement of the present model should be clearly focused on considering the solid sludge phase, in spite of high computational effort

(increasing number of phases, make more complex simulations). The design of settlers by using CFD models (De Clercq, 2003) is an initial starting point, since a wide range of settling models are proposed (Takács et al., 1991) and could be incorporated within the biological reactions. As far as we know, only a single study (Lei and Ni, 2014) has so far developed simulations by incorporating biological models and considering three phases (sludge, wastewater and dissolved oxygen) to simulate an oxidation ditch. In this study, the sludge phase was incorporated as a pseudo-solid phase, considering it as a liquid phase with rheological properties closer to the solid phase (viscous material).

The simulation of these ternary systems (biomass, liquid and gas) make necessary defining properly the physical and rheological sludge properties in order to be incorporated within the hydrodynamics simulation. This would facilitate the incorporation of biomass transport and reaction models. Further research should be done to introduce mass transference models. The introduction of biomass phase could be done as a granular or biofilm. In case of granulation, additional models of particles size distribution (Nopens et al., 2005) and settling models (Takács et al., 1991) could be used to support the hydrodynamic models and get more reliable results. This is of particular interest in the case of the anammox process, which has tendency to have granular biomass showing large settling velocities and a wide range of particle sizes (Lu et al., 2012).

For the simulation of systems with biofilm attachment (as in MFC), the use of CFDs could be supplied by additional models which account the attachment/detachment rates. For the particular case of MFC reactors, the main model improvement could be addressed by simulating the electrode material (granular graphite, stainless steel, among others) as a porous zone, in which values of porosity and pressure losses should be accounted. Then

the biological model introduced in this zone, considering wall reactions. The bottle neck of applying CFDs for a full simulation of activated sludge system is the high computational effort needed for modelling the growth and decay of microorganisms, due to the large difference in time scale for bio and physic processes.

As a final summary, the simulations results combining CFD and biological models have demonstrated to be a powerful tool to simulate the biological and physical processes occurring inside the reactors, obtaining new insights into process performance and design assessment. This became a new paradigm in the design and optimization of process, and allows the user to get larger information than those experimentally available. However, to be able to re-design and optimize reactors, the introduction of sludge phase is a key parameter to fulfil this objective.

CONCLUSIONS

Chapter 8. **General Conclusions**

The main goal of this thesis was the integration of both Computational Fluid Dynamics (CFD) and biological models (Activated Sludge Models, ASM) for supporting the design of biological wastewater technologies. This model integration was applied in two novel biological reactor designs for nutrient removal. Simulated results demonstrated the feasibility of integrating these models and how it resulted in a powerful tool to get deep knowledge about the internal flux and species distribution. Moreover it revealed information not available in conventional models. The main conclusions obtained in this work are listed below:

Coupling CFD and biological models:

- For the CFD simulations, the Ansys Fluent® solver was used to solve the simulations. This software contained wide range of models and sub-models to perform a wide range of simulations. In this sense, clear objectives and expected results may be previously well defined in order to choose the proper models for the simulations. The proper model definition will involve finer results and lower simulation times.
- The discretization (meshing) works is the most critic process since it determines the quality of the results. It should be a compromise between fine quality results and low simulation time and effort. Additionally the precision and reliability of the results could be also influenced by the model selection.
- Biological model need to be integrated to the hydrodynamic simulation as the source term in the mass balances for each individual chemical species. To do it, special software functions are necessary to introduce biokinetic equations within the mass balances. For the particular case of Ansys Fluent software, this was integrated by the development of user-defined functions, a special code developed. This tool permitted to map

the internal concentrations distributions of the species, as a function of its flow distribution and biological reactions.

- The hydrodynamic simulation of a biological reactor is of special interest in systems with heterogeneous flow distribution or a complex internal configuration. The full description of velocities profiles, residence time distribution and substrate/phases distribution could be simulated in the new reactor, in order to improve its design. It was a clear advantage in front conventional biological model based on ideal flux, generally mixing conditions.
- Residence time distribution (RTD) was also simulated by a tracer and the hydraulic retention time and the degree of mixing conditions could be estimated. Moreover, it was useful to detect death zones and zones of unequal distribution flux.
- The CFD permitted also to calculate the removal rate at each computational point of the domain in order to measure the zones of maximum/minimum removal rates and identify the necessary reactor improvements to optimize nutrient removal.

MFC reactorsimulation

The integrated modeling tool (CFD + ASM) was applied to a MFC anodic chamber to evaluate different electrode material considering their geometry, composition and electrical properties. From this study was stated that:

- The use of granular graphite and stainless steel mesh favored the flux distribution throw the MFC anodic chamber. The large recirculation ratio produced a clear preferable way of flow when operating with a rod graphite electrode. The introduction of such materials produced a better flux distribution;
- Substrate was immediately removed from the influent stream. The high recirculation stream made the substrate to circulate in a half part of the

chamber connecting the influent stream and both recirculation streams. For this reason, substrate concentration at the outflow stream was practically zero.

- The introduction of granular graphite and stainless steel mesh produced a clear deviation between the global hydraulic retention time (0,4 d and 0,5 d for granular and stainless steel plus rod graphite, respectively) and the mean hydraulic residence time distribution (14,5 and 11,6 d, respectively). This is explained by the large recirculation ratio compared to the influent stream, which produced substrate to be large time in circulation between both recirculation streams.
- Maximum removal rate was achieved close to the inlet stream of the system, as a maximum concentration of substrate was achieved at this point. In the zone close to the outflow stream, the removal rate was clearly lower because lower concentrations of substrate reaching this zone.
- In case of MFC anodic chamber,the large recirculation produced that half part of the anodic chamber (close to the influent stream). has the substrate circulating. Then the system is able to treat higher loading rate in order to increase the system efficiency.

Modelling anammox reactor

The integration of both modelling tools was also tested to evaluate a novel anammox reactor configuration with internal plates regularly distributed along the reactor domain and a large recirculation stream (in comparison with the influent stream) to maintain the biogranules fluidized. The simulation results obtained by integrating both models permitted to conclude that:

- The use of internal plates produced internal recirculation streams inside the reactor which could favor the mass transfer of substrate to the granules and also enhanced flow distribution inside the reactor.
- A flux distribution (up and down) was detected in the column despite the bottom part of reactor had a dead zone. From the overall reactor volume, the up-flow velocities represented a 53 % of the volume, a 43 % of the volume being down-flow velocities, and the rest represented death zones or really low velocities (low to 20 $m \cdot h^{-1}$).
- The RTD demonstrated that the flux conditions in the reactor were close to the ideal mixing conditions and it was promoted by the large recirculation ratio.
- The species distribution analysis along the ananmmox reactor evidenced the high removal rate at the lower part of the column while the rest of the column remained at low substrate concentrations.
- In order to improve the overall performance, lateral feeding streams along the column reactor height could be applied increasing substrate concentration and therefore the removal rate.
- The simulation study could be enhanced to obtain more reliable simulations by including a new phase in the multiphase approach: solid phase representing the sludge involved in the biological processes.


APPENDIX

Chapter 9. **Appendix**

9.1 Model development

9.1.1 Mass conservation equation

The governing equations of a fluid flow are developed based on three fundamental laws of physics: i) the mass of a fluid is conserved, ii) the rate of change of fluid particle is equal to the sum of forces on the fluid particle (Newton's second law), iii) the rate of change of energy is equal to the sum of the rate of heat added to the fluid particle and the rate of work done on it (first thermodynamics' law).

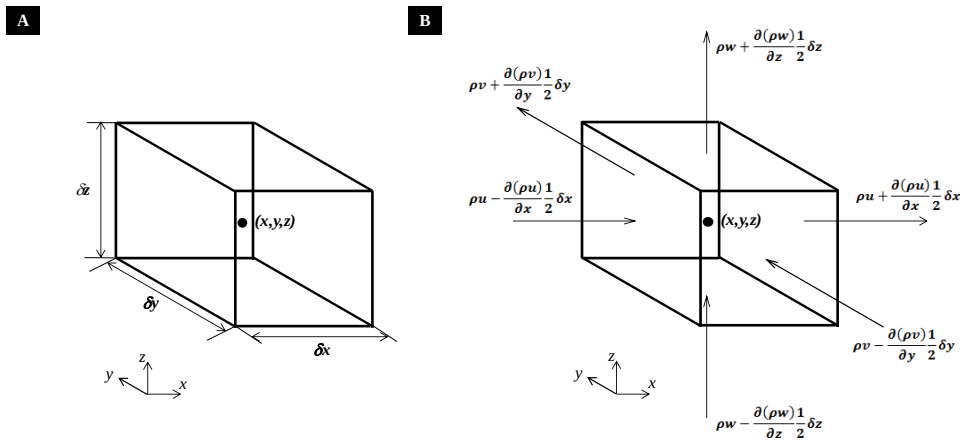

Figure 9.1 Representation of a fluid element in a coordinated system for the development of the mass flow. B) Schematic mass flow balance applied to the fluid element.

Based on these assumptions, one could analyze the flow around a particle of fluid. If one takes an element at macroscopic scale. The mass conservation applied to the fluid particle should be developed balancing the rate of increase of mass on the fluid particle and the net rate of flow of mass into it. From Figure 9.1, one could do the balance (Equation 9.1):

$$\begin{aligned}\frac{\partial}{\partial t}(\rho\delta x\delta y\delta z) \quad = \quad & \left(\rho u - \frac{\partial(\rho u)}{\partial x}\frac{1}{2}\delta x\right)\delta y\delta z - \left(\rho u + \frac{\partial(\rho u)}{\partial x}\frac{1}{2}\delta x\right)\delta y\delta z \\ & + \left(\rho v - \frac{\partial(\rho v)}{\partial y}\frac{1}{2}\delta y\right)\delta x\delta z - \left(\rho v + \frac{\partial(\rho v)}{\partial y}\frac{1}{2}\delta y\right)\delta x\delta z \\ & + \left(\rho w - \frac{\partial(\rho w)}{\partial z}\frac{1}{2}\delta z\right)\delta x\delta y - \left(\rho v + \frac{\partial(\rho w)}{\partial z}\frac{1}{2}\delta y\right)\delta x\delta y \end{aligned} \quad (9.1)$$

Rate of increase of mass in Fluid element — *Net rate of flow of mass into fluid element*

From which it is obtained the mass conservation (continuity) equation for a three dimensional and unsteady flow (Equation 9.2):

$$\frac{\partial \rho}{\partial t} + div(\rho \mathbf{u}) = 0 \quad (9.2)$$

Note that the *div* refers to the divergence vector: $div = \partial/\partial x + \partial/\partial y + \partial/\partial z$. The Equation 9.2 could be simplified in the case of incompressible fluid, which is simplified to (Equation 9.3):

$$div(\rho \mathbf{u}) = 0 \quad (9.3)$$

9.1.2 Momentum equation

The momentum equation is developed base on the Newton's second law, which state that the rate of increase of momentum in a fluid particle is equal to the sum of forces on this fluid particle. There are two kind of forces applied to a particle fluid: i) the surface force which are distinguished between pressure (*p* – normal stress) forces and viscous forces (τ – surfaces forces), and ii) the body forces (gravitational, Coriollis, centrifugal and

electromagnetic forces). The second group of forces (body) are usually accounted as source momentum terms, and the surface forces are usually accounted separately within the momentum equation. If one balance the different forces at each direction of flow (x,y and z), the momentum equations could be obtained as (Figure 9.2):

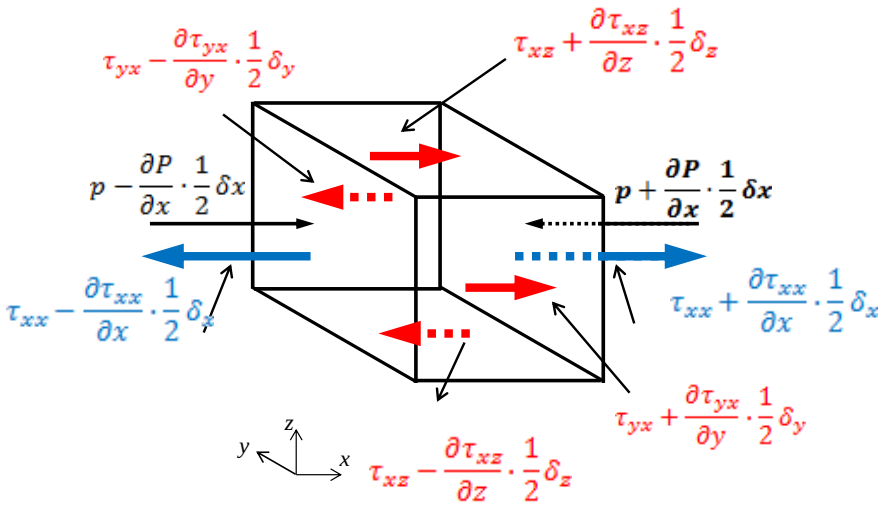

Figure 9.2 Sum of *x*-forces. Momentum balances applied for a fluid element, applied only for the x-direction. Identical vectors should be applied for the rest of directions but changing its nomenclature.

$$\rho \frac{Du}{Dt} = \frac{\partial(-p + \tau_{xx})}{\partial x} + \frac{\partial \tau_{yx}}{\partial y} + \frac{\partial \tau_{zx}}{\partial z} + S_{Mx} \tag{9.4}$$

$$\rho \frac{Dv}{Dt} = \frac{\partial \tau_{xy}}{\partial x} + \frac{\partial(-p + \tau_{yy})}{\partial y} + \frac{\partial \tau_{zy}}{\partial z} + S_{My} \tag{9.5}$$

$$\rho \frac{Dw}{Dt} = \frac{\partial \tau_{xz}}{\partial x} + \frac{\partial \tau_{yz}}{\partial y} + \frac{\partial(-p + \tau_{zz})}{\partial x} + S_{Mz} \tag{9.6}$$

from which *D/Dt* represents the substantial derivative which is defined as (Equation 9.7):

$$\frac{D\emptyset}{Dt} = \frac{\partial \emptyset}{\partial t} + u\frac{\partial \emptyset}{\partial x} + v\frac{\partial \emptyset}{\partial y} + w\frac{\partial \emptyset}{\partial z} = \frac{\partial \emptyset}{\partial t} + \boldsymbol{u} \cdot \boldsymbol{grad}(\emptyset) \tag{9.7}$$

Being ***u*** the velocity vector, and *u, v, w* each dimension of velocity vector.

Regarding the formulation of the stress tensor (τ), the major part of the fluids used in this study –water and air/nitrogen gas– are considered to be Newtonian and isotropic fluids. The first concept is related to how the molecules of a fluid particle are arranged themselves being exposed to a strain. In a Newtonian fluid the viscous stress is directly proportional to the deformation (strain) rate. The three dimensional expression for a Newtonian compressible fluid is related to the linear deformation (μ) and to the volumetric deformation (λ), as it follows:

$$\tau_{ii} = 2\mu\left(\frac{\partial u_i}{\partial x_i}\right) + \lambda \cdot div\, \boldsymbol{u} \tag{9.8}$$

$$\tau_{ij} = 2\mu\left(\frac{\partial u_i}{\partial x_j} + \frac{\partial u_j}{\partial x_i}\right) + \lambda \cdot div\, \boldsymbol{u} \tag{9.9}$$

$$div\, \boldsymbol{u} = \sum_{i=1}^{3} \frac{\partial u_i}{\partial x_i} \tag{9.10}$$

The effect of the parameter λ is less important in the equation particularly for gases and incompressible fluids, since the term and for gases (air/nitrogen) it has been defined to be equal to 2/3·μ. For a incompressible fluid – such water- the divergence vector of velocity (div **u**) is equal to zero,

and then the stress tensor is just twice the local rate of linear deformation times the dynamic viscosity.

For this, replacing the stress viscosity (τ) to the Equations 9.3-9.5 and reordering terms, the Navier-Stokes formulas were obtained (Equation 9.11-9.13)

$$\rho\frac{\partial u}{\partial x}+\rho div(u\boldsymbol{u})=-\frac{\partial P}{\partial x}+div\big(\mu\ grad(\boldsymbol{u})\big)+\ S_{Mx} \tag{9.11}$$

$$\rho\frac{\partial v}{\partial y}+\rho div(\boldsymbol{v}\boldsymbol{u})=-\frac{\partial P}{\partial y}+div\big(\mu\ grad(\boldsymbol{u})\big)+\ S_{My} \tag{9.12}$$

$$\rho\frac{\partial w}{\partial z}+\rho div(w\boldsymbol{u})=-\frac{\partial P}{\partial z}+div\big(\mu\ grad(\boldsymbol{u})\big)+\ S_{Mz} \tag{9.13}$$

9.1.3 Energy equation

The energy equation is developed based on the first thermodynamics law: the rate of change of energy in a fluid particle is produced by the change in the work done over the particle and the heat added into the particle (Equation 9.14) .

$$\begin{matrix}rate\ of\ increase\\ of\ energy\ of\\ fluid\ particle\end{matrix}\quad=\quad\begin{matrix}head\ added\ to\\ fluid\ particle\end{matrix}+\begin{matrix}work\ done\ on\ the\\ fluid\ particle\end{matrix} \tag{9.14}$$

The mathematical model of the energy equation is defined as follows:

$$\rho\frac{DE}{Dt} = \begin{matrix} -div(p\boldsymbol{u}) + \\ \left[\frac{\partial(u\tau_{xx})}{\partial x}+\frac{\partial(u\tau_{yx})}{\partial y}+\frac{\partial(u\tau_{zx})}{\partial z}+\frac{\partial(v\tau_{xy})}{\partial x}+\right. \\ \left.+\frac{\partial(v\tau_{yy})}{\partial y}+\frac{\partial(v\tau_{yz})}{\partial x}+\frac{\partial(w\tau_{xz})}{\partial x}+\frac{\partial(w\tau_{yz})}{\partial y}+\frac{\partial(w\tau_{zz})}{\partial z}\right]+ \end{matrix}\Bigg\} \begin{matrix} work\ by \\ sufrace \\ stress \end{matrix}$$
$$+div(k\cdot grad\ T) \quad \} \begin{matrix} heat \\ conduction \end{matrix}$$
$$+S_E \quad \} \begin{matrix} addit\ energy \\ source \end{matrix} \tag{9.15}$$

$$\rho\frac{D\left[\frac{1}{2}(u^2+v^2+w^2)\right]}{Dt} = \begin{matrix} -\boldsymbol{u}\cdot grad(p)+\mathbf{u}\left(\frac{\partial\tau_{xx}}{\partial x}+\frac{\partial\tau_{yx}}{\partial y}+\frac{\partial\tau_{zx}}{\partial z}\right)+ \\ +v\left(\frac{\partial\tau_{xy}}{\partial x}+\frac{\partial\tau_{yy}}{\partial y}+\frac{\partial\tau_{yz}}{\partial z}\right)+ \\ +w\left(\frac{\partial\tau_{xz}}{\partial x}+\frac{\partial\tau_{yz}}{\partial y}+\frac{\partial\tau_{zz}}{\partial z}\right)+\mathbf{u}\cdot S_M \end{matrix} \tag{9.16}$$

From which the two first terms of the equations were derived from the work added by the surfaces forces to the fluid particle, and the other two terms were derived from the heat conduction through the fluid particle boundaries. The term of E indicates the energy of the fluid particle, which is defined by the internal energy (i) plus the kinetic energy ($1/2 \cdot (u^2+v^2+w^2)$). The kinetic energy equation could be introduced by multiplying each spatial component of the momentum equation by the correspondent velocity component, and resulting in Equation 9.16

From which SM means any external momentum source. If one subtracts Equation 9.14 from Equation 9.15, one could obtain the equation of the Chapter 2 of this thesis, defined in terms of internal energy (Equation 9.17):

$$\rho \frac{Di}{Dt} = \begin{matrix} -p \cdot div(\boldsymbol{u}) + \\ \left[\frac{\partial(u\tau_{xx})}{\partial x} + \frac{\partial(u\tau_{yx})}{\partial y} + \frac{\partial(u\tau_{zx})}{\partial z} + \frac{\partial(v\tau_{xy})}{\partial x} + \right. \\ \left. + \frac{\partial(v\tau_{yy})}{\partial y} + \frac{\partial(v\tau_{yz})}{\partial x} + \frac{\partial(w\tau_{xz})}{\partial x} + \frac{\partial(w\tau_{yz})}{\partial y} + \frac{\partial(w\tau_{zz})}{\partial z}\right] + \\ +div(k \cdot grad\ T) + S_E \end{matrix} \quad (9.17)$$

For an incompressible fluid (*div* ***u*** = 0) – such the major systems included in these thesis - the internal energy is directly proportional to the temperature by means of specific heat (c): i = cT. So the first term of the equation can be removed and the term in the equation is expressed as a: $\rho c\, DT/Dt$. Additionally, in this kind of systems, the tensor vector is considered to be constant, so its spatial variations could be also removed ($\partial \tau_{ii}/\partial x_j = 0$).

9.1.4 Modelling Turbulence

The turbulence motion is related to the chaotic motion of fluid molecules. The main characteristics of the turbulent motion are(Andersson, 2012): i)

irregularity: it is chaotic, occurred in a different spatial directions and different time scales, as well at different rates, ii) diffusivity: the turbulence motion allows a faster mixing rate, momentum and energy transport compared to the molecular diffusion. This is really important in chemical processes, iii) dissipation of turbulent kinetic energy: the turbulence energy is dissipated from large eddy scales to smaller scales. The larger eddies are broken up to smaller, and finally the energy at smaller scales is dissipated in form of molecular viscosity, iv) continuum: the turbulence is encountered at the different flow scales and it permit the continuity of the flow.

For the modelling of fully developed turbulent flows, it is a high computational cost to resolve eddies produced by direct resolution of the Navier-Stokes equations (Direct Numerical Solution) for an incompressible fluid. Despite the increase in the computer capacity, it is necessary to find any form to resolve the turbulence flow for any case with a high number of eddies. Several models had been developed to avoid this. This was accomplished by the development of Reynolds equations.

In a turbulent flow, any flow property φ (such pressure or velocity, among others) is mathematically described as a sum of an average value Φ (steady) of this property and its fluctuation φ' over time (Equation 9.18):

$$\varphi = \Phi + \varphi' \tag{9.18}$$

The steady value is determined as (Equation 9.19):

$$\Phi = \frac{1}{\Delta t}\int_0^{\Delta t} \varphi(t)\, dt \tag{9.19}$$

As one could state, the mean value of the fluctuations (φ') became zero. It is feasible to measure the value of the root mean square of the fluctuations. A useful value to measure the turbulence, its the kinetic energy (per unit mass), defined as (Equation 9.20):

$$k = \frac{1}{2}\left(\overline{u'^2} + \overline{v'^2} + \overline{w'^2}\right) \tag{9.20}$$

Note that *u', v', w'* represents fluctuations of each component of the velocity vector in Cartesian coordinates. Additionally, the turbulence intensity (T_i) is linked to the kinetic energy and to a reference mean flow velocity (U_{ref}) (Equation 9.21):

$$T_i = \frac{\left(\frac{2}{3}k\right)^{1/2}}{U_{ref}} \tag{9.21}$$

Replacing the continuity and Navier-Stokes equations (for instantaneous velocity), in an incompressible fluid with constant viscosity, and applying the velocitiy (*u = U+u' ; v = V+v'; w = W+w'*) and pressure (*p = P + p'*) decomposition, one could obtain the following set of equations (Equation 9.22 – 9.25):

$$div\ u = div\ U = 0 \tag{9.22}$$

$$\frac{dU}{dt} + div(U\mathrm{U}) = -\frac{1}{\rho}\frac{\partial P}{\partial x} + \nu div\ grad\ U + \left[-\frac{\partial \overline{u'^2}}{\partial x} - \frac{\partial \overline{u'v'}}{\partial y} - \frac{\partial \overline{u'w'}}{\partial z}\right] + S_{Mx} \tag{9.23}$$

$$\frac{dU}{dt} + div(V\mathrm{U}) = -\frac{1}{\rho}\frac{\partial P}{\partial y} + \nu div\ grad\ V + \left[-\frac{\partial \overline{u'v'}}{\partial x} - \frac{\partial \overline{v'^2}}{\partial y} - \frac{\partial \overline{v'w'}}{\partial z}\right] + S_{My} \tag{9.24}$$

$$\frac{dU}{dt} + div(W\mathrm{U}) = -\frac{1}{\rho}\frac{\partial P}{\partial z} + \nu div\ grad\ W + \left[-\frac{\partial \overline{u'w'}}{\partial x} - \frac{\partial \overline{v'w'}}{\partial y} - \frac{\partial \overline{w'^2}}{\partial z}\right] + S_{Mz} \tag{9.25}$$

From which ν variable denotes kinematic viscosity. The resulting equations of applying the decomposition are known as the Reynolds Average Navier Stokes (RANS) equation.

The right hand in the momentum equations is the added term due to the time decomposition, and is called the Reynolds stress. The Reynolds stress is not directly a stress applied to the fluid (such with the viscous stress), is a transport of momentum due to the velocity fluctuations. For a high turbulence flow, the Reynolds stress could be clearly bigger than the viscous stress.

The resolution of these equations including the Reynolds stress terms involves extra independent variables (extra additional stresses) and for this,

six new constraints should be defined to resolve the system. Additionally, resolving the transport on a scalar in a turbulent flow, there are also incorporated the turbulent terms. The time average equation (Equation A26) for a transport of a scalar is presented here (Equation 9.26):

$$\frac{\partial \Phi}{\partial t} + div(\Phi \mathbf{U}) = \mathrm{div}(\Gamma_{\Phi}^{*} grad\ \Phi) + \left[-\frac{\partial \overline{\mathrm{u}'\varphi'}}{\partial \mathrm{x}} - \frac{\partial \overline{\mathrm{v}'\varphi'}}{\partial \mathrm{y}} - \frac{\partial \overline{\mathrm{w}'\varphi'}}{\partial \mathrm{z}} \right] + \mathrm{S}_{\Phi} \tag{9.26}$$

As mentioned above, in the resolution of RANS equations, it is necessary to close the resolution of the Partial Differential Equations. In a wide range of applications of simulations, it is not necessary to define exactly each turbulence eddy, it is enough to evaluate how it is affecting over the flow, so it is necessary to define the effect of the Reynolds Stress terms in the momentum and scalar transport equations. The models based on the Reynolds averaged equations are presented here:

- Zero equation model: mixing length
- Two equations models: k-e models
- Algebraic/stress models

The zero order and two order equation models are based on the assumption that there exists and analogy between the viscous stress and the Reynolds stress. As could be observed through the different equations developed above, these stress terms appears all on the right hand of momentum equations. For an incompressible isothermal flow, the turbulence tends to decay, except when a shear rate is applied over the fluid. Additionally, the turbulent stress tends to increase when the deformation rate is increased.

For such reason, the Boussinesq approximation was formulated in such manner that the turbulent (Reynolds) stress could be considered directly proportional to rate of deformation. Next equations expressed such analogy (Equation 9.27 – 9.28):

$$\tau_{ij} = \mu e_{ij} = \mu\left(\frac{\partial u_i}{\partial x_j} + \frac{\partial u_j}{\partial x_i}\right) \qquad viscous\ stress \tag{9.27}$$

$$\tau_{ij} = -\rho\overline{u_i' u_j'} = \mu_t\left(\frac{\partial u_i}{\partial x_j} + \frac{\partial u_j}{\partial x_i}\right) \quad Reynolds\ stress \tag{9.28}$$

Note that the suffix i-j denotes any of the Cartesians coordinates *(x,y,z)*. It could be also expressed a kinematic turbulent viscosity ($v_t = \mu_t/\rho$). The turbulent scalar transport equation could be also developed similarly, since it could be defined to be proportional to the gradient of the scalar (Equation 9.29):

$$-\rho\overline{u_i'\varphi'} = \Gamma_t \frac{\partial \Phi}{\partial x_i} \tag{9.29}$$

The value Γ_t is defined as the turbulent diffusivity. Eddy mixing involves the turbulent transport of momentum, heat and mass, so it is expected that both values of turbulent viscosity (μ_t) and turbulent diffusivity (Γ_t) are proportional. There is a ratio to balance its difference, known as Schmidt number, that balances the turbulent viscosity over the turbulent diffusivity. In CFD modelling works, it is usual to work with values ranging 0.5 and 1. The definition of the Schmidt number is presented here (Equation 9.30):

$$Sc_t = \frac{\mu_t}{\rho\Gamma_t} \tag{9.30}$$

9.1.4.1 k-ε model

As mentioned above, the mixing model is only to accomplish for such situations of two dimensional mixing layers, boundary layers, among others. In systems where both diffusion or convection processes could not be neglected, it is necessary to develop further models to resolve the turbulence phenomena. The k-ε model (Equations 9.31-9.33) is focused in the turbulent kinetic energy (k), and the phenomena affecting its variation:

$$K = \frac{1}{2}(U^2 + V^2 + W^2) \tag{9.31}$$

$$k = \frac{1}{2}\left(u'^2 + v'^2 + w'^2\right) \tag{9.32}$$

$$k(t) = K + k \tag{9.33}$$

The governing equations of the mean flow kinetic energy (K) – developed by multiplying Reynolds equations (Equation 9.19-9.21) with each correspondent velocity component – and for the turbulent kinetic energy (k) – obtained by multiplying the Navier Stokes equation by each velocity fluctuation component – are presented here (Equation 9.34-9.35):

$$\frac{\partial(\rho K)}{\partial t} + div(\rho K\mathbf{U}) = div\left(-P\mathbf{U} + 2\mu\mathbf{U}E_{ij} - \rho\mathbf{U}\overline{u_i' u_j'}\right) - 2\mu E_{ij}\,E_{ij} + \rho\overline{u'_i u_j'}\cdot E_{ij}$$

$$\underset{change\ of\ K}{Rate\ of} + \underset{by\ convection}{Transp.\ of\ K} = \underset{by\ pressure}{Transp.\ of\ K} + \underset{by\ viscous\ stress}{Transp.\ of\ K} + \underset{by\ Reynolds\ stress}{Transp.\ of\ K} - \underset{of\ K}{Dissipation} + \underset{production}{Turbulence} \quad (9.34)$$

$$\frac{\partial(\rho K)}{\partial t} + div(\rho K\mathbf{U}) = div\left(-\overline{p'\mathbf{u}'} + 2\mu\overline{\mathbf{u}'e'_{ij}} - \rho\frac{1}{2}\overline{u_i'\cdot u_i' u_j'}\right) - 2\mu\overline{e'_{ij}e'_{ij}} - \rho\overline{u'_i u_j'}\cdot E_{ij}$$

$$\underset{change\ of\ k}{Rate\ of} + \underset{by\ convection}{Transp.\ of\ k} = \underset{by\ pressure}{Transp.\ of\ k} + \underset{by\ viscous\ stress}{Transp.\ of\ k} + \underset{by\ Reynolds\ stress}{Transp.\ of\ k} - \underset{of\ k}{Dissipation} + \underset{production}{Turbulence} \quad (9.35)$$

From which the term rate of deformation tensor was introduced, $e_{ij}(t)$, which could be also separated in the mean flow and fluctuating component: $e_{ij}(t) = E_{ij} + e'_{ij}$. Both equations are similar, but from the second one it could be stated that the appearance of the fluctuating terms shows that the turbulent kinetic energy is governed by the turbulent interactions. Is interesting to analyze the viscous dissipation term: $-2\mu\overline{e'_{ij}e'_{ij}}$ which has a negative value, that means the dissipation of energy caused by the smallest turbulent eddies. For this reason, it is necessary to define the rate of dissipation per unit of mass: $\varepsilon = 2\nu\overline{e'_{ij}e'_{ij}}$ (from which ν denotes the kinematic viscosity). The resolution of both equations has a lot of uncertain terms. This motivated the development of different models to try to disclaim the impact of the turbulence over the flow.

The standard k-e model, assumes that the turbulent viscosity (units of $m^2 \cdot s^{-1}$) is proportional to a turbulent velocity scale ϑ ($m \cdot s^{-1}$) and to a length scale ℓ (units of m), being C a dimensionless constant of proportionality (Equation 9.36):

$$\mu_t = C\vartheta\ell \tag{9.36}$$

Both ϑ (Equation 9.35) an ℓ (Equation 9.36) parameters could be expressed as a function of turbulent kinetic energy (k) and dissipation rate (ε). A dimensional study was developed to define a velocity scale (ϑ) and length scale (ℓ):

$$\vartheta = k^{1/2} \tag{9.37}$$

$$\ell = \frac{k^{3/2}}{\varepsilon} \tag{9.38}$$

The introduction of such small eddies variable (ε) has sense, since the energy obtained by the largest eddies from the mean flow is proportional to the rate of converting these eddies to smaller and dissipating eddies, at high Reynolds number. As mentioned above, one could express the eddy viscosity as (Equation 9.39):

$$\mu_t = C\rho\vartheta\ell = \rho C_\mu \frac{k^2}{\varepsilon} \tag{9.39}$$

With the C_μ being a dimensionless constant. Then the standard k-ε model used these equations (Equation 9.40-9.42):

$$\frac{\partial(\rho k)}{\partial t} + div(\rho k\mathbf{U}) = div\left[\frac{\mu_t}{\sigma_k} grad\ k\right] + 2\mu_t E_{ij} \cdot E_{ij} - \rho\varepsilon \tag{9.40}$$

$$\frac{\partial(\rho\varepsilon)}{\partial t} + div(\rho\varepsilon\mathbf{U}) = div\left[\frac{\mu_t}{\sigma_k} grad\ \varepsilon\right] + C_{l\varepsilon}\frac{\varepsilon}{k}2\mu_t E_{ij} \cdot E_{ij} - C_{2\varepsilon}\rho\frac{\varepsilon^2}{k} \tag{9.41}$$

$$\begin{matrix} Rate\ of \\ change\ of\ k\ or\ \varepsilon \end{matrix} + \begin{matrix} Transport\ of\ k\ or \\ \varepsilon\ by\ convection \end{matrix} = \begin{matrix} Transport\ of\ k\ or \\ \varepsilon\ by\ diffusion \end{matrix} + \begin{matrix} Production\ of \\ k\ or\ \varepsilon \end{matrix} \_ \begin{matrix} Destruction \\ k\ or\ \varepsilon \end{matrix} \quad (9.42)$$

Where well defined and validated values the constants C_{μ}=0.09, σ_k=1.00, σ_{ε}=1.30, $C_{1\varepsilon}$=1.44, C_{2C} =1.92. The Boussinesq extended relation (Equation 9.43) was developed to solve the Reynolds stress:

$$-\rho\overline{u_i'u_j'} = \mu_t\left(\frac{\partial U_i}{\partial x_j} + \frac{\partial U_j}{\partial x_i}\right) - \frac{2}{3}\rho k\delta_{ij} = 2\mu_t E_{ij} - \frac{2}{3}\rho k\delta_{ij} \quad (9.43)$$

From which the parameter δ_{ij} is the Kronecker delta (Equation 9.44):

$$\begin{cases} \delta_{ij} = 1\ if\ i = j \\ \delta_{ij} = 0\ if\ i \neq j \end{cases} \quad (9.44)$$

It should be keep in mind that the Boussinesq approximation is developed for an isotropic model for the Reynolds stress and assumes that normal stresses are equal. The standard k-ε model is a widely used model. However, few limitations were encountered due the imposition proceeding of the Boussinesq approximation, which imposes isotropic flows. Other problematic about this model was found on the way of developing the dissipation equation. Additionally, the parameters should be adjusted for each simulation. It was necessary to develop improved model to face the limitations from the standard model. The most accepted variations (and formulated in Fluent software), are the RNG and realizable k-ε models.

The RNG k-ε model, was formulated with a new energy dissipation equation, incorporating a new source term, S_E (Equation 9.45-9.47):

$$\frac{\partial(\rho\varepsilon)}{\partial t} + div(\rho\varepsilon\mathbf{U}) = \\ = div\left[\frac{\mu_t}{\sigma_k} grad\ \varepsilon\right] + C_{l\varepsilon}\frac{\varepsilon}{k}2\mu_t E_{ij}\cdot E_{ij} - C_{2\varepsilon}\rho\frac{\varepsilon^2}{k} \\ - S_E \tag{9.45}$$

$$S_E = \frac{C_\mu \eta^3(1-\eta/\eta_0)\varepsilon^2}{(1+\beta\eta^3)k} \tag{9.46}$$

$$\eta = \frac{k}{\varepsilon}\sqrt{2S_{ij}S_{ij}} \tag{9.47}$$

From which both parameters η_0 and β had calibrated values. The introduction of this additional source is useful for situations with high strain rate; this additional term involves a smaller destruction of dissipation rate, and then reducing turbulent kinetic energy, reducing the effective viscosity. For this, this model is useful in situations with swirling flows and strong curvature. It should be noted that this model is not useful for jets and plumes, for which standard model is more useful.

The realizable model is focused in the Reynolds stress tensor (eq 24), which by definition, must be negative, because of the negative sign and a product of turbulent velocities (either positive or negative). Otherwise, in such situations with larger strain (E_{ij}) the sign could become positive. What is doing the realizable model is regulate the value of C_μ in order to avoid the

Reynold stress term to become positive. This model is useful for those situations with high strain such curvature streamlines or rotational systems.

9.1.5 Multiphase models

The multiphase modelling is the art of solving mass, momentum and energy equations for two or more phases, and including the interactions between the two or more phases. There is a wide range of multiphase systems. A classification of industrial processes – based on the multiphase simulations - is given by the next table (Table 9.1):

Table 9.1 **Multiphase flows cases**

Continuous phase + dispersed phase	***Industrial application***
Gas + solid flows	Pneumatic conveying, fluidized beds, solid separation (filters, cyclones)
Liquid – solid flows	Stirred vessels, liquid-solid separation, hydraulic conveying
Gas-liquid (droplets) flows	Spray drying, spray cooling, spray painting
Liquid-droplet flows	Mixing, separations, extraction
Liquid-gas (bubble) flows	Flotation, aeration, bubble columns

When defining multiphase flows, it is necessary to define several concepts. The first one is the volume fraction, defined as the volume that one (dispersed or secondary) phase is occupying in a determined volume, which is usually a computational cell volume. The volume fraction (α) is defined in Equation 9.48:

$$\alpha = \frac{\sum_{i=1}^{N} V_i}{V} \tag{9.48}$$

From which *N* means the number of secondary or dispersed phases (not including the primary or continuous phase), *Vi* is the volume occupied by the secondary phase, and *V* is the total volume (computational cell). As one could state, the sum of all the volume fractions (including the primary phase) must be equal to Flows are classified in two groups regarding the secondary phase volume fraction: i) diluted flows, in which the particle motion is only affected by the fluid forces (drag and lift); ii) dense flows, in which the particles movement is controlled by collisions between particles (such in fluidized beds) or by the continuous contact between particles. There are other parameters which are used when modelling particles or droplets. The use of these parameters has not been used in this thesis, because only liquid-gas systems have been modelled.

Regarding the modelling of multiphase systems, there are several approaches. All of them would be mentioned and briefly explained, but a deep development will be done for those methods used in this thesis (gas-liquid simulations). Two kind of approaches existed: the Eulerian-Lagrangian methods and Euler-Euler methods. The main difference between these two approaches remains in the treatment of the dispersed (secondary) phase.

In the first case, the Eulerian-Lagrangian methods treat the primary phase as a continuum solving the Navier-Stokes equations. For the secondary phase, the movement of each particle is modelled, treating each particle as perfectly spherical and really small, by the second Newton's Law. Continuous and particle phases could exchange momentum, mass and energy. The use of

this method is limited to really low volume fractions of secondary phase (lower to 10%).

The Eulerian-Eulerian approach treats both fluid and the dispersed phases as interprenating continua: the momentum, mass and energy equations were solved for each phase. These equations are usually closed by the use of empirical equations. Three models exist using this approach: VOF model, mixture model and Euler model. The mixture model resolves the equations for the mixture and to describe the secondary phases uses the relative velocity between mixture and dispersed phases. This model is useful for sedimentation, bubbly flows or stirred reactors, among others. The Euler model is more complex because it resolves one momentum equation and one continuity equation for each phase. It is used in a bubble columns, risers or fluidized beds, among others.

9.1.6 Eulerian model

The equations of the Eulerian model are based on the above mentioned volume fraction α -equation 46). The sum of all the fractions should be equal to one, and the effective ($\rho_q{}'$) density of each phase is the product of the volume fraction of the phase and its density (ρ_q). The mass conservation equation is developed as follows (Equation 9.49):

$$\frac{\partial}{\partial t}\left(\alpha_q \rho_q\right) + \nabla \cdot \left(\alpha_q \rho_q \overrightarrow{v_q}\right) = \sum_{\mathrm{p=1}}^{\mathrm{N}} \left(\dot{\mathrm{m}}_{\mathrm{pq}} - \dot{\mathrm{m}}_{\mathrm{qp}}\right) + \mathrm{S_q} \qquad (9.49)$$

From which $\overrightarrow{v_q}$ is the velocity of the phase q, N is the number of phases, $\dot{\mathrm{m}}_{\mathrm{pq}}$ is the mass transfer from phase p to phase q, and $\dot{\mathrm{m}}_{\mathrm{qp}}$ and you are able to

model them separately. The term S_q involves any mass source term at phase q.

The momentum equation for a *qth* phase is (Equation 9.50):

$$\frac{\partial}{\partial t}\left(\alpha_q \rho_q \boldsymbol{u}_q\right) + \nabla \cdot \left(\alpha_q \rho_q \boldsymbol{u}_q \boldsymbol{u}_q\right) = -\alpha_q \nabla p + \nabla \cdot \bar{\tau}_q + \alpha_q \rho_q \vec{g} + \\ + \sum_{p=1}^{n} \left(\vec{R}_{pq} + \dot{m}_{pq} \boldsymbol{u_{pq}} - \dot{m}_{qp} \boldsymbol{u_{qp}}\right) + \vec{F}_q + \vec{F}_{add,q} \quad (9.50)$$

From which $\vec{F}_q$ is an external body force, $\vec{F}_{add,q}$ incorporates phases forces which included the lift forces, virtual mass forces, wall lubricant forces and turbulent dispersion forces. All of them are included or not depending on the specification of each simulation case. The term $\vec{R}_{pq}$ incorporated interaction forces between phases. Regarding the term $\bar{\tau}_q$ is defined as (equation 9.51):

$$\bar{\tau}_q = \alpha_q \mu_q \left(\nabla \boldsymbol{u_q} + \boldsymbol{u_q^T}\right) + \alpha_q \left(\lambda_q - \frac{2}{3}\mu_q\right) \nabla \boldsymbol{u_q} \bar{I} \cdot \quad (9.51)$$

From which μ_q and λ_q are the shear and bulk viscosity of the q phase, respectively.

An important parameter to define mass and momentum transfer between phases, is the well-known interfacial area between phases. The interfacial area (A_P) – equation 50 - is obtained by the ratio between the surface area and the volume of spherical bubble (Equation 9.52):

$$A_i = \frac{\pi {d_p}^2}{\frac{1}{6}\pi {d_p}^3} = \frac{6}{d_p} \tag{9.52}$$

In fact, when modelling a multiphase model, such in case of Eulerian model, it is necessary to relate this interfacial area to the volume fraction (α_q – Equation 9.53):

$$A_i = \frac{6(1-\alpha_p)}{d_p} \tag{9.53}$$

It is also necessary to define how the bubbles or droplets (secondary phase) are interacting with the primary phase. In this sense, the exchange coefficient is defined as (Equation 9.54):

$$K_{pq} = \frac{\rho_p f}{6\tau_p} d_p A_i \tag{9.54}$$

From which f is the drag function (explained later) and the parameter τ_p refers to the particulate (bubble/droplet) relaxation time, and it is defined as (equation 9.55):

$$\tau_p = \frac{\rho_p {d_p}^2}{18\mu_q} \tag{9.55}$$

Being d_p the diameter of the secondary phase. Regarding the drag function – above mentioned – is a function which includes the drag coefficient that depends on the Reynolds number. There are several models defined on the drag coefficients and momentum exchange, depending on the fluid-fluid pair. Ansys Fluent(Ansys, 2009) incorporates a wide ranges of it. For the simulations used in this study - water-nitrogen multiphase simulations – the Schieller – Naumann Model was used (Equation 9.56):

$$f = \frac{C_D Re}{24} \tag{9.56}$$

Where C_D is the drag coefficient, and Re refers to the Reynolds number. In this sense, the drag coefficient (C_D – Equation 9.57) is defined by:

$$C_D = \begin{cases} 24(1 + 0.15Re^{0.687})/Re & Re \leq 1000 \\ 0.44 & Re \geq 1000 \end{cases} \tag{9.57}$$

Which in this case, *Re* (Equation 9.58) is referred to the relative Reynolds number, which is defined as:

$$Re = \frac{\rho_q \left| \overrightarrow{v_p} - \overrightarrow{v_q} \right|}{\mu_q} d_p \tag{9.58}$$

From which *q* is the primary phase and p is the secondary phase.

9.2 Solver theory – Solution Methods and Solution Controls

Solution Methods is the step in the simulation after defining materials and models used. Those methods are distinguished between spatial and temporary discretization. Regarding the resolution of general scalar equations, the scalar values are in general stored in the cell centres. However, when resolving convective-diffusive fluxes, it is necessary to define the flux through the cell faces to resolve the convective terms (it is important to know about the flux direction, and average the net flux through the cell). To do it, the upwind approach was developed to calculate the flow through cells and resolve numerically the general transport equation within the overall domain. The upwind scheme used the values of the upstream cells to calculate the flux at the actual cell. In Ansys Fluent® there are developed four different upwind methods: first order upwind, second order upwind, power law and QUICK. Ansys Fluent® defined the first order upwind in such manner that the flow through a face is identical to the value of the upstream cell. The power-law determines the face value of a variable solving the exact solution of one-dimensional convection-diffusion equation. The second order upwind scheme, the variable quantities at the faces cells are calculated from two cells upstream. This methodology required the determination of the scalar variable gradient for the prediction of the new value. Regarding the QUICK

method (*Quadratic Upstream Interpolation for Convective Kinetics*) is a method of high order, which is based in a combination of the second-order upwind and the central differencing methods. This later method is used for quadrilateral o hexahedral meshes, and performs better the solution when the structured grid is oriented to the flow direction. The software also incorporated more sophisticated methods, which were not used in the development of this thesis. To obtain further information about the development of the exposed methods, one should refer the Ansys Fluent® Theory Guide(Ansys, 2009).

Additionally, the solution methods for the pressure-velocity coupling need also to be defined (*Pressure-Velocity Coupling* from the Solution Methods). An additional constraint in the resolution of the Navier Stokes equations relies in the difficulty of resolving these equations: the convective terms of each momentum equation had no-linear terms (ρu^2) and the difficulty to resolve the pressure variable (which appeared in all the momentum equations) for which no additional pressure equation was formulated. The SIMPLE (*Semi Implicit-Methods for Pressure Linked equations*) algorithm was designed to solve both problematic. The SIMPLEC and PISO methods were improved methods, and the later was specially formulated for multiphase flows. Further information about these methods was explained in Versteeg and Malalasekera, 1995. In cases where the simulations are complex, it is recommended starting the solution with first order methods and after few simulations one could chance to more useful methods.

Last but not least, it is necessary to determine how the solution obtained after each iteration is controlled in order to properly achieves the final solution convergence. In Ansys Fluent® the solution controls are defined in the “Solution Control” panel. The iteratively resolution of flow equations

should follow convergence criterion: in order to obtain reliable from the simulations.

Each of the successive iterations used the value (result) obtained in the previous one (old value) to calculate a new solution for the flow equations. In this sense, a first consideration is the adjustment of the under-relaxation factor values.

The under-relaxation factors are parameters that acts as a buffer of the new solution obtained with respect to the old solution in the iterations. These factors are implemented in the solution of the variables, at least in flow field variables (pressure, momentum and velocities). Hence, the new value, resulting from each iteration, is calculated based on the value predicted in the current iteration and the old value obtained in the previous iteration. The mathematical definition of the under-relaxation factor is presented in Equation 9.59:

$$\emptyset^{new\ value} = \alpha \cdot \emptyset^{new,predicted} + (1 - \alpha) \cdot \emptyset^{old} \tag{9.59}$$

The adjustment of the relaxation factors is a critical point: large values are supposed to accelerate the convergence but could induce to heavy instabilities in the solution and consequently tend to divergence. In opposite, low relaxation values give more stable solution but dramatically increase the time invested to reach convergence. Hence, a good compromise must be achieved. Usually in Ansys Fluent®, the modeller may use the default under-relaxation factors and reduce these values depending on is the ongoing solution.

When modelling cases involving turbulent flows multiphase systems, it is often recommendable to resolve the case by computing the solution sequentially: first solving equations related to flow (pressure, momentum and velocities) and then adding into the solution the rest of equations (turbulence, species equations, multiphase). This technique was followed in the all simulation studies developed in this Thesis.

Finally, the user must choose which variables will be monitored during the CFD simulations. The default monitor shows the residuals profiles as a function of iterations, which allows supervising the convergence of the system. However, it is possible to calculate average, integrals of variables, or also the mass flow. It could be done for a boundary condition, a particular defined plane, lines or points of interest, or maybe for the whole fluid domain. It is also possible to create new variables or custom calculations.

As mentioned above, the convergence of the solution is the parameter used to decide when a simulation is concluded. Since it is not possible to compare the numerical solution to the real solution (i.e. the solution obtained by resolving analytically the equation), it is necessary to define a criteria to stop the simulation. The convergence criteria considers that "when no cell value differs by more than a small threshold (e.g. 0.01) from iteration to iteration, the solution has converged" (Andersson, 2012). Since the studies developed in this Thesis were formulated in a pressure based solver, the definition of the residuals given by Ansys Fluent® (Ansys, 2009) is as follows. The conservation of an arbitrary variable ϕ in a discredited computational cell P is defined as (Equation 9.60):

$$a_P \phi_P = \sum_{nb} a_{nb} \phi_{nb} + b \tag{9.60}$$

From which a_P represents the centre coefficient, a_{nb} the influence coefficients for the neighbouring cells, and b is the contribution of the constant part of the source term (Sc) in the equation S = Sc + Sp ϕ and of the boundary conditions. Equation 18 can be also expressed as (Equation 9.61):

$$a_P = \sum_{nb} a_{nb} - S_P \tag{9.61}$$

If the Equation 9.18 is applied to the whole domain of points P, and it is summed, it results in a unscaled value of the residuals of variable ϕ. It is preferable to calculate the scale value which is the Residual computed by Ansys Fluent® and is formulated as follows (for a pressure based solver; (Equation 9.62):

$$R^{\phi} = \frac{\sum_{cells\ P} \left| \sum_{nb} a_{nb} \phi_{nb} + b - a_p \phi_P \right|}{\sum_{cells\ P} \left| a_p \phi_P \right|} \tag{9.62}$$

For the simulation works developed in this Thesis, the criterion value for convergence was formulated as: $1 \cdot 10^{-3}$ for continuity, turbulence parameters and energy parameters and $1 \cdot 10^{-6}$ for species.

9.3 User defined funcions

9.3.1 Microbial Fuel Cells

The routines developed to perform the MFC simulations are presented here:

```
DEFINE_ADJUST(recirculacio_sortida,domain)
{
    int    zoneID=8;//    cas    malla    id:60050
//40033;//30026;//60050;//pensar en canviar-ho per
cada cas

    Thread *t = Lookup_Thread(domain,zoneID);

    face_t f;
    real ac;
    real sumac=0.;
    real prot;
    real sumprot=0.;
    real acetatR=0.;
    real mac, mprot;
    real tot;
    real sumtot=0.;
    real sumacetatR=0.;
    real velocity;
    real NV_VEC(A);
    begin_f_loop(f,t)
    {

        F_AREA(A,f,t);
        ac=C_YI(f,t,0); //
        //prot=C_YI(f,t,0);
        //F_UDMI(f,t,18)=prot;

        velocity                                    =
sqrt(F_U(f,t)*F_U(f,t)+F_V(f,t)*F_V(f,t)+F_W(f,t)*
F_W(f,t));

        mac = velocity*F_R(f,t)*NV_MAG(A)*ac;

        sumac += mac;

        tot = velocity*F_R(f,t)*NV_MAG(A)*1;
```

```
          sumtot += tot;

     }end_f_loop(f,t)

     CACETAT = sumac/sumtot;

}

DEFINE_PROFILE(conc_recircACETAT,t,nv)
{
     face_t f;

     begin_f_loop(f,t)
     {
          F_PROFILE(f,t,nv)=CACETAT;

     }end_f_loop(c,t)

}

DEFINE_SOURCE(mean_age_source,c,t,dS,eqn)
{
          double source=C_R(c,t);

          dS[eqn]=0.0;

          return source;
     }

DEFINE_ON_DEMAND(intensitat)
{

     double xa[ND_ND], vol = 0., acetat_removed=
0., cod_removed= 0., cabal= 0., intensity= 0.,
methane=0., intensity2= 0., methane2=0.,
conversio= 0., orr= 0., qa =0., qm=0., qa2 = 0.,
qm2 = 0.;
     int ncelles;

     Domain *domini;

     Thread *t;
     face_t f;
```

```
      Thread *tf;
      cell_t c;

      domini=Get_Domain(1);

      conversio = 0.0;

      thread_loop_c(t,domini)
      {

            begin_c_loop_all(c,t)
            {

                  C_CENTROID(xa,c,t);

                  intensity = 0.;
                  //cas3: xc[0] > -1.05e-1 && xc[1] <
0.086 && xc[0] < 0.94e-1
                  //cas2 granular nou : xc[0] > -
0.0935 && xc[1] < 0.092 && xc[0] < 0.107
                  if (xa[0] > -0.0935 && xa[1] <
0.092 && xa[0] < 0.107)
                  {

                              ncelles = ncelles +1;
                              vol     =     vol     +
C_VOLUME(c,t); //volum total

                              qa      =      qa     +
C_UDMI(c,t,0)*0.5*C_VOLUME(c,t); /* kg S seg-1 */
                              qm      =      qm     +
C_UDMI(c,t,1)*0.25*C_VOLUME(c,t);   /* kg S seg-1
*/
                              qa2     =     qa2     +
C_UDMI(c,t,0);
                              qm2     =     qm2     +
C_UDMI(c,t,1);

                  }


            }end_c_loop_all(c,t)

      }
```

```
    qa2 = qa2 / ncelles;
    qm2 = qm2 / ncelles;

    intensity = qa*1000*8*96485000/60;
    methane = qm*0.3*86400*1e6;

    intensity2 = qa2*0.5*vol*1000*8*96485000/60;
    methane2 = qm2*vol*0.25*0.3*86400*1e6;

    printf("volum     total     fluid     (Litres)
%g\n",vol*1000);

    printf("qa average (kgs·KgX·seg-1) %g\n",qa2);
    printf("qa average (kgS·kgX·seg-1) %g\n",qm2);

    printf("qa term (kgs·seg-1) %g\n",qa);
    printf("qa term (kgs·seg-1) %g\n",qm);

    printf("intensitat(mA)   experimental   %g\n",
intensity);
    printf("methane(mg/dia)   experimental   %g\n",
methane);

    printf("intensitat(mA)     2nmètode     %g\n",
intensity2);
    printf("methane(mg/dia)     2nmètode     %g\n",
methane2);

    methane = 0.;
    intensity = 0.;
    methane2 = 0.;
    intensity2=0.;
    qa = 0.;
    qm = 0.;
    qa2=0.;
    qm2=0.;
    vol = 0.;

}

DEFINE_INIT(entrada_acetat,domain)
{
    cell_t ca;
    Thread *ta;
```

```
      real xp[ND_ND];

      thread_loop_c(ta,domain)
      {

            begin_c_loop_all(ca,ta)
            {

                  C_CENTROID(xp,ca,ta);

                  if  (xp[0]  >  0.94e-1  &&  xp[1]  <
0.03)
                  {
                        C_YI(ca,ta,1)=0.0005;
                        C_UDMI(ca,ta,6)=1;

                  }else
                  {
                        C_YI(ca,ta,1)=5e-6;
                  }


            }end_c_loop_all(ca,ta)

      }

}
```

9.3.2 Anammox reactor

```
#include "udf.h"
#include "pdf_props.h"
#include "pdf_table.h"
#include "math.h"
#include "mem.h"
```

```
#include "materials.h"
#include "sg_mem.h"
#include "threads.h"

#define UDS_SOLID 0   /*
VSS/COD = 1.42  */
#define UDS_AMONI 1
#define UDS_NITRITE 2
#define UDS_NITRATE 3
#define UDS_NITROGEN 4

#define C_UDS_SOLID(c,t) C_UDSI(c,t,UDS_SOLID)
#define C_UDS_AMONI(c,t) C_UDSI(c,t,UDS_AMONI)
#define C_UDS_NITRITE(c,t) C_UDSI(c,t,UDS_NITRITE)
#define C_UDS_NITRATE(c,t) C_UDSI(c,t,UDS_NITRATE)
#define C_UDS_NITROGEN(c,t) C_UDSI(c,t,UDS_NITROGEN)

#define TARGET_THREAD_ID1 7
#define TARGET_THREAD_ID2 6
#define TARGET_THREAD_ID3 10
#define TARGET_THREAD_ID4 1

static real kamx_nh4=0.7e-3;   /*kg N·m-3* _____ en
realitat s'ha d'usar kgN/KgTOt, per això dividim per
densitat (kg/m3) ! */
static real kamx_no2=0.55e-3; /*kg N·m-3 _____ en
realitat s'ha d'usar kgN/KgTOt, per això dividim per
densitat (kg/m3) !*/
static real mu_max_amx=8.3e-7; /*s-1*/ //NI et al ,
0.003 h-1

static real Y_AMX=0.164; /*kgDQO·kgN*/
static real i_n_bm=0.07; /*kgHN·kgDQO*/

static real f_Xh_TSS = 0.777;
```

```
static real mu_H=4e-5;
static real eta_g=0.8;

static real K_S=10e-6;

static real K_NO = 0.56e-6;

static real sigma_t = 0.7;

static real g=-9.81;

static real rho_water = 998.2;
static real rho_solid = 1450; /*dry particle*/

real CSOLID, CAMONI, CNITRITE;
DEFINE_DIFFUSIVITY(uds_diffusivity,c,t,i)
{
      return C_MU_EFF(c,t) / sigma_t;

}

DEFINE_PROPERTY(cell_density,c,t)
{
      real conc_solid, rho_total;

      conc_solid = C_UDSI(c,t,0);

      rho_total                                          =
rho_water/(1+conc_solid*(rho_water/rho_solid-1));

      return rho_total;

}
```

```
DEFINE_SOURCE(nh4_nxrate_multiph,c,t,ds,eqn)
      {
            Thread *tm = THREAD_SUPER_THREAD(t);

            real X_AMX;

            double x_ac[ND_ND];

            real den, CNH4, CNO2, source_amon;

            X_AMX = C_UDS_SOLID(c,t)/1.42; /*kg COD ·
            m-3*/ // la ratio VSS/COD = 1.41


            /*den=C_R(c,t); */

            C_CENTROID(x_ac,c,t);

            CNH4 = C_YI(c,t,0)*998*14/18;// KgN·m-3
            CNO2 = C_YI(c,t,1)*998*14/46;

            if ((x_ac[1] >= -0.99))
            {
                        if  ((CNH4  >=  0)  &&  (CNO2  >=
0))
                        {


                                    source_amon=(-
1)*(1/Y_AMX+i_n_bm)*mu_max_amx*(CNH4/(CNH4+kamx_nh4)
)*(CNO2/(CNO2+kamx_no2))*(X_AMX);         //kg N · m-
3·s-1

      /*C_UDMI(c,tm,0)=mu_max_amx*(CNH4/(CNH4+kamx_nh
4))*(CNO2/(CNO2+kamx_no2))*(X_AMX*den);*/


                        }
                        else
```

```
                        {
                              source_amon=-1e-12;
                              /*C_UDMI(c,tm,0)=1e-30;*/

                        }
            }
            else
            {
                  source_amon=-1e-50;
            }


            C_UDMI(c,tm,0)=source_amon*18/14;     //kg
NH4+ m-3 s-1


            C_UDMI(c,tm,3)                                =
            mu_max_amx*(CNH4/(CNH4+kamx_nh4))*(CNO2/(
            CNO2+kamx_no2))*(X_AMX);


            ds[eqn]=(-1)*(1/Y_AMX+i_n_bm)*(1)*(-
            1)*(1/Y_AMX+i_n_bm)*mu_max_amx*(kamx_nh4/
            ((CNH4+kamx_nh4)*(CNH4+kamx_nh4)))*(CNO2/
            (CNO2+kamx_no2))*(X_AMX);
            return source_amon*18/14; /*kg NH4 m-3 s-
1*/


}


DEFINE_SOURCE(no2_nxrate_multiph,c,t,ds,eqn)
{

      Thread *tm = THREAD_SUPER_THREAD(t);


      real X_AMX;


      double x_ac[ND_ND];
```

```
      real den, CNH4, CNO2, source_nitrite;

      X_AMX = C_UDS_SOLID(c,t)/1.42; /*kg COD · m-3*/
// la ratio VSS/COD = 1.41


      /*den=C_R(c,t); */

      C_CENTROID(x_ac,c,t);

      CNH4 = C_YI(c,t,0)*998*14/18;// KgN·m-3
      CNO2 = C_YI(c,t,1)*998*14/46;

      if (x_ac[1] >= -0.99)
      {
            if ((CNH4 >= 0) && (CNO2 >= 0))
            {

                  source_nitrite          =          -
(1/Y_AMX+(5/3)*1.52-
(4/3)*(14/32))*mu_max_amx*(CNH4/(CNH4+kamx_nh4))*(CN
O2/(CNO2+kamx_no2))*(X_AMX); //kg N · m-3·s-1


            }
            else
            {
                  source_nitrite=-1e-12;
            }
      }
      else
      {
            source_nitrite=-1e-50;
      }

      C_UDMI(c,tm,1)=source_nitrite*46/14;  //kg  No2-
m-3 s-1
```

```
      ds[eqn]=(-1)*(1/Y_AMX+(5/3)*1.52-
(4/3)*(14/32))*(CNH4/(CNH4+kamx_nh4))*(X_AMX)*(kamx_
no2/((CNO2+kamx_no2)*(CNO2+kamx_no2)));


      return source_nitrite*46/14;


}


DEFINE_SOURCE(no3_nxrate_multiph,c,t,ds,eqn)
{


      Thread *tm = THREAD_SUPER_THREAD(t);


      real X_AMX;


      double x_ac[ND_ND];
      real den, CNH4, CNO2, source_nitrate;


      X_AMX = C_UDS_SOLID(c,t)/1.42; /*kg COD · m-3*/
// la ratio VSS/COD = 1.41



      /*den=C_R(c,t); */


      C_CENTROID(x_ac,c,t);


      CNH4 = C_YI(c,t,0)*998*14/18;// KgN·m-3
      CNO2 = C_YI(c,t,1)*998*14/46;


      if (x_ac[1] >= -0.99)
      {
            if ((CNH4 >= 0) && (CNO2 >= 0))
            {
```

```
            source_nitrate                                  =
            +1.52*mu_max_amx*(CNH4/(CNH4+kamx_nh4))*(
            CNO2/(CNO2+kamx_no2))*(X_AMX);



            }
            else
            {
                  source_nitrate=+1e-12;
            }
      }
      else
      {
            source_nitrate=+1e-50;
      }


      C_UDMI(c,tm,2)=source_nitrate*46/14;  //kg  No2-
m-3 s-1 eps ! esta equivocat !


      ds[eqn]=0;
      return source_nitrate*46/14;
      //aixo has de multiplicar-ho per (14/46)*62


}


DEFINE_SOURCE(factorMODIFICAT_N2gas,c,t,dS,eqn)
{


      Thread *tm=THREAD_SUPER_THREAD(t);


      real  source,  rho_total,  X_AMX,  CNH4,  CNO2,
term;


      real x_ac[ND_ND];


      /*rho_total = C_R(c,mixture_thread);
```

```
      X_AMX = C_UDS_SOLID(c,t)*1.5; */

      term = C_UDMI(c,tm,3);

      C_CENTROID(x_ac,c,t);

      if (x_ac[1] > -0.99)
      {

            source      =      (2/Y_AMX+(2/3)*(1.52)-
(4/3)*(14/32))*term;
            C_UDMI(c,tm,5)=(2/Y_AMX+(2/3)*(1.52)-
(4/3)*(14/32));

            /*C_UDMI(c,mixture_thread,3) = source; */
            dS[eqn] = 0;

            C_UDMI(c,tm,6)=source;
      }
      else
      {
            dS[eqn]=1e-15;

            source = 1e-15;
            /*C_UDMI(c,mixture_thread,3) = source; */

      }

      return source;
      C_UDMI(c,tm,4) = source; /*inutil perque cada
vegada que el fas return, ja deu passar a zero el
source fixa't que el cudmi(c,t,6)=source; no marca 0
*/

}
```

```
/*-------------------- DEGASSING BOUNDARY CONDITION -
------------ */


DEFINE_PROFILE(vel_nitro_x,tf_sec,i)
{
      Thread *tf_mix = THREAD_SUPER_THREAD(tf_sec);
      Thread                  *tc_sec                 =
THREAD_SUB_THREAD(THREAD_T0(tf_mix),1);


      face_t f;


      begin_f_loop(f,tf_sec)
      {
            F_PROFILE(f,tf_sec,i)                     =
C_U(F_C0(f,tf_mix),tc_sec);


      }
      end_f_loop(f,tf_sec)


}


DEFINE_PROFILE(vel_nitro_y,tf_sec,i)
{
      Thread *tf_mix = THREAD_SUPER_THREAD(tf_sec);
      Thread                  *tc_sec                 =
THREAD_SUB_THREAD(THREAD_T0(tf_mix),1);


      face_t f;


      begin_f_loop(f,tf_sec)
      {
            F_PROFILE(f,tf_sec,i)                     =
C_V(F_C0(f,tf_mix),tc_sec);


      }
```

```
      end_f_loop(f,tf_sec)


}


DEFINE_PROFILE(vel_nitro_z,tf_sec,i)
{
      Thread *tf_mix = THREAD_SUPER_THREAD(tf_sec);
      Thread                  *tc_sec                  =
THREAD_SUB_THREAD(THREAD_T0(tf_mix),1);


      face_t f;


      begin_f_loop(f,tf_sec)
      {
            F_PROFILE(f,tf_sec,i)                      =
C_W(F_C0(f,tf_mix),tc_sec);
      }
      end_f_loop(f,tf_sec)


}


DEFINE_PROFILE(vel_aigua_x,tf_prim,i)
{
      Thread *tf_mix = THREAD_SUPER_THREAD(tf_prim);
      Thread                  *tc_prim                 =
THREAD_SUB_THREAD(THREAD_T0(tf_mix),0);


      face_t f;


      begin_f_loop(f,tf_prim)
      {
            F_PROFILE(f,tf_prim,i)                     =
C_V(F_C0(f,tf_mix),tc_prim);


      }
```

```
      end_f_loop(f,tf_prim)

}

DEFINE_PROFILE(vel_aigua_z,tf_prim,i)
{
      Thread *tf_mix = THREAD_SUPER_THREAD(tf_prim);
      Thread                *tc_prim                =
THREAD_SUB_THREAD(THREAD_T0(tf_mix),0);

      face_t f;

      begin_f_loop(f,tf_prim)
      {
            F_PROFILE(f,tf_prim,i)                  =
C_W(F_C0(f,tf_mix),tc_prim);

      }
      end_f_loop(f,tf_prim)

}

DEFINE_PROFILE(vof_air, tf_sec, i)
{
      Thread *tf_mix = THREAD_SUPER_THREAD(tf_sec);
      Thread                *tc_sec                 =
THREAD_SUB_THREAD(THREAD_T0(tf_mix),1);

      face_t f;

      begin_f_loop(f, tf_sec)
      {
            F_PROFILE(f,          tf_sec,i)         =
C_VOF(F_C0(f,tf_mix),tc_sec);
      }
      end_f_loop(f, tf_sec)
```

```
}
/*_____________________        RECIRCULATION STREAM,
AVOIDING GAS TO SCAPE --------------------*/

DEFINE_PROFILE(REC_vel_nitro_x,tf_sec,i)
{
      Thread *tf_mix = THREAD_SUPER_THREAD(tf_sec);
      Thread                 *tc_sec                =
THREAD_SUB_THREAD(THREAD_T0(tf_mix),1);

      face_t f;

      begin_f_loop(f,tf_sec)
      {
            F_PROFILE(f,tf_sec,i) = 0.;

      }
      end_f_loop(f,tf_sec)

}

DEFINE_PROFILE(REC_vel_nitro_y,tf_sec,i)
{
      Thread *tf_mix = THREAD_SUPER_THREAD(tf_sec);
      Thread                 *tc_sec                =
THREAD_SUB_THREAD(THREAD_T0(tf_mix),1);

      face_t f;

      begin_f_loop(f,tf_sec)
      {
            F_PROFILE(f,tf_sec,i) = 0.;

      }
```

```
      end_f_loop(f,tf_sec)

}

DEFINE_PROFILE(REC_vel_nitro_z,tf_sec,i)
{
      Thread *tf_mix = THREAD_SUPER_THREAD(tf_sec);
      Thread                *tc_sec                =
THREAD_SUB_THREAD(THREAD_T0(tf_mix),1);

      face_t f;

      begin_f_loop(f,tf_sec)
      {
            F_PROFILE(f,tf_sec,i) = 0.;

      }
      end_f_loop(f,tf_sec)

}

DEFINE_PROFILE(REC_vof_air, tf_sec, i)
{
      Thread *tf_mix = THREAD_SUPER_THREAD(tf_sec);
      Thread                *tc_sec                =
THREAD_SUB_THREAD(THREAD_T0(tf_mix),1);

      face_t f;

      begin_f_loop(f, tf_sec)
      {
            F_PROFILE(f, tf_sec,i) = 0.;
      }
      end_f_loop(f, tf_sec)
```

```
}

DEFINE_ADJUST(recirculacio_solids,domain)
{
     int zoneID=10; //posar el codi ID de la bc de
recirculacio

     FILE *fp;

     Thread *t = Lookup_Thread(domain,zoneID);
     Thread *subthread = THREAD_SUB_THREAD(t,0);

     face_t f;

     real mac, mac2, mac3, mag, velocity, solid,
tot, sumtot, sumac, sumac2, sumac3, currenttime,
amoni, nitrite;

     cell_t c;

     Thread *tc;

     real NV_VEC(A);

     currenttime = CURRENT_TIME;
     fp                                              =
fopen("Csolid_recirculatDEGASSING_3.txt","a");

     begin_f_loop(f,subthread)
     {

          F_AREA(A,f,subthread);   /*Get   the   area
vector*/

          mag=NV_MAG(A);  /*Magnitude   of   the   area
vector*/
```

```
            c=F_C0(f,subthread);

            tc=F_C0_THREAD(f,subthread);

            solid=C_UDSI(c,tc,0);//kg VSS m-3
            amoni = C_YI(c,tc,0);
            nitrite = C_YI(c,tc,1);

            velocity                                        =
sqrt(F_U(f,subthread)*F_U(f,subthread)+F_V(f,subthre
ad)*F_V(f,subthread)+F_W(f,subthread)*F_W(f,subthrea
d));

            mac                                             =
velocity*F_R(f,subthread)*NV_MAG(A)*solid;
            mac2                                            =
velocity*F_R(f,subthread)*NV_MAG(A)*amoni;
            mac3                                            =
velocity*F_R(f,subthread)*NV_MAG(A)*nitrite;

            sumac += mac;
            sumac2 += mac2;
            sumac3 += mac3;

            tot                                             =
velocity*F_R(f,subthread)*NV_MAG(A)*1;

            sumtot += tot;

      }end_f_loop(f,subthread)

      CSOLID = sumac/sumtot;
      CAMONI = sumac2/sumtot;
      CNITRITE = sumac3/sumtot;

      printf("C Solid recirculat = %g\n",CSOLID);
```

```
      fprintf(fp,"TEMPS_FLOW %g (seconds) and C_solid
:  %g  velocity:  %g  ,  suma_flux_scalar:  %g  ,
suma_flux_total:   %g   \n",currenttime,   CSOLID,
velocity, sumac, sumtot);


      //sumac = 0.;
      //sumtot = 0.;


      fclose(fp);
}


DEFINE_PROFILE(solids_aigua,tf_prim,i)
{


      real currenttime;
      Thread *tf_mix = THREAD_SUPER_THREAD(tf_prim);
      Thread *tc_prim = THREAD_SUB_THREAD(tf_mix,0);


      face_t f;


      FILE *fp2;


      currenttime = CURRENT_TIME;


      fp2=fopen("Conc_recirc_entradaDEGASSING_3.txt",
"a");
      begin_f_loop(f,tf_prim)
      {
            F_PROFILE(f,tf_prim,i)                    =
(35.29*CSOLID/35.63);


      }
      end_f_loop(f,tf_prim)


      fprintf(fp2,"time_flow %g (seconds) and C_solid
: %g\n",currenttime, CSOLID);
```

```
      fclose(fp2);

}

DEFINE_PROFILE(rec_amoni,tf_prim,i)
{

      real currenttime;
      Thread *tf_mix = THREAD_SUPER_THREAD(tf_prim);
      Thread *tc_prim = THREAD_SUB_THREAD(tf_mix,0);

      face_t f;

      begin_f_loop(f,tf_prim)
      {
            F_PROFILE(f,tf_prim,i)                    =
(35.29*CAMONI+0.34*(560e-6)*(18/14))/35.63;   /*   KG
NH4 / KGTOT -> PERQUÈ QUADRIN LES UNITATS S'HAURIA
DE MULTIPLICAR A DALT I A BIAX PER LA DENSITAT, PERÒ
ES LA MATEIXA A DAL I A BAIX I SE SIMPLIFICA */

      }
      end_f_loop(f,tf_prim)



}

DEFINE_PROFILE(rec_nitrite,tf_prim,i)
{

      real currenttime;
      Thread *tf_mix = THREAD_SUPER_THREAD(tf_prim);
      Thread *tc_prim = THREAD_SUB_THREAD(tf_mix,0);

      face_t f;
```

```
      begin_f_loop(f,tf_prim)
      {
            F_PROFILE(f,tf_prim,i)                    =
(35.29*CNITRITE+0.34*(739.5e-6)*(46/14))/35.63;


      }
      end_f_loop(f,tf_prim)



}


DEFINE_PROFILE(solids_profile_multiphase, t, i)
{


      face_t f;


      Domain *mixture_domain;
      mixture_domain = Get_Domain(1);


      begin_f_loop(f,THREAD_SUB_THREAD(THREAD_SUPER_T
HREAD(t),0))
      {


            F_PROFILE(f,t,i)                          =
C_UDSI(F_C0(f,THREAD_SUB_THREAD(THREAD_SUPER_THREAD(
t),0)),THREAD_T0(THREAD_SUB_THREAD(THREAD_SUPER_THRE
AD(t),1)),0);


      }end_f_loop(f,THREAD_SUB_THREAD(THREAD_SUPER_TH
READ(t),0))


}


/* ----------------------------limit_UDS.c----------
---------------------------- */
DEFINE_ADJUST(limit_UDS,d)
```

```
{

      int phase_domain_index = 0;

      Domain                *subdomain                =
DOMAIN_SUB_DOMAIN(d,phase_domain_index);
      cell_t c;
      Thread *t;
      real n;

      /*loop over cell threads*/
      sub_domain_loop(subdomain,
d,phase_domain_index)
      {

            thread_loop_c(t,subdomain)
            {
                  /* loop over cells in thread */
                  begin_c_loop(c, t)
                  {
                  /*Set values to zero if negative*/
                        if(C_UDSI(c,t,0)<0)
                        {

      C_UDSI(c,t,UDS_SOLID)=0.0;
                              n = n+1;

                        }

                  }end_c_loop_all(c, t)

            }

      }
```

```
}
/* ------------------------------end limit_UDS.c------
-------------------------------- */



static int last_ts = -1;

DEFINE_ADJUST(first_iter_only, domain)
{
      int curr_ts;
      curr_ts = N_TIME;
      if (last_ts != curr_ts)
      {
      last_ts = curr_ts;
      }
      printf("C Solid recirculat = %g\n",CSOLID);

}

DEFINE_EXECUTE_AT_END(calcul_biomassa_total)
{

      FILE *fa;

      Domain *d;

      real volume;
      real biomassa;
      real densitait_acc;
      real currenttime;
      real vol_tot=0.;
      real av_bio=0.;
      real av_bio2=0.;
```

```
      real densitat_acc = 0.;
      int ncel = 0;

      Thread *t;
      cell_t c;

      d = Get_Domain(2);

      currenttime = CURRENT_TIME;

      fa=fopen("concentracion_mitjana_segons_iteracio
DEGASSING_3.txt","a");

      thread_loop_c(t,d)
      {
            begin_c_loop_all(c,t)
            {
                  ncel = ncel + 1;
                  volume = C_VOLUME(c,t);
                  biomassa = C_UDSI(c,t,0);

                  vol_tot = volume + vol_tot;
                  densitat_acc    =    densitat_acc    +
C_R(c,t);
                  av_bio        =        av_bio        +
biomassa*volume*C_R(c,t);

            }
            end_c_loop_all(c,t)

            av_bio = av_bio/vol_tot;
            av_bio2                                    =
(av_bio/vol_tot)/(densitat_acc/ncel);
            fprintf(fa, " Flow time : %g (seconds)
Vol promig = %g (L) i av_biomassa = %g    i %g
(W)\n",currenttime, vol_tot,av_bio);
```

```
      }

      fclose(fa);
}

DEFINE_ON_DEMAND(calcul_instant_biomassa_total)
{

      FILE *f1;

      Domain *d;

      real volume;
      real biomassa;
      real density;

      real vol_tot=0.;
      real av_bio=0.;
      real av_bio2=0.;
      int ncells =0;

      Thread *t;
      cell_t c;

      d = Get_Domain(2);

      f1=fopen("average_concentrationDEGASSING_3.txt"
,"w");

      thread_loop_c(t,d)
      {
            begin_c_loop_all(c,t)
            {
```

```
                ncells = ncells +1 ;
                volume = C_VOLUME(c,t);
                biomassa = C_UDSI(c,t,0);

                vol_tot = volume + vol_tot;

                av_bio = av_bio + biomassa*volume;

          }
          end_c_loop_all(c,t)

          av_bio = av_bio/vol_tot;
          fprintf(f1,"   Vol   promig   =   %g   i
av_biomassa = %g \n",vol_tot,av_bio);
     }

     fclose(f1);
}

DEFINE_UDS_FLUX(uds_fluxamx_ok_NOU_BRANNOCK,f,t,i)
{

     Thread *t0, *t1 = NULL, *tm;
     cell_t c0, c1 = -1;

     real NV_VEC(psi), NV_VEC(A);
     real  flux,  conc_solid,  vel_solid,  rho_total,
scalar;

     t0 = THREAD_T0(t);
     c0 = F_C0(f,t);

     /*tm = THREAD_SUPER_THREAD(t); */
```

```
     if (NULL != THREAD_T1(t)) /* si es una cara
interna, que té cel·la c1 ... */
     {
          t1 = THREAD_T1(t);
          c1 = F_C1(f,t);

     }else /*so es qualsevol boundary face*/
     {
          t1 = NULL;
          c1 = -1;
     }

     F_AREA(A,f,t);

     F_FLUX(f,t);

     if (NULL == t1) /*si esta en una bc*/
     {
          scalar = 0;

     }
     else
     {
          rho_total = (C_R(c0,t0)+C_R(c1,t1)/2.);

          conc_solid                              =
((C_UDS_SOLID(c0,t0)+C_UDS_SOLID(c1,t1))/2.);    //kg
VSS m-3

          vel_solid = -1.39e-3; /* MODFICIADA AL
071015 PERQUÈ HA DE SER PER SOTA DE LA FLUIDITZACIÓ
! -> AIXÒ DELS FULLS DE XLS ERA EL MODEL DE LU nou
veure      fulla      excel      recalculada      -
(1/100)*158.22*1*pow(1.5e-3,1.428)*pow((-
0.0282*1.5e-3+1.0489-0.998),0.7143); */

          /*F_UDMI(f,t,1)=vel_solid; */
```

```
            NV_D(psi, =, 0., vel_solid, 0.);
            NV_S(psi,*=, rho_total);

            scalar = NV_DOT(psi,A);
      }
      //F_UDMI(f,tm,4)=conc_solid;

      //F_UDMI(f,tm,5)= scalar; /*kg s-1*/

      flux = F_FLUX(f,t) + scalar;

      /*F_UDMI(f,tm,6) = flux; */

      if (i== UDS_SOLID)
      {
            return flux;
      }
      else
      {
            return 0.;
      }

}


DEFINE_UDS_FLUX(settling_flux_amx,f,tf,i)
{
  cell_t c0=F_C0(f,tf),c1=F_C1(f,tf);
  Thread *t0=THREAD_T0(tf),*t1=THREAD_T1(tf), *tm =
THREAD_SUPER_THREAD(tf);
  real face_concentration;
  real       gravity_vector[]={0,1,0},area[ND_ND];/*
Gravity vector (0,1,0)-------------------------------
---------------------------------            !!!!!!!
*/


  if ((t1==NULL)||(THREAD_TYPE(tf)==THREAD_F_WALL))
```

```
    /* if this is a boundary zone or a 0-thickness
wall */
    face_concentration=F_UDSI(f,tf,0);
  else
    /* if this an interior face, the face value is
the average of the upstream and downstream cells */

face_concentration=.5*(C_UDSI(c0,t0,0)+C_UDSI(c1,t1,
0));
  /* F_AREA macro stores the components (Ax,Ay) of
the area vector on the array area */
  F_AREA(area,f,tf);


  /*F_UDMI(f,tm,7) = face_concentration; */


  if (THREAD_TYPE(tf)==THREAD_F_WALL)
    return 0.;
  else
    return          F_FLUX(f,tf)+C_R(c0,t0)*(-1.39e-
3)*NV_DOT(gravity_vector,area);


 /*   F_UDMI(f,tm,8)   =   F_FLUX(f,tf)+C_R(c0,t0)*(-
1.39e-3)*NV_DOT(gravity_vector,area);*/


     /*if   the   face   is   parallel   to   the
gravity_vector, NV_DOT(gravity_vector,area) = 0 */
     /*if   the   face   is   perpendicular   to   the
gravity_vector, NV_DOT(gravity_vector,area) = 1 */
}


DEFINE_INIT(my_init_function, mixture_domain)
{


     int phase_domain_index;
     cell_t cell;
     Thread *cell_thread;
     Domain *subdomain;
```

```
     real xc[ND_ND];

     /* loop over all subdomains (phases) in the
superdomain (mixture) */
     sub_domain_loop(subdomain,      mixture_domain,
phase_domain_index)
     {

          if (DOMAIN_ID(subdomain) == 2)

          /* loop over all cell threads in the
secondary phase domain */

          thread_loop_c (cell_thread,subdomain)
          {

               /* loop over all cells in secondary
phase cell threads */
               begin_c_loop_all (cell,cell_thread)
               {


     C_CENTROID(xc,cell,cell_thread);
                    if (xc[1] >= -0.99)
                    {

                         if (xc[1] <= 0.215505)
                         {

                              /*     set     volume
fraction to 1 for centroid */

     C_UDSI(cell,cell_thread,0)=1.9; //kg VSS/kg TOT

                         }
```

```
                              if (xc[1] > 0.215505)
                              {

                                    if (xc[1] <= 0.30)

                                    {
                                          /*  set  volume
fraction to 1 for centroid */

      C_UDSI(cell,cell_thread,0)=1.57;   //kg   VSS/kg
TOT

                                    }

                              }
                        }


                  }
                  end_c_loop_all (cell,cell_thread)

            }
      }

}

DEFINE_INIT(my_init_function2, mixture_domain)
{

      int phase_domain_index;
      cell_t cell;
      Thread *cell_thread;
      Domain *subdomain;

      real xc[ND_ND];
```

```
     /* loop over all subdomains (phases) in the
superdomain (mixture) */
     sub_domain_loop(subdomain,      mixture_domain,
phase_domain_index)
     {

          if (DOMAIN_ID(subdomain) == 2)

          /* loop over all cell threads in the
secondary phase domain */

          thread_loop_c (cell_thread,subdomain)
          {

               /* loop over all cells in secondary
phase cell threads */
               begin_c_loop_all (cell,cell_thread)
               {


     C_CENTROID(xc,cell,cell_thread);
                    if (xc[1] >= -0.99)
                    {

                         if (xc[1] <= 1)
                         {

                              /*     set     volume
fraction to 1 for centroid */

     C_UDSI(cell,cell_thread,0)=1.15;   //kg   VSS/kg
TOT

                         }

                    }
```

```
                    }
                    end_c_loop_all (cell,cell_thread)

                }
            }
}
```

9.4 Supporting Information anode hidrodynamics in biolectrochemical systems

9.4.1 Governing equations in the hydrodynamics simulation

The continuity equation was defined as (Equation 9.63):

$$\frac{\partial \rho}{\partial t} + \nabla(\rho \vec{v}) = S_m \tag{9.63}$$

The momentum conservation equation was (Equation 9.64-9.65):

$$\frac{\partial}{\partial t}(\rho \vec{v}) + \nabla(\rho \overrightarrow{v\,v}) = -\nabla \mathrm{p} + \nabla \cdot (\bar{\tau}) + \rho \vec{\mathrm{g}} + \vec{\mathrm{F}} \tag{9.64}$$

$$\vec{\tau} = \mu\left[(\nabla\vec{v} + \nabla\vec{v}^{T}) - \frac{2}{3}\nabla\cdot\vec{v}I\right] \quad (9.65)$$

which for an incompressible fluid (water) , the divergence of u became 0, and then the momentum equation is redefined as (Equation 9.66):

$$\frac{\partial u}{\partial t} + (u\cdot\nabla)u - \nu\nabla^{2}u = -\nabla\left(\frac{p}{\rho_0}\right) + g \quad (9.66)$$

9.4.2 Source acetate consumption

The source of acetate concentration by means of biological activity is defined in Equation 9.63, with the included parameters defined in Equations 9.67 and 9.69, respectively.

$$\frac{\mathrm{dS}}{\mathrm{dt}} = -\mathrm{q_a X_a} - \mathrm{q_m X_m} \quad (9.67)$$

$$q_{=} = q_a^{max}\cdot\frac{S}{K_{sa}+S}\cdot\frac{M_{ox}}{M_{ox}+K_M} \quad (9.68)$$

$$q_m = q_m^{max} \cdot \frac{S}{S + K_{sm}} \tag{9.69}$$

The oxidation reaction of acetate is presneted in Equation 9.70:

$$CH_3COO^- + 2H_2O \rightarrow 2CO_2 + 7\,H^+ + 8e^- \tag{9.70}$$

9.4.3 Current generation and methane production rates equations:

The intensity was calculated as (Equation 9.71):

$$i(mA) = q_a(KgS \cdot kgX \cdot s^{-1}) \cdot X_a(kgX \cdot m^{-3}) \cdot V_{liq}(m^3) \cdot \cdot \frac{1000\ mole\ S}{60KgS} \cdot \frac{8\ mole\ e^-}{1\ mole\ S} \cdot \frac{96485000\ mC}{1\ mole\ e-} \tag{9.71}$$

And the methane generation was calculated as (Equation 9.72)

$$Q(mgCH_4 \cdot day^{-1}) = q_m(KgS \cdot kgX \cdot s^{-1}) \cdot X_m(kgX \cdot m^{-3}) \cdot \cdot V_{liq}(m^3) \cdot Y(m^3CH_4 \cdot KgS^{-1}) \cdot \frac{86400\ s}{1\ day} \cdot \frac{10^6 mg}{1\ m^3} \tag{9.72}$$

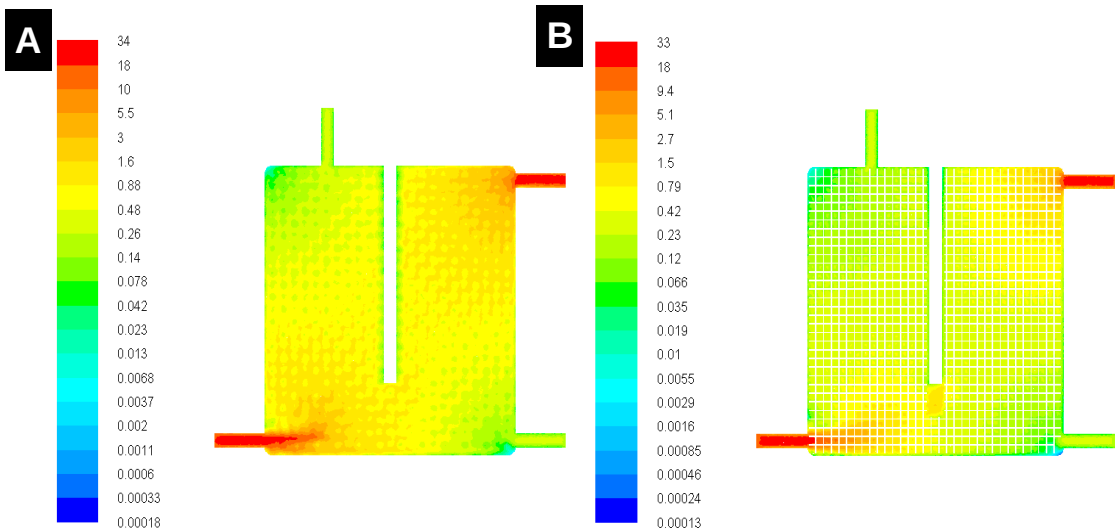

Figure 9.3 Reynolds profiles (logarithmic scales) for the simulations cases of : a) rod graphite + granular graphite (225.44 $m^2 \cdot m^{-3}$ NAC, HRT 9.55 h), and b) rod graphite + stainless steel meshes (Case 3, b: 13.81 $m^2 \cdot m^{-3}$ NAC, HRT 12.08 h) as electrode materials.

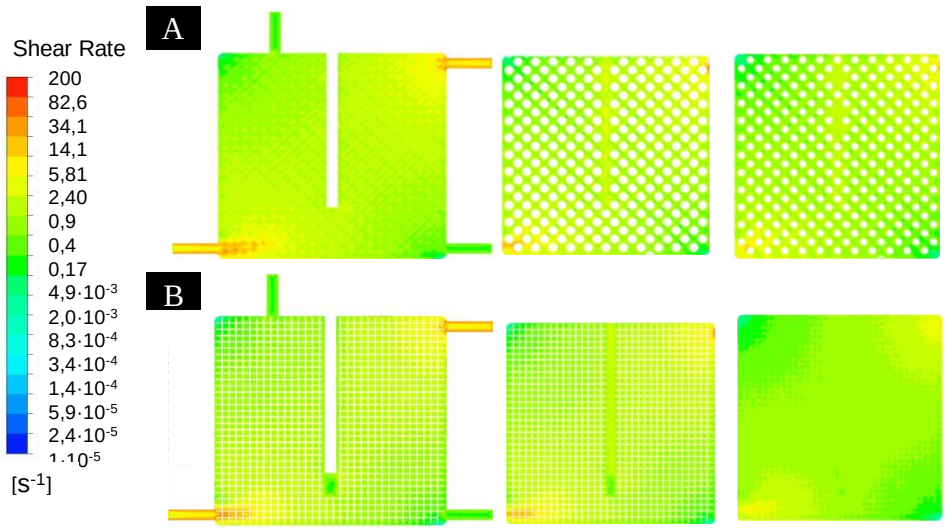

Figure 9.4 Shear stress profiles distribution for two different cases: a) rod graphite + granular graphite (225.44 $m^2 \cdot m^{-3}$ NAC, HRT 9.55 h), and b) rod graphite + stainless steel meshes (Case 3, b: 13.81 m^2/m^{-3} NAC, HRT 12.08 h) as electrode materials.

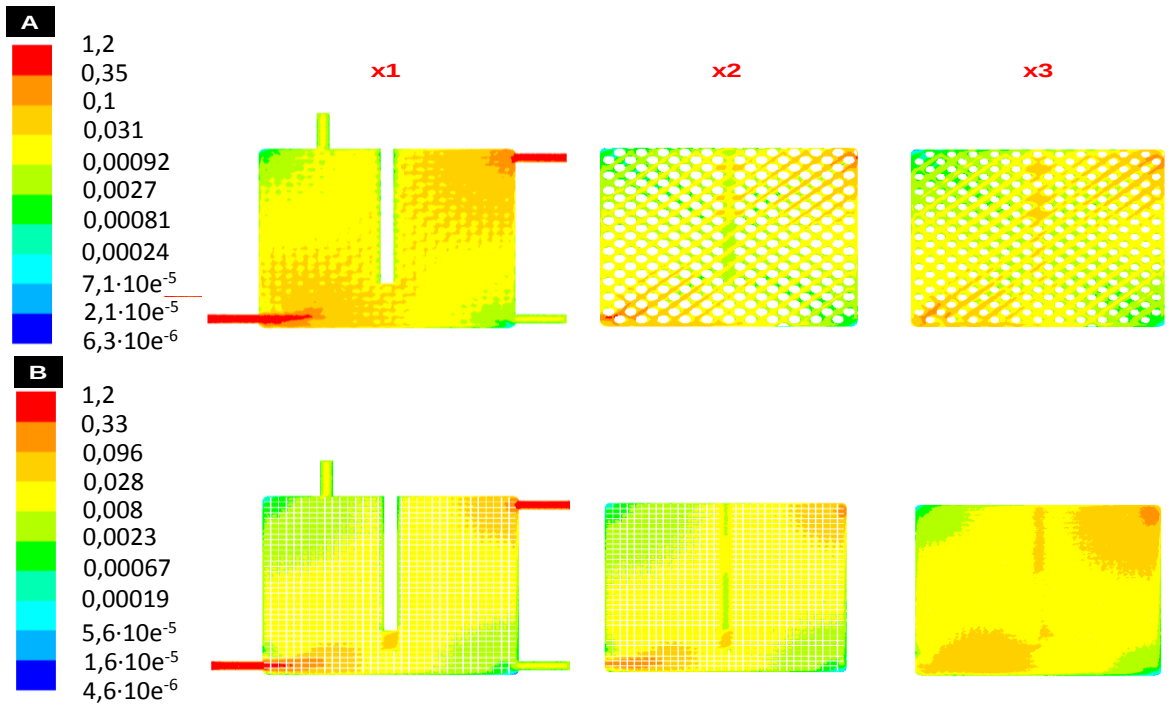

Figure 9.5 Peclet number profiles (logarithmic scales) for the simulations cases of a) rod graphite + granular graphite (225.44 $m^2 \cdot m^{-3}$ NAC, HRT 9.55 h), and b) rod graphite + stainless steel meshes (13.81 $m^2 \cdot m^{-3}$ NAC, HRT 12.08 h) as electrode materials. Values measured at three different sections of the anodic chamber (x1, x2 and x3 – See Figure 1).

REFERENCES

References

Aelterman, P., Versichele, M., Marzorati, M., Boon, N., Verstraete, W., 2008. Loading rate and external resistance control the electricity generation of microbial fuel cells with different three-dimensional anodes. Bioresour. Technol. 99, 8895–8902.

Ahn, Y., Hatzell, M.C., Zhang, F., Logan, B.E., 2014. Different electrode configurations to optimize performance of multi-electrode microbial fuel cells for generating power or treating domestic wastewater. J. Power Sources 249, 440–445.

Alvarado, A., Vedantam, S., Goethals, P., Nopens, I., 2012. A compartmental model to describe hydraulics in a full-scale waste stabilization pond. Water Res. 46, 521–530.

Andersson, B.E.A., 2012. Computational Fluid Dynamics for Engineers. Cambridge University Press.

Andersson, R., Andersson, B., Chopard, F., Norén, T., 2004. Development of a multi-scale simulation method for design of novel multiphase reactors. Chem. Eng. Sci. 59, 4911–4917.

Anon, 1980. Boiler Dynamics and control in nuclear power stations 2, PROCEEDINGS OF THE INTERNATIONAL CONFERENCE, 2ND, 1979. Conv. - Batter. Counc. Int.

Ansys, 2009. Ansys fluent theory guide, Inc Northbrook IL.

Arnaldos, M., Amerlinck, Y., Rehman, U., Maere, T., Van Hoey, S., Naessens, W., Nopens, I., 2015. From the affinity constant to the half-saturation index: Understanding conventional modeling concepts in novel wastewater treatment processes. Water Res. 70, 458–470.

Arrojo, B., Figueroa, M., Mosquera-Corral, A., Campos, J.L., Méndez, R., 2008. Influence of gas flow-induced shear stress on the operation of the Anammox process in a SBR. Chemosphere 72, 1687–1693.

Arrojo, B., Mosquera-Corral, A., Campos, J.L., Méndez, R., 2006. Effects of mechanical stress on Anammox granules in a sequencing batch reactor (SBR). J. Biotechnol. 123, 453–463.

Batlle-Vilanova, P., Puig, S., Gonzalez-Olmos, R., Vilajeliu-Pons, A., Balaguer, M.D., Colprim, J., 2015. Deciphering the electron transfer mechanisms for biogas upgrading to biomethane within a mixed culture biocathode. RSC Adv. 52243–52251.

Batlle-Vilanova, P., Puig, S., Gonzalez-Olmos, R., Vilajeliu-Pons, A., Bañeras, L., Balaguer, M.D., Colprim, J., 2014. Assessment of biotic and abiotic graphite cathodes for hydrogen production in microbial electrolysis cells. Int. J. Hydrogen Energy 39, 1297–1305.

Bentzen, T.R., Ratkovich, N., Madsen, S., Jensen, J.C., Bak, S.N., Rasmussen, M.R., 2012. Analytical and numerical modelling of Newtonian and non-Newtonian liquid in a rotational cross-flow MBR. Water Sci. Technol. 66, 2318–2327.

Bond, D.R., Lovley, D.R., 2003. Electricity Production by Geobacter sulfurreducens Attached to Electrodes. Appl. Environ. Microbiol. 69, 1548–1555.

Boni, A.A., 1978. Numerical simulation of flame propagation in internal combustion engines. SAE Prepr.

Brannock, M.W.D., 2003. Computational Fluid Dynamics Tools for the Design of Mixed Anoxic Wastewater Treatment Vessels.

Brannock, M.W.D., De Wever, H., Wang, Y., Leslie, G., 2009. Computational fluid dynamics simulations of MBRs: Inside submerged versus outside submerged membranes. Desalination 236, 244–251.

Cockx, A., Do-Quang, Z., Liné, A., Roustan, M., 1999. Use of computational

fluid dynamics for simulating hydrodynamics and mass transfer in industrial ozonation towers. Chem. Eng. Sci. 54, 5085–5090.

Coma, M., Puig, S., Pous, N., Balaguer, M.D., Colprim, J., 2013. Biocatalysed sulphate removal in a BES cathode. Bioresour. Technol. 130, 218–223.

Corominas, L.P.D. thesis, 2006. Control and optimization of an SBR for nitrogen removal : from model control and optimization of an SBR for nitrogen removal. Universitat de Girona.

Crider, J.E., Foss, A.S., 1966. Computational studies of transients in packed tubular chemical reactors. AIChE J. 12, 514–522.

Dalmau, M., Rodriguez-Roda, I., Ayesa, E., Odriozola, J., Sancho, L., Comas, J., 2013. Development of a decision tree for the integrated operation of nutrient removal MBRs based on simulation studies and expert knowledge. Chem. Eng. J. 217, 174–184.

Dapena-Mora, A., Arrojo, B., Campos, J.L., Mosquera-Corral, A., M�ndez, R., 2004a. Improvement of the settling properties of Anammox sludge in an SBR. J. Chem. Technol. Biotechnol. 79, 1417–1420.

Dapena-Mora, A., Van Hulle, S.W.H., Campos, J.L., Méndez, R., Vanrolleghem, P. a., Jetten, M., 2004b. Enrichment of Anammox biomass from municipal activated sludge: Experimental and modelling results. J. Chem. Technol. Biotechnol. 79, 1421–1428.

De Clercq, B., 2003. Fluid dynamics of settling tanks: development of experiments and rheological, settling, and scraper submodels.

Dewan, A., Beyenal, H., Lewandowski, Z., 2008. Scaling up microbial fuel cells. Environ. Sci. Technol. 42, 7643–7648.

Dhenge, R.M., Fyles, R.S., Cartwright, J.J., Doughty, D.G., Hounslow, M.J., Salman, A.D., 2010. Twin screw wet granulation: Granule properties.

Chem. Eng. J. 164, 322–329.

Di Lorenzo, M., Scott, K., Curtis, T.P., Head, I.M., 2010. Effect of increasing anode surface area on the performance of a single chamber microbial fuel cell. Chem. Eng. J. 156, 40–48.

Fan, J., Lu, S.-G., Qiu, Z.-F., Wang, X.-X., Li, W.-Z., 2009. An activated sludge model based on activated sludge model number 3 for full-scale wastewater treatment plant simulation. Environ. Technol. 30, 641–649.

Fayolle, Y., Cockx, A., Gillot, S., Roustan, M., Héduit, A., 2007. Oxygen transfer prediction in aeration tanks using CFD. Chem. Eng. Sci. 62, 7163–7171.

Fernández, I., Bravo, J.I., Mosquera-Corral, A., Pereira, A., Campos, J.L., Méndez, R., Melo, L.F., 2014. Influence of the shear stress and salinity on Anammox biofilms formation: modelling results. Bioprocess Biosyst. Eng. 37, 1955–1961.

Fiset, E., Puig, S., 2015. Modified Carbon Electrodes : A New Approach for Bioelectrochemical Systems. J. Bioremediation Biodegrad. 6, 1–2.

Fogler, H.S., 2006. Elements of chemical reaction engineering, Prentice Hall PTR international series in the physical and chemical engineering sciences.

Galí, A., Dosta, J., van Loosdrecht, M.C.M., Mata-Alvarez, J., 2007. Two ways to achieve an anammox influent from real reject water treatment at lab-scale: Partial SBR nitrification and SHARON process. Process Biochem. 42, 715–720.

Ganigué, R., Puig, S., Batlle-Vilanova, P., Balaguer, M.D., Colprim, J., 2015. Microbial electrosynthesis of butyrate from carbon dioxide. Chem. Commun. 51, 3235–3238.

Ganigué, R., Volcke, E.I.P., Puig, S., Balaguer, M.D., Colprim, J., Sin, G., 2010. Systematic model development for partial nitrification of landfill leachate in a SBR. Water Sci. Technol. 61, 2199–2210.

Garcia-Ochoa, F., Gomez, E., 2009. Bioreactor scale-up and oxygen transfer rate in microbial processes: an overview. Biotechnol. Adv. 27, 153–176.

Gimbun, J., Rielly, C.D., Nagy, Z.K., 2009. Modelling of mass transfer in gas-liquid stirred tanks agitated by Rushton turbine and CD-6 impeller: A scale-up study. Chem. Eng. Res. Des. 87, 437–451.

Gresch, M., Armbruster, M., Braun, D., Gujer, W., 2011. Effects of aeration patterns on the flow field in wastewater aeration tanks. Water Res. 45, 810–818.

Gujer, W., Henze, M., Mino, T., Loosdrecht, M.C.M. Van, 1999. Activated sludge model No. 3. Water Sci. Technol.

Henze, M., Gujer, W., Mino, T. and Van Loosdrecht, M.C.M. (2000), 2000. Activated Sludge Models: ASM1, ASM2, ASM2d and ASM3, Scientific and technical report n^{o}9. IWA Publishing, London.

Henze, M., Gujer, W., Mino, T., van Loosdrecht, M.C.M., 2000. Activated Sludge Models ASM1, ASM2, ASM2d and ASM3. IWA Publ. 121.

Hijnen, W.A.M., Beerendonk, E.F., Medema, G.J., 2006. Inactivation credit of UV radiation for viruses, bacteria and protozoan (oo)cysts in water: A review. Water Res. 40, 3–22.

Hreiz, R., Latifi, M.A., Roche, N., 2015. Optimal design and operation of activated sludge processes: State-of-the-art. Chem. Eng. J. 281, 900–920.

Huang, Q., Yang, C., Yu, G., Mao, Z.-S., 2010. CFD simulation of hydrodynamics and mass transfer in an internal airlift loop reactor

using a steady two-fluid model. Chem. Eng. Sci. 65, 5527–5536.

Ieropoulos, I., Winfield, J., Greenman, J., 2010. Effects of flow-rate, inoculum and time on the internal resistance of microbial fuel cells. Bioresour. Technol. 101, 3520–3525.

Janex, M., Savoye, P., Doquang, Z., Blatchleyiii, E., Laine, J., 1998. Impact of water quality and reactor hydrodynamics on wastewater disinfection by UV, use of CFD modeling for performance optimization. Water Sci. Technol. 38, 71–78.

Jeppsson, U., Pons, M.N., Nopens, I., Alex, J., Copp, J.B., Gernaey, K. V., Rosen, C., Steyer, J.P., Vanrolleghem, P.A., 2007. Benchmark simulation model no 2: General protocol and exploratory case studies 56, 67–78. doi:10.2166/wst.2007.604

Jeremiasse, A.W., Hamelers, H.V.M., Buisman, C.J.N., 2010. Microbial electrolysis cell with a microbial biocathode. Bioelectrochemistry 78, 39–43.

Jin, R.C., Yang, G.F., Ma, C., Yu, J.J., Zhang, Q.Q., Xing, B.S., 2012. Influence of effluent recirculation on the performance of Anammox process. Chem. Eng. J. 200–202, 176–185.

Karpinska, A.M., Bridgeman, J., 2015. CFD-Aided Modelling of Activated Sludge Systems – A Critical Review. Water Res. 88, 861–879.

Kim, H., Lim, H., Wie, J., Lee, I., Colosimo, M.F., n.d. Optimization of modified ABA2 process using linearized ASM2 for saving aeration energy. Chem. Eng. J. 251, 337–342.

Kim, J., Kim, H., Kim, B., Yu, J.,. Computational fluid dynamics analysis in microbial fuel cells with different anode configurations. Water Sci. Technol. 69, 1447–1452.

Lackner, S., Gilbert, E.M., Vlaeminck, S.E., Joss, A., Horn, H., van Loosdrecht, M.C.M., 2014. Full-scale partial nitritation/anammox experiences – An application survey. Water Res. 55, 292–303.

Laurent, J., Samstag, R.W., Ducoste, J.M., Griborio, A., Nopens, I., Batstone, D.J., Wicks, J.D., Saunders, S., Potier, O., 2014. A protocol for the use of computational fluid dynamics as a supportive tool for wastewater treatment plant modelling. Water Sci. Technol. 70, 1575–1584.

Le Moullec, Y., Gentric, C., Potier, O., Leclerc, J.P., 2010. CFD simulation of the hydrodynamics and reactions in an activated sludge channel reactor of wastewater treatment. Chem. Eng. Sci. 65, 492–498.

Ledezma, P., Donose, B.C., Freguia, S., Keller, J., 2015. Oxidised stainless steel: A very effective electrode material for microbial fuel cell bioanodes but at high risk of corrosion. Electrochim. Acta 158, 356–360.

Lei, L., Ni, J., 2014. Three-dimensional three-phase model for simulation of hydrodynamics, oxygen mass transfer, carbon oxidation, nitrification and denitrification in an oxidation ditch. Water Res. 53, 200–214.

Lim, S.J., Park, W., Kim, T.-H., Shin, I.H., 2012. Swine wastewater treatment using a unique sequence of ion exchange membranes and bioelectrochemical system. Bioresour. Technol. 118, 163–169.

Logan, B.E., Hamelers, B., Rozendal, R., Schröder, U., Keller, J., Freguia, S., Aelterman, P., Verstraete, W., Rabaey, K., 2006. Microbial fuel cells: Methodology and technology. Environ. Sci. Technol. 40, 5181–5192.

Lopes, R.J.G., Quinta-Ferreira, R.M., 2010a. Assessment of CFD Euler–Euler method for trickle-bed reactor modelling in the catalytic wet oxidation of phenolic wastewaters. Chem. Eng. J. 160, 293–301.

Lopes, R.J.G., Quinta-Ferreira, R.M., 2010b. Evaluation of multiphase CFD models in gas–liquid packed-bed reactors for water pollution

abatement. Chem. Eng. Sci. 65, 291–297.

Lopes, R.J.G., Quinta-Ferreira, R.M., 2009. CFD modelling of multiphase flow distribution in trickle beds. Chem. Eng. J. 147, 342–355.

López, H., Puig, S., R., G., Ruscalleda, M., Balaguer, M.D., Colprim, J., 2008. Start-up and enrichment of a granular anammox SBR to treat high nitrogen load wastewaters. J. Chem. Technol. Biotechnol. 241, 233–241.

Lotti, T., Milano, P., Lotti, T., Kleerebezem, R., Erp, C. Van, Kip, T., Hendrickx, T.L.G., 2014. Anammox growth on pretreated municipal wastewater. Environ. Sci. Technol. 48, 7874–7880.

Lu, H.-F., Zheng, P., Ji, Q.-X., Zhang, H.-T., Ji, J.-Y., Wang, L., Ding, S., Chen, T.-T., Zhang, J.-Q., Tang, C.-J., Chen, J.-W., 2012. The structure, density and settlability of anammox granular sludge in high-rate reactors. Bioresour. Technol. 123, 312–317.

Mavriplis, D.J., 1996. Mesh Generation and adaptivity for complex geometries and flows, Handbook Of Computational Fluid Mechanics. Academic Press.

Michie, I.S., Kim, J.R., Dinsdale, R.M., Guwy, A.J., Premier, G.C., 2014. The influence of anodic helical design on fluid flow and bioelectrochemical performance. Bioresour. Technol. 165, 13–20.

Nevin, K.P., Hensley, S. a., Franks, A.E., Summers, Z.M., Ou, J., Woodard, T.L., Snoeyenbos-West, O.L., Lovley, D.R., 2011. Electrosynthesis of organic compounds from carbon dioxide is catalyzed by a diversity of acetogenic microorganisms. Appl. Environ. Microbiol. 77, 2882–2886.

Ni, B.-J., Chen, Y.-P., Liu, S.-Y., Fang, F., Xie, W.-M., Yu, H.-Q., 2009. Modeling a granule-based anaerobic ammonium oxidizing (ANAMMOX) process.

Biotechnol. Bioeng. 103, 490–499.

Nopens, I., Beheydt, D., Vanrolleghem, P.A., 2005. Comparison and pitfalls of different discretised solution methods for population balance models: A simulation study. Comput. Chem. Eng. 29, 367–377.

Park, D.H., Zeikus, J.G., 2003. Improved fuel cell and electrode designs for producing electricity from microbial degradation. Biotechnol. Bioeng. 81, 348–355.

Pham, H.T., Boon, N., Aelterman, P., Clauwaert, P., De Schamphelaire, L., van Oostveldt, P., Verbeken, K., Rabaey, K., Verstraete, W., 2008. High shear enrichment improves the performance of the anodophilic microbial consortium in a microbial fuel cell. Microb. Biotechnol. 1, 487–496.

Picioreanu, C., Head, I.M., Katuri, K.P., van Loosdrecht, M.C.M., Scott, K., 2007. A computational model for biofilm-based microbial fuel cells. Water Res. 41, 2921–2940.

Picioreanu, C., Vrouwenvelder, J.S., van Loosdrecht, M.C.M., 2009. Three-dimensional modeling of biofouling and fluid dynamics in feed spacer channels of membrane devices. J. Memb. Sci. 345, 340–354.

Pinto, R.P., Srinivasan, B., Manuel, M.-F., Tartakovsky, B., 2010. A two-population bio-electrochemical model of a microbial fuel cell. Bioresour. Technol. 101, 5256–5265.

Pocaznoi, D., Calmet, A., Etcheverry, L., Erable, B., Bergel, A., 2012. Stainless steel is a promising electrode material for anodes of microbial fuel cells. Energy Environ. Sci. 5, 9645–9652.

Pous, N., Koch, C., Vilà-Rovira, A., Balaguer, M.D., Colprim, J., Mühlenberg, J., Müller, S., Harnisch, F., Puig, S., 2015. Monitoring and engineering reactor microbiomes of denitrifying bioelectrochemical systems. RSC Adv. 5, 68326–68333.

Pous, N., Puig, S., Coma, M., Balaguer, M.D., Colprim, J., 2013. Bioremediation of nitrate-polluted groundwater in a microbial fuel cell. J. Chem. Technol. Biotechnol. 88, 1690–1696.

Puig, S., Coma, M., Desloover, J., Boon, N., Colprim, J., Balaguer, M.D., 2012. Autotrophic denitrification in microbial fuel cells treating low ionic strength waters. Environ. Sci. Technol. 46, 2309–2315.

Ratkovich, N., Bentzen, T.R., 2013. Comparison of four types of membrane bioreactor systems in terms of shear stress over the membrane surface using computational fluid dynamics. Water Sci. Technol. 68, 2534–2544.

Rehman, U., Vesvikar, M., Maere, T., Guo, L., Vanrolleghem, P.A., Nopens, I., 2015. Effect of sensor location on controller performance in a wastewater treatment plant 71, 700–708.

Rochex, A., Godon, J.-J., Bernet, N., Escudié, R., 2008. Role of shear stress on composition, diversity and dynamics of biofilm bacterial communities. Water Res. 42, 4915–4922.

Ruscalleda, M., 2011. Treatment of mature urban landfill leachates by anammox process. Universitat de Girona.

Ruscalleda, M., Puig, S., Mora, X., López, H., Ganigué, R., Balaguer, M.D., Colprim, J., 2010. The effect of urban landfill leachate characteristics on the coexistence of anammox bacteria and heterotrophic denitrifiers. Water Sci. Technol. 61, 1065–1071.

Samstag, R.W., Ducoste, J.J., Griborio, A., Nopens, I., Batstone, D.J., Wicks, J.D., Saunders, S., Wicklein, E.A., Kenny, G., Laurent, J., 2016. CFD for wastewater treatment: An overview. Water Sci. Technol. 74, 549–563.

Scaglione, D., Ficara, E., Corbellini, V., Tornotti, G., Teli, A., Canziani, R., Malpei, F., 2015. Autotrophic nitrogen removal by a two-step SBR

process applied to mixed agro-digestate. Bioresour. Technol. 176, 98–105.

Scaglione, D., Ruscalleda, M., Ficara, E., Balaguer, M.D., Colprim, J., 2012. Response to high nitrite concentrations of anammox biomass from two SBR fed on synthetic wastewater and landfill leachate. Chem. Eng. J. 209, 62–68.

Strous, M., Heijnen, J.J., Kuenen, J.G., Jetten, M.S.M., 1998. The sequencing batch reactor as a powerful tool for the study of slowly growing anaerobic ammonium-oxidizing microorganisms. Appl. Microbiol. Biotechnol. 50, 589–596.

Strous, M., Van Gerven, E., Zheng, P., Kuenen, J.G., Jetten, M.S.M., 1997. Ammonium removal from concentrated waste streams with the anaerobic ammonium oxidation (Anammox) process in different reactor configurations. Water Res. 31, 1955–1962.

Takács, I., Patry, G.G., Nolasco, D., 1991. A dynamic model of the clarification-thickening process. Water Res. 25, 1263–1271.

Takács, I., Vanrolleghem, P. a, Wett, B., Murthy, S., 2007. Elemental balance based methodology to establish reaction stoichiometry in environmental modeling. Water Sci. Technol. 56, 37–41.

Tang, C.-J., He, R., Zheng, P., Chai, L.-Y., Min, X.-B., 2013. Mathematical modeling of high-rate Anammox UASB reactor based on granular packing patterns. J. Hazard. Mater. 250–251, 1–8.

Tang, C.-J., Zheng, P., Wang, C.-H., Mahmood, Q., Zhang, J.-Q., Chen, X.-G., Zhang, L., Chen, J.-W., 2011. Performance of high-loaded ANAMMOX UASB reactors containing granular sludge. Water Res. 45, 135–144.

Ter Heijne, A., Liu, F., Van Rijnsoever, L.S., Saakes, M., Hamelers, H.V.M., Buisman, C.J.N., 2011. Performance of a scaled-up Microbial Fuel Cell

with iron reduction as the cathode reaction. J. Power Sources 196, 7572–7577.

Torres, C.I., Lee, H.-S., Rittmann, B.E., 2008. Carbonate species as OH- carriers for decreasing the pH gradient between cathode and anode in biological fuel cells. Environ. Sci. Technol. 42, 8773–8777.

van der Star, W.R.L., Abma, W.R., Blommers, D., Mulder, J.-W., Tokutomi, T., Strous, M., Picioreanu, C., van Loosdrecht, M.C.M., 2007. Startup of reactors for anoxic ammonium oxidation: experiences from the first full-scale anammox reactor in Rotterdam. Water Res. 41, 4149–4163.

van der Star, W.R.L., Miclea, A.I., van Dongen, U.G.J.M., Muyzer, G., Picioreanu, C., van Loosdrecht, M.C.M., 2008. The membrane bioreactor: a novel tool to grow anammox bacteria as free cells. Biotechnol. Bioeng. 101, 286–294.

Van Hulle, S.W.H., Vandeweyer, H.J.P., Meesschaert, B.D., Vanrolleghem, P. a., Dejans, P., Dumoulin, A., 2010. Engineering aspects and practical application of autotrophic nitrogen removal from nitrogen rich streams. Chem. Eng. J. 162, 1–20.

Vangsgaard, A.K., Mauricio-Iglesias, M., Gernaey, K. V, Smets, B.F., Sin, G., 2012. Sensitivity analysis of autotrophic N removal by a granule based bioreactor: Influence of mass transfer versus microbial kinetics. Bioresour. Technol. 123, 230–41.

Versteeg, H., Malalasekera, W., 1995. An introduction to computational fluid dynamics the finite volume method. Willey, New York.

Vilajeliu-Pons, A., Bañeras, L., Puig, S., Molognoni, D., Vilà-Rovira, A., Amo, E.H. Del, Balaguer, M.D., Colprim, J., 2016a. External resistances applied to MFC affect core microbiome and swine manure treatment efficiencies. PLoS One 11, 1–20.

Vilajeliu-Pons, A., Puig, S., Carmona-Martínez, A., Bernet, N., Coma, M., Aulenta, F., Colprim, J., Balaguer, M.D., 2016b. Electroactive Biofilms in Water and Air Pollution Treatment, in: Romani, A.M., Balaguer, M.D. (Eds.), Aquatic Biofilms.

Vilajeliu, A., Bañeras, L., Puig, S., Molognoni, D., Vilà-Rovira, A., Amo, E.H.-D., Balaguer, M.D., Colprim, J., 2016. External resistances applied to MFC affect core microbiome and swine manure treatment efficiencies. PLoS One 11. doi:10.1371/journal.pone.0164044

Vilar-Sanz, A., Puig, S., García-Lledó, A., Trias, R., Balaguer, M.D., Colprim, J., Bañeras, L., 2013. Denitrifying bacterial communities affect current production and nitrous oxide accumulation in a microbial fuel cell. PLoS One 8, e63460.

Volcke, E.I.P., Picioreanu, C., De Baets, B., van Loosdrecht, M.C.M., 2012. The granule size distribution in an anammox-based granular sludge reactor affects the conversion--implications for modeling. Biotechnol. Bioeng. 109, 1629–1636.

Wang, X., Ding, J., Ren, N.-Q., Liu, B.-F., Guo, W.-Q., 2009. CFD simulation of an expanded granular sludge bed (EGSB) reactor for biohydrogen production. Int. J. Hydrogen Energy 34, 9686–9695.

Wei, J., Liang, P., Huang, X., 2011. Recent progress in electrodes for microbial fuel cells. Bioresour. Technol. 102, 9335–44.

Wicklein, E., Batstone, D.J., Ducoste, J., Laurent, J., Griborio, A., Wicks, J., Saunders, S., Samstag, R., Potier, O., Nopens, I., 2016. Good modelling practice in applying computational fluid dynamics for WWTP modelling. Water Sci. Technol. 73, 969–982.

Wrighton, K.C., Virdis, B., Clauwaert, P., Read, S.T., Daly, R. a, Boon, N., Piceno, Y., Andersen, G.L., Coates, J.D., Rabaey, K., 2010. Bacterial

community structure corresponds to performance during cathodic nitrate reduction. ISME J. 4, 1443–1455.

Wu, B., 2012. Integration of mixing, heat transfer, and biochemical reaction kinetics in anaerobic methane fermentation. Biotechnol. Bioeng. 109, 2864–2674.

Wyffels, S., Van Hulle, S.W.H., Boeckx, P., Volcke, E.I.P., Van Cleemput, O., Vanrolleghem, P. a, Verstraete, W., 2004. Modeling and simulation of oxygen-limited partial nitritation in a membrane-assisted bioreactor (MBR). Biotechnol. Bioeng. 86, 531–542.

Yang, Q., Peng, Y., Liu, X., Zeng, W., Mino, T., Satoh, H., 2007. Nitrogen removal via nitrite from municipal wastewater at low temperatures using real-time control to optimize nitrifying communities. Environ. Sci. Technol. 41, 8159–8164.

Yu, L., Ma, J., Frear, C., Zhao, Q., Dillon, R., Li, X., Chen, S., 2013. Multiphase modeling of settling and suspension in anaerobic digester. Appl. Energy 111, 28–39.

Zhang, Y., Sun, J., Hu, Y., Li, S., Xu, Q., 2012. Bio-cathode materials evaluation in microbial fuel cells: A comparison of graphite felt, carbon paper and stainless steel mesh materials. Int. J. Hydrogen Energy 37, 16935–16942.

Zhou, M., Chi, M., Luo, J., He, H., Jin, T., 2011. An overview of electrode materials in microbial fuel cells. J. Power Sources 196, 4427–4435.